(12)

AFGL-TR-82-0021

GRAVITY GRADIOMETER SURVEY AND REAL TIME TECHNIQUES FOR IMPROVING INERTIAL NAVIGATION SYSTEM ACCURACY

Daniel B. DeBra
John V. Breakwell
Eugene Wells

Stanford University
Guidance & Control Laboratory
Department of Aeronautics and Astronautics
Stanford, California 94305

Final Report
January 1978 - December 1981

December 1981

Approved for public release; distribution unlimited

AIR FORCE GEOPHYSICS LABORATORY
AIR FORCE SYSTEMS COMMAND
UNITED STATES AIR FORCE
HANSCOM AFB, MASSACHUSETTS 01731

Unclassified

SECURITY CLASSIFICATION OF THIS PAGE (When Data Entered)

(12)

REPORT DOCUMENTATION PAGE	READ INSTRUCTIONS BEFORE COMPLETING FORM
1. REPORT NUMBER: AFGL-TR-82-0021	2. GOVT ACCESSION NO.: AD-A114 636
	3. RECIPIENT'S CATALOG NUMBER:
4. TITLE (and Subtitle): Gravity Gradiometer Survey and Real Time Techniques for Improving Inertial Navigation System Accuracy	5. TYPE OF REPORT & PERIOD COVERED: Final Report Jan 78 - Dec 1981
	6. PERFORMING ORG. REPORT NUMBER:
7. AUTHOR(s): Daniel B. DeBra, John V. Breakwell, Eugene Wells	8. CONTRACT OR GRANT NUMBER(s): F19628-78-C-0038
9. PERFORMING ORGANIZATION NAME AND ADDRESS: Stanford University, Guidance & Control Laboratory, Dept. Aeronautics & Astronautics, Stanford, CA 94305	10. PROGRAM ELEMENT, PROJECT, TASK AREA & WORK UNIT NUMBERS: 63701 B, 320103AE
11. CONTROLLING OFFICE NAME AND ADDRESS: Air Force Geophysics Laboratory, Hanscom AFB, MA 01731, Monitor: James Hammond/LWG	12. REPORT DATE: December 1981
	13. NUMBER OF PAGES: 124
14. MONITORING AGENCY NAME & ADDRESS(if different from Controlling Office)	15. SECURITY CLASS. (of this report): Unclassified
	15a. DECLASSIFICATION/DOWNGRADING SCHEDULE

16. DISTRIBUTION STATEMENT (of this Report)

Approved for public release; distribution unlimited.

17. DISTRIBUTION STATEMENT (of the abstract entered in Block 20, if different from Report)

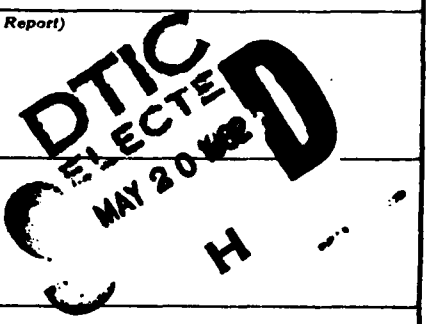

18. SUPPLEMENTARY NOTES

19. KEY WORDS (Continue on reverse side if necessary and identify by block number)

gravity survey, gravity gradiometer, inertial navigation, system accuracy, second-order model, Heller model, cross-track position error, real-time models, covariance comparisons,

20. ABSTRACT (Continue on reverse side if necessary and identify by block number)

see back side

DD FORM 1 JAN 73 1473 EDITION OF 1 NOV 65 IS OBSOLETE

Unclassified

SECURITY CLASSIFICATION OF THIS PAGE (When Data Entered)

Abstract

As inertial navigation instrumentation has become more advanced, the errors associated with imprecise knowledge of the true gravity vector have become significant. With the development of the moving base gravity gradiometer, ongoing for the past ten years, a means for detecting the true gravity vector is available. This research explores both real time and a priori schemes for using the gradiometer information to reduce the position and velocity error associated with an inertial navigation system.

In the real time application, information derived from the gradiometer is filtered to produce estimates of position and velocity error. The problem is to derive accurate filters in the presence of an inherently transcendental gravity field. Conventional Kalman filters are very cumbersome to apply in this instance. However, the sensitivity of inertial navigation systems at Schuler frequency makes it possible to neglect errors outside of a narrow band of frequencies centered at Schuler frequency. This approximation leads to low order filters which may be applied with surprising accuracy.

For the survey application, the gradiometer is used to establish a reference gravity model to be used in open loop inertial navigation system operation. By determining the root mean squared values of the resulting position and velocity errors, it is possible to evaluate the effectiveness of the survey scheme and to compare the survey application with the real time gradiometer application. Again, analytic and numeric covariance methods are used to do these analyses.

TABLE OF CONTENTS

LIST OF FIGURES

LIST OF TABLES

LIST OF TABLES (Cont)

LIST OF SYMBOLS

A		specific force
a		Schuler frequency velocity error estimation filter constant
AS		area surveyed
$A_j (j = 1, \ldots, 4)$		transition symbols
B		a posteriori gravity perturbation factor
b		first order Schuler frequency position error estimation filter constant(s)
c		zero order Schuler frequency position error estimation filter constant(s)
C_1, C_2		contours enclosing the left and right half complex plane respectively
$C_{\ell m}$		normalized potential coefficient of degree, ℓ, and order m
D	Ch. III	vertical deflection ensemble correlation distance
D	Ch. V	zero correlation matrix
D	App. A	the length of the vector $(\bar{R}_{(\theta} - \bar{r})$
D_i		depth below the earth's surface of the ith layer in Heller's model
$d\Omega$		small area on earth's surface
d	Ch. III	vertical deflection ensemble characteristic distance
d		first order low frequency position error estimation filter constant
e		zero-order low-frequency position error estimation filter constant
$E(\ )$	App. B	expected value
F		state transition matrix
F'		equivalent state transition matrix
$f(\ )$		perturbation potential of estimate transition function
G		process noise transition matrix

G'		equivalent process noise transition matrix
g		gravity perturbation
H		matrix relating gradient perturbation components to actual measured quantities
h_1		height above sea level where quantity is to be estimated
h_2		height above sea level where survey is taken
h_1'		height above ith layer of Heller's model, $(D_i + h_1)$, where quantity is to be estimated
h_2'		height above ith layer of Heller's model $(D_i + h_2)$ where survey is taken
$\bar{J}_{\ell m}$		fully normalized potential coefficients of degree ℓ and order m
K_1		modified Bessel function of first order
$K_{\ell m}$		normalizing constant
k		Schuler damping constant
k'		optimal k for minimum estimate error variance
k_j $(j=1, \ldots, 5)$		low frequency spatial spectral density coefficients
$k_j^A(j=1, \ldots, 3)$		low frequency time spectral density coefficients
$k_j^B(j=3, 4)$		low frequency time spectral density coefficients
$k_j^C(j=5)$		low frequency time spectral density coefficient
L	Ch. II	latitude
L		low frequency factor (ℓ+) coefficient
M		power spectral density matrix
m	Ch. IV	number of measurements
N		number of survey measurements
$P_\ell(\ )$		Legendre polynomial of degree ℓ
$\bar{P}_{\ell m}(\ )$		fully normalized Legendre function of degree ℓ and order m

q_2		power spectral density associated with the external velocity measurement noise
R		power spectral density matrix of the white noise measurement error vector ($\bar{\epsilon}$).
$R_\oplus$		nominal earth radius
$r_j (j=1, 2)$		diagonal members of the measurement error power spectral density matrix (R)
r		distance from earth's center to some point above the earth's surface
$S_{\ell m}$		normalized potential coefficient of degree ℓ and order m
s		Laplace variable
T		process-measurement noise power spectral density matrix
U		earth's surface potential
V		carrier vehicle velocity in an earth-fixed frame
V_{cir}		satellite velocity
V^m		externally measured velocity
w		process noise
w'		equivalent process noise
w_1		white noise associated with the second order gravity perturbation model
$W_j (j=1, 2)$		estimate error characteristic matrix
X		state vector
x_1		Markov Process state variable
x, y, z	Ch. III	position coordinates in-track, cross-track, and vertical respectively
$\bar{Y}_{\ell m}$		a portion of the spherical harmonic expansion for the earth's potential (defined in App. A)
z	Ch. III	height above the earth's surface
z	Ch. IV	measurement

z_i (i=1, ..., 3)		height above the ith layer of Heller's model

Greek Symbols

α		low frequency cross-track filter constant for position error estimation
$\bar{\alpha}$		angle which denotes the direction of $\bar{\omega}^s$
β		Markov parameter
$\bar{\beta}$		low frequency cross-track filter pole
γ		gravity gradient
Γ		gravity gradient perturbation or difference gradient
Δ		satellite distance spacing
$\Delta(\ )$		small change in indicated quantity
δ		Dirac delta
δ	App. A	Kronecker delta
δ_1		low frequency factor damping constant
δ_2		frequency constant in low frequency factor
$\bar{\delta}$		ground track divergence angle for low altitude polar orbit
δV		INS velocity error
δR		INS position error
δV^m		external velocity measurement error
ϵ		measurement noise (assumed white)
η		gradiometer accuracy
$\bar{\eta}$		quantity to be estimated from survey data
θ, θ'		latitude coordinates
μ	Ch. II	total accelerometer error
μ		the universal gravitational constant times the mass of the earth

ξ	App. C	transition symbol
σ		root mean squared value
$\sigma^2_{\bar{J}_\ell}$		root mean squared potential coefficient variation
$\Phi(\ )$		power spectral density
Φ_i		power spectral density of ith white noise level in Heller's model
ϕ		modified form of the external velocity measurement filter
Φ, Φ'	Ch. III App. A App. B	longitudinal coordinates
Ψ		velocity or position error filter(s) for gradiometer measurements
Ψ	Ch. II	small angle misalignment between platform and computer frames
Ψ	App. A	angle between two unit vectors defined by spherical coordinate sets $(1, \theta, \Phi)$ and $(1, \theta' \Phi')$
Ψ'		velocity or position error filter for external velocity measurement
ω		frequency variable
$\lvert\bar{\omega}\rvert$		magnitude of two dimensional frequency vector, $(\omega_x^2+\omega_y^2)^{\frac{1}{2}}$
ω_N		low frequency factor natural frequency
Ω	Ch. II	earth's rotation rate
Ω	Ch. IV	gradiometer rotation rate
Ω_i		normalized in-track frequency variable $(\Omega_i = 2z_i\omega_x)$

List of Symbols (Cont)

Superscripts

AF		analytic formula
AO		approximately optimal
c		computed quantity
HM		Heller Model
KF		Kalman Filter
LF		low frequency
NI		numerically integrated
s		spatial variation
SOM		second order (gravity perturbation) model
SO		suboptimal
t		time variation
T		transpose
^		estimated quantity
.		time derivative of scalar quantity
-		vector quantity
-	App. A	fully normalized quantity
=		second-order tensor
*		complex conjugate
( ) × ( )		matrix size designator
~		estimate error
$( )^{-1}$		inverse

List of Symbols (Cont)

Subscripts

cir		circular
E		east-pointing direction
ℓ		low frequency
ℓ, m	Ch. III App. A App. B	degree and order respectively
N		north-pointing direction
s		Schuler frequency
x		in-track direction
y		cross-track direction
z		vertical direction (positive downward)
1-D		one dimensional
2-D		two dimensional

Miscellaneous

(+)	positive Schuler factor
(-)	negative Schuler factor
(+')	modified positive Schuler factor
(-')	modified negative Schuler factor
$\lvert\ \rvert$	determinant
$\circledast$	convolution
$(\ )^{(\ )}$	exponential
$\triangleq$	defined as

Abbreviations

BHM	Baseline Heller model
CT	cross-track
E	Eötvos
EVM	external velocity measurement
E/EVM	excluding the external velocity measurement
GEM	Goddard Earth Model
GS	gradiometer survey
IHM	improved Heller Model
INS	inertial navigation system
IT	in-track
I/EVM	including the external velocity measurement
(ℓ+)	positive low frequency factor
(ℓ-)	negative low frequency factor
m	meter
mm	millimeter
PSD	power spectral density
RGG	rotating gravity gradiometer
rms	root mean squared
sec	second
SOM	second-order (gravity perturbation) model
SS	satellite survey
TC	time constant

Chapter I

INTRODUCTION

A. PROBLEM STATEMENT

For inertial navigation a gyro stabilized platform is used to spatially orient accelerometers which measure specific force. Specific force is the vector (difference) of the quantity to be determined, inertial acceleration, and gravity. Therefore to isolate inertial acceleration the true gravity vector must be found. It cannot be measured directly from a moving vehicle because it is inseparable from the effects of inertial acceleration. However, the gradients of the gravity field are separable from those of a linear acceleration field (zero if nonrotating) thus making it possible to calculate the changes in gravity. By spatially integrating these changes on-line, variations in the true gravity vector may be determined. If these variations are used in conjunction with periodic platform leveling and position fixes, the true gravity vector can be found. It is now a simple matter to difference the true and assumed (from a reference gravity model) gravity vectors to obtain the gravity perturbation vector. The horizontal components of the gravity perturbation vector represent the deflections of the vertical uncertainties of which cause errors in the horizontal inertial navigation channels.

The problem addressed by this research is to determine how to use the gradiometer to most effectively reduce the gravity deflection error contribution to the inertial navigation system (INS) horizontal position and velocity outputs. This is distinct from the greater question of how large the geodetic error is when compared with the instrument errors in the inertial navigation system. A discussion of this separate question is given by Hildebrant, et al., [1] and shows, for instance, that the geodetic portion of the total inertial navigation velocity error budget may be as high as 70% in state-of-the-art systems. There are two ways to use the gradiometer to improve inertial navigation. The first way is to estimate in real time the velocity and position errors propagating

in the INS basic output loop. In reality this portion of the problem primarily involves the derivation and evaluation of approximate low-order filters for velocity and position error estimation. Approximate filters are advantageous because they circumvent the problems which arise from working with inherently transcendental gravity field spectra. The second method is to survey the area which the INS carrier vehicle is to traverse. Using this information the reference gravity model contained in the INS output loop is updated to reduce the residual between true and reference gravity. This involves updating the gravity perturbation power spectrum and subsequently determining rms position and velocity error for survey parameter optimization and real time comparisons.

Since navigation on the surface of the earth is generally more important than vertical position, this research will focus on only the horizontal channels of a locally level INS, though some of the methods could be applied to the vertical channel.

B. GRADIOMETER DEVELOPMENT AND PREVIOUS WORK

Moving base gravity gradiometers have been under development for the past 15 years. This development, done under the auspices of the Air Force, Navy and the Defense Mapping Agency, resulted in two workable gradiometers: one by the Bell Laboratories [2], and one by the Draper Labs [3]. The Bell instrument was chosen by the Navy as the most advantageous design for their application, and will be used when reference to hardware is necessary. The Bell instrument is commonly called a "rotating gravity gradiometer" (RGG) because the measurement unit is actually rotated to separate spectrally the gradient signals from outside disturbances.

The gradiometer research done at Stanford began in 1972 under the auspices of the U.S. Air Force Geophysics Laboratory. Pelka's dissertation [4] dealt with improving the accuracy of the Hughes' (prototype) gradiometer using on-line parameter estimation and control techniques. Subsequent studies by DeBra, Breakwell, Schaechter, and

Kurosaki dealt with the development of gravity models used to determine the performance of the gradiometer in mapping the earth's gravity field [5]. The culmination of this work describes the use of a gravity gradiometer aboard a horizontally moving vehicle to estimate gravity deflection and anomaly [6]. Gradiometer derived improvements of inertial navigation and gravity survey work are presented in this dissertation.

C. NEW RESULTS

Whereas most previous research on gradiometers has dealt with the instruments themselves, the research reported here deals with the processing of gradiometer data both in real time and after the fact (the latter being called the "survey" use). No other investigators have addressed these aspects of the problem as they have been addressed here.

Specific contributions are:

1. The development of a method for deriving approximate Wiener filters for estimation of INS position and velocity error;
2. The statistical evaluation of these filters to determine relative and absolute optimality;
3. The statistical evaluation of various survey schemes for update of the reference gravity model;
4. Development of an improved version of Heller's gravity model to portray more accurately the perturbation potential in light of the latest gravity data available.

D. THESIS OUTLINE

The full inertial navigation system error equations and the assumptions used to simplify them for use in this research are presented in Chapter II.

Chapter III presents three statistical gravity perturbation models used in the covariance analyses presented in Chapters V and VII. The first model is rational (the reason for its use) but somewhat inaccurate. The second and third models are transcendental but are representative of the most accurate gravity perturbation models available.

In Chapter IV the basic theory used in deriving approximate real time filters is shown, along with examples, for a wide spectrum of measurement combinations.

Several filters obtained in Chapter IV are evaluated and compared by covariance methods in Chapter V.

In Chapter VI the theory used in analyzing the effect of a gravity survey on INS performance is developed.

In Chapter VII covariance data for the survey scheme is computed and compared with data obtained from the real time application. The ultimate goal of this comparison is to determine which gradiometer application is most desirable under a given set of conditions.

In Chapter VIII the conclusions and future recommendations of this research are presented.

Chapter II

INERTIAL NAVIGATION ERROR EQUATIONS

Before looking at the error equations associated with conventional inertial navigation systems (INSs) it is instructive to examine the basic navigation loop used throughout this research. Figure II-1 is a schematic of this loop. Note that some type of external velocity measurement (V^m) is assumed for damping of Schuler oscillations.

A. FULL INERTIAL NAVIGATION SYSTEM ERROR EQUATIONS

The error equations relating the gravity perturbations to INS position and velocity error have been developed in detail by Heller [7]. These equations assume an INS mechanized in a local-level wander-azimuth frame and coordinatized in a local-level north-pointing frame. The full position and velocity error equations for the horizontal channels of an INS are given below [from Ref. 7]:

$$\begin{aligned}\dot{\delta V}_N = {} & \mu_N - A_z\psi_E + A_E\psi_z - \omega_s^2\delta R_N + g_N \\ & - \left(2\Omega \sin L + \frac{V_E}{R_\oplus} \tan L\right) \delta V_E \\ & + \frac{V_N}{R_\oplus} \delta V_z - k\delta V_N - kV_E\psi_z + kV_z\psi_E + k\delta V_N^m \ ; \end{aligned} \tag{2.1}$$

$$\begin{aligned}\dot{\delta V}_E = {} & \mu_E + A_z\psi_N - A_N\psi_z - \omega_s^2\delta R_E + g_E + \left(2\Omega \sin L \right. \\ & \left. + \frac{V_E}{R_\oplus} \tan L\right)\delta V_N + \left(2\Omega \cos L + \frac{V_E}{R_\oplus}\right)\delta V_z \\ & - k\delta V_E - kV_z\psi_N + kV_N\psi_z + k\delta V_E^m \ ; \end{aligned} \tag{2.2}$$

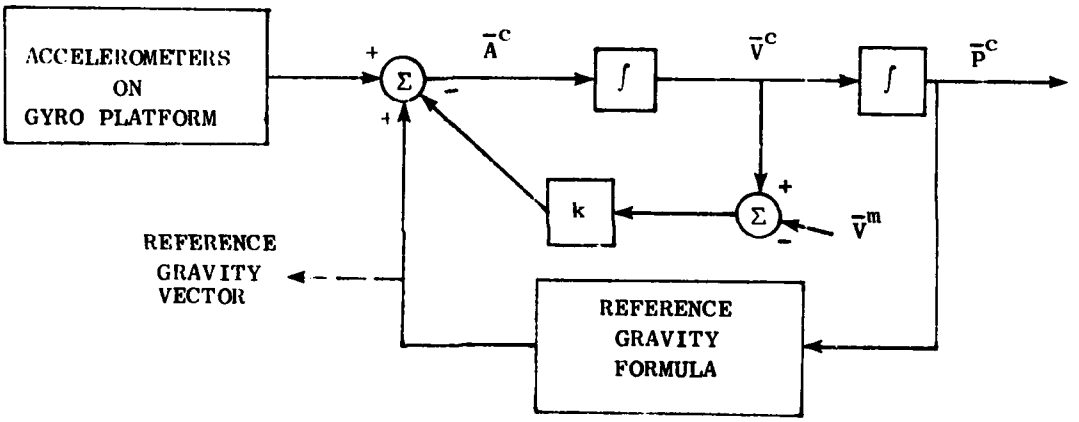

FIG. II-1 SCHEMATIC OF BASIC NAVIGATION LOOP

$$\delta\dot{R}_N = \delta V_N - \frac{V_E}{R_D} \tan L \, \delta R_E - \frac{V_N}{R_D} \delta R_z \; ; \qquad (2.3)$$

$$\delta\dot{R}_E = \delta V_E + \frac{V_E}{R_D} \tan L \, \delta R_N - \frac{V_E}{R_D} \delta R_z \; . \qquad (2.4)$$

B. SIMPLIFYING ASSUMPTIONS AND RESULTING ERROR EQUATIONS

The error equations are linear thus allowing different error contributors to be superposed. In order to focus on gravity induced errors the nongravitational error sources in (2.1) to (2.4) (i.e., accelerometer bias, μ, platform misalignment, ψ, etc.) may be set aside [1]. Furthermore, the north and east equations may be decoupled without limitation to research objectives. Therefore the following assumptions have been made.

1) The carrier vehicle travels due north*;

2) There are no platform misalignment or accelerometer bias errors;

3) The carrier vehicle altitude is fixed;

4) The earth is nonrotating.

With these assumptions the horizontal channel error equations become

$$\delta\dot{V}_x = -\omega^2 \delta R_x - k[\delta V_x - \delta V_x^m] + g_x \qquad (2.5)$$

$$\delta\dot{V}_y = -\omega_s^2 \delta R_y - k[\delta V_y - \delta V_y^m] + g_y \qquad (2.6)$$

$$\delta\dot{R}_x = \delta V_x \qquad (2.7)$$

$$\delta\dot{R}_y = \delta V_y \; . \qquad (2.8)$$

---

* This assumption is simply a manifestation of the particular north-east down coordinate system chosen in (2.1) through (2.4). Equations (2.5) through (2.8) would remain the same had another local-level coordinate system been selected to coincide with the in-track (x) and cross-track (y) directions of a vehicle traveling other than north. Thus the analysis done here applies to a carrier vehicle traveling in any direction over a non-rotating earth.

Note that since the carrier vehicle travels due north this direction will henceforth be denoted in-track (x subscript) and the easterly direction denoted cross-track (y subscript).

Chapter III

STATISTICAL GRAVITY PERTURBATION MODELS

A stochastic study of INS position and velocity error requires that the gravity perturbation terms in Eqs. (2.5) and (2.6) be statistically modeled. Three models were used in this study. The first is a relatively inaccurate rational model used solely for Kalman filter comparisons, as a rational model is necessary for a Kalman realization. The last two models have the same basic form, the only difference being a slight parameter modification in the final version to fit observed data more closely. These models are transcendental but portray more accurately the earth's actual gravity field. All three of these models were developed by the processing of empirical data such as that collected by Rice [8].

A. SECOND-ORDER MODEL

The details of this model are fully detailed by Kasper [9] and reiterated by Heller [10]. To summarize briefly, it is a second-order model consisting of zero mean white noise put through a shaping filter as shown in Fig. III-1.

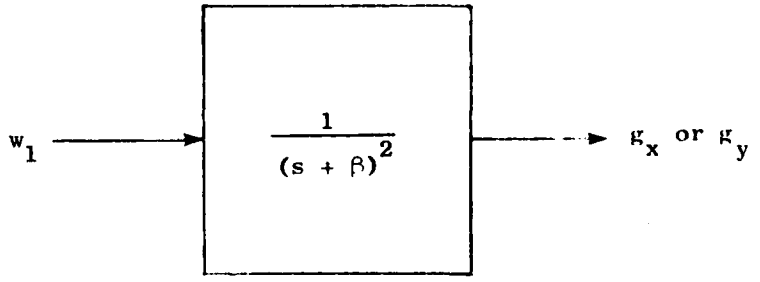

FIG. III-1 SECOND-ORDER GRAVITY PERTURBATION MODEL

The Markov parameter β is defined as

$$\beta = V_x/d^* \quad . \tag{3.1}$$

where d is the vertical deflection ensemble characteristic distance.

---

* The constant d in Kasper's model is related to the more commonly known correlation distance (D) by the relation: $D = 2.146d$.

This model may be used in either the in-track or cross-track directions. However, the Kalman filter comparisons need only be done cross-track to demonstrate the accuracy of the approximate filters. The spectral density of the white noise w_1, is given as

$$q_1 = 4\beta^3\sigma_{g_y}^2 \quad . \tag{3.2}$$

where

$$\sigma_{g_y}^2 = E\{w_1^2\} \quad .$$

A state space description of this model, required in Ch. V, may be written as

$$\begin{bmatrix} \dot{x}_1 \\ \dot{g}_y \end{bmatrix} = \begin{bmatrix} -\beta & 0 \\ 1 & -\beta \end{bmatrix} \begin{bmatrix} x_1 \\ g_y \end{bmatrix} + \begin{bmatrix} w_1 \\ 0 \end{bmatrix} \quad , \tag{3.3}$$

where x_1 is a Markov Process state variable.

B. BASELINE HELLER MODEL

This statistical model was developed by Heller [11] and describes perturbations in the earth's surface potential away from an ellipsoidal geoid as fictitious white noise potential fluctuations restricted to a few thin layers below the earth's surface. The model, as shown below, is defined by the power spectral density (PSD) of surface potential fluctuations

$$\Psi_{\Delta U}^{s}(\bar{\omega}^s;\ z = 0) = \Phi_{\Delta U}^{s}(|\bar{\omega}^s|;\ 0) = \sum_{i=1}^{3} \lambda_i e^{-2|\bar{\omega}^s| D_i} \tag{3.4}$$

where

$$\bar{\omega} = \begin{bmatrix} \omega_x \\ \omega_y \end{bmatrix} .$$

The values for the depths (D_i's) and PSDs (Φ_i's) of the three layers of interest given by Heller are listed in Table III-1.

Table III-1

BASELINE HELLER MODEL PARAMETERS

i	D_i (km)	Φ_i (km^6/sec^4)
1	16.3	7.1×10^{-8}
2	92.5	1.07×10^{-4}
3	390.5	1.16×10^{-2}

To determine the relationship between surface potential fluctuations and potential fluctuations at an altitude z above the earth's surface it facilitates analysis to work with a "flat earth" approximation [12] to Poisson's upward continuation formula for the earth's potential. Poisson's upward continuation formula is given by

$$\Delta U(r, \theta, \phi) = \frac{R_\oplus (r^2 - R_\oplus^2)}{4\pi} \oint \frac{\Delta U(R_\oplus, \theta', \phi')}{(r^2 + R_\oplus^2 - 2\bar{r} \cdot \bar{R}_\oplus)^{3/2}} \, d\Omega' \qquad (3.5)$$

where the direction of the vector $\bar{r}$ is determined by the (r, θ, ϕ) spherical coordinate set, and the direction of $\bar{R}_\oplus$ is determined by the set $(R_\oplus, \theta', \phi')$. The integration of (3.5) is done over the entire earth's surface. The details of the derivation of (3.5) are given in App. A. Making the "flat earth" approximation ($z \ll R_\oplus$) to (3.5)

$$\Delta U(x, y; z) = \frac{z}{2\pi[x^2 + y^2 + z^2]^{3/2}} \otimes \Delta U(x, y; 0) \qquad (3.6)$$

where $\otimes$ denotes convolution in two dimensions. Taking the fourier transform of (3.6) yields

$$\Delta U(\bar{\omega}^s;\ z) \ = \ e^{-z|\bar{\omega}^s|}\Delta U(\bar{\omega}^s;\ 0)\ . \tag{3.7}$$

This allows (3.4) to be rewritten as

$$\Phi^s_{\Delta U}(\bar{\omega}^s;\ z) \ = \ e^{-2|\bar{\omega}^s|z}\Phi^s_{\Delta U}(\bar{\omega}^s;\ 0) \ = \ \sum_{i=1}^{3} \Phi_i e^{-2z_i|\bar{\omega}^s|}\ . \tag{3.8}$$

Because Heller has modeled the potential perturbations it is a simple matter to obtain from (3.8) the two dimensional PSD expressions for any of the gravity or gravity gradient perturbation components. In fact, the two dimensional spectral density matrix relating g_x, g_y g_z, Γ_{yz}, Γ_{zz} is given by Kurosaki and Breakwell [13] as

$${}^s[M]_{2\text{-}D} = \sum_{i=1}^{3} \Phi_i e^{-2z_i|\bar{\omega}|} \begin{bmatrix} \omega_x^2 & \omega_x\omega_y & j\omega_x|\bar{\omega}| & -\omega_x\omega_y|\bar{\omega}| & -j\omega_x|\bar{\omega}|^2 \\ \omega_x\omega_y & \omega_y^2 & j\omega_y|\bar{\omega}| & -\omega_y^2|\bar{\omega}| & -j\omega_y|\bar{\omega}|^2 \\ -j\omega_x|\bar{\omega}| & -j\omega_y|\bar{\omega}| & |\bar{\omega}|^2 & j\omega_y|\bar{\omega}|^2 & -|\bar{\omega}|^3 \\ -\omega_x\omega_y|\bar{\omega}| & -\omega_y^2|\bar{\omega}| & -j\omega_y|\bar{\omega}|^2 & \omega_y^2|\bar{\omega}|^2 & j\omega_y|\bar{\omega}|^3 \\ j\omega_x|\bar{\omega}|^2 & j\omega_y|\bar{\omega}|^2 & -|\bar{\omega}|^3 & -j\omega_y|\bar{\omega}|^3 & |\bar{\omega}|^4 \end{bmatrix}$$

where all ω's indicate spatial frequency variation.

The spectral-density matrix along the line $y = 0$ is required because the carrier vehicle is, by definition, always traveling in-track. This matrix is obtained by performing the following operation:

$$ {}^{s}[M]_{1\text{-}D} = \frac{1}{2\pi} \int_{-\infty}^{\infty} {}^{s}[M]_{2\text{-}D}\, d\omega_y^s \,. \qquad (3.9) $$

The results of this operation are again shown by Breakwell and Kurosaki [13] as

$$ {}^{s}[M]_{1\text{-}D} = \sum_{i=1}^{3} \frac{\Phi_i}{\pi(2z_i)^3} $$

$$ \times \begin{bmatrix} \Omega_i^3 K_1(\Omega_i) & 0 & -j\Omega_i^3 K_1'(\Omega_i) & 0 & -j\frac{\Omega_i}{2z_i} K_1''(\Omega_i) \\ 0 & \Omega_i^3[K_1''(\Omega_i)-K_1(\Omega_i)] & 0 & \frac{\Omega_i^4}{2z_i}[K_1'''(\Omega_i)-K_1'(\Omega_i)] & 0 \\ j\Omega_i^3 K_1'(\Omega_i) & 0 & \Omega_i^3 K_1''(\Omega_i) & 0 & \frac{\Omega_i^4}{2z_i} K_1'''(\Omega_i) \\ 0 & \frac{\Omega_i^4}{2z_i}[K_1'''(\Omega_i)-K_1'(\Omega_i)] & 0 & \frac{\Omega_i^5}{(2z_i)^2}[K_1''''(\Omega_i)-K_1''(\Omega_i)] & 0 \\ \frac{j\Omega_i^4}{2z_i} K_1''(\Omega_i) & 0 & \frac{\Omega_i^4}{2z_i} K_1'''(\Omega_i) & 0 & \frac{\Omega_i^5}{(2z_i)^2} K_1''''(\Omega_i) \end{bmatrix} \qquad (3.10) $$

where

$K_1(\Omega_i)$ = modified Bessel function of first order

Ω_i = normalized frequency variable ($\Omega_i = 2z_i\omega_x^s$)

$'$ = differentiation with respect to the variable Ω_i.

Although in ${}^{s}[M]_{1\text{-}D}$ the designated states are g_x, g_y, and g_z, the PSDs of the in-track spatial derivatives of these quantities Γ_{xx}, Γ_{xy}, Γ_{xz} are easily obtained by multiplication by $j\omega_x^s$. In addition, Γ_{yy} may be found through the application of Laplace's equation $\Gamma_{xx} + \Gamma_{yy} + \Gamma_{zz} = 0$.

The zero correlations in (3.10) are interesting because they show which gradient perturbation components may be used to estimate g_x and g_y in Eqs. (2.5) and (2.6). The zero correlation between g_y, Γ_{xy} and the other states indicates that the optimal estimate of g_y should involve only the measurements Γ_{xy} and Γ_{yz}. The optimal estimate of g_x, on the other hand, should use only Γ_{xx}, Γ_{xz}, Γ_{zz} (or Γ_{yy}).

Spectral separation considerations to be explained in Ch. V dictate that a low frequency approximation to (3.10) be available. Such an approximation was developed by Breakwell and Kurosaki [13] and is shown below.

$$ {}^{s}[M]^{LF}_{1-D} = \begin{bmatrix} -k_1 s^2 & 0 & k_2 s & 0 & -2k_3 s \\ 0 & 2k_3 & 0 & -6k_4 & 0 \\ -k_2 s & 0 & 2k_3 & 0 & -6k_4 \\ 0 & -6k_4 & 0 & 24k_5 & 0 \\ 2k_3 s & 0 & -6k_4 & 0 & 24k_5 \end{bmatrix} \tag{3.11} $$

where

$$ k_j = \frac{1}{\Pi} \sum_{i=1}^{3} \frac{\phi_i}{(2z_i)^j} \tag{3.12} $$

and

$$ s = j\omega_x^s \, . \tag{3.13} $$

C. IMPROVED HELLER MODEL

In the course of this research it became necessary to improve Heller's baseline model with the latest gravity data available in an attempt to shorten the characteristic times of certain low frequency poles, to be introduced in the next chapter. The process and result of this improvement will be discussed here.

The data used to improve the baseline Heller model (BHM) was the Goddard Earth Model (GEM) 10 data published by NASA [14]. In the GEM 10 studies done by the NASA the earth's potential was described in the standard spherical harmonic form given below:

$$U(r, \theta, \phi) = \frac{\mu}{R_D} \sum_{\ell=0}^{\infty} \sum_{m=0}^{\ell} \left(\frac{R_D}{r}\right)^{\ell+1} \bar{P}_{\ell m}(\sin\theta) \times [C_{\ell m} \cos m\phi + S_{\ell m} \sin m\phi] \tag{3.14}$$

where the $C_{\ell m}$'s and $S_{\ell m}$'s determined from satellite data actually define GEM 10.

If it is assumed that the gravity model used in an INS is at least as accurate as GEM 10 then the rms potential coefficient error estimates for GEM 10 taken from Ref. 14 (p. 55) should equal the rms potential coefficient variation ($\sigma_{\bar{J}_\ell}$) of the Heller model. The relation defining the mean-squared potential coefficient variation for both the spherical and Heller models is derived in App. B and summarized as

$$\sigma^2_{\bar{J}_\ell} = \sum_{m=0}^{n} \frac{C^2_{\ell m}+S^2_{\ell m}}{2\ell+1} = \left(\frac{R_D}{\mu}\right)^2 \frac{1}{4\pi} \sum_{i=1}^{3} \frac{\Phi_i}{(R_D-D_i)^2} \left(\frac{R_D-D_i}{R_D}\right)^{2\ell+2} . \tag{3.15}$$

By substituting the GEM 10 rms coefficient error estimates in for $C_{\ell m}$ and $S_{\ell m}$ in (3.15) the PSD of the deepest layer of Heller's model may be adjusted so that (3.15) is roughly satisfied at low frequency. Recalling that the reason for this exercise is to adjust low frequency pole characteristic times, only Φ_3 need be adjusted as this value has the largest effect on low frequency behavior while its influence dies out at high frequency. A satisfactory match was obtained by reducing Φ_3 by a factor of 10. Figure III-2 shows the results of this change. Thus the IHM (improved Heller model) parameters are the same as those given in Table III-1 except that

$$\Phi_3 = 1.16 \times 10^{-3} \text{ km}^6/\text{sec}^4 . \tag{3.16}$$

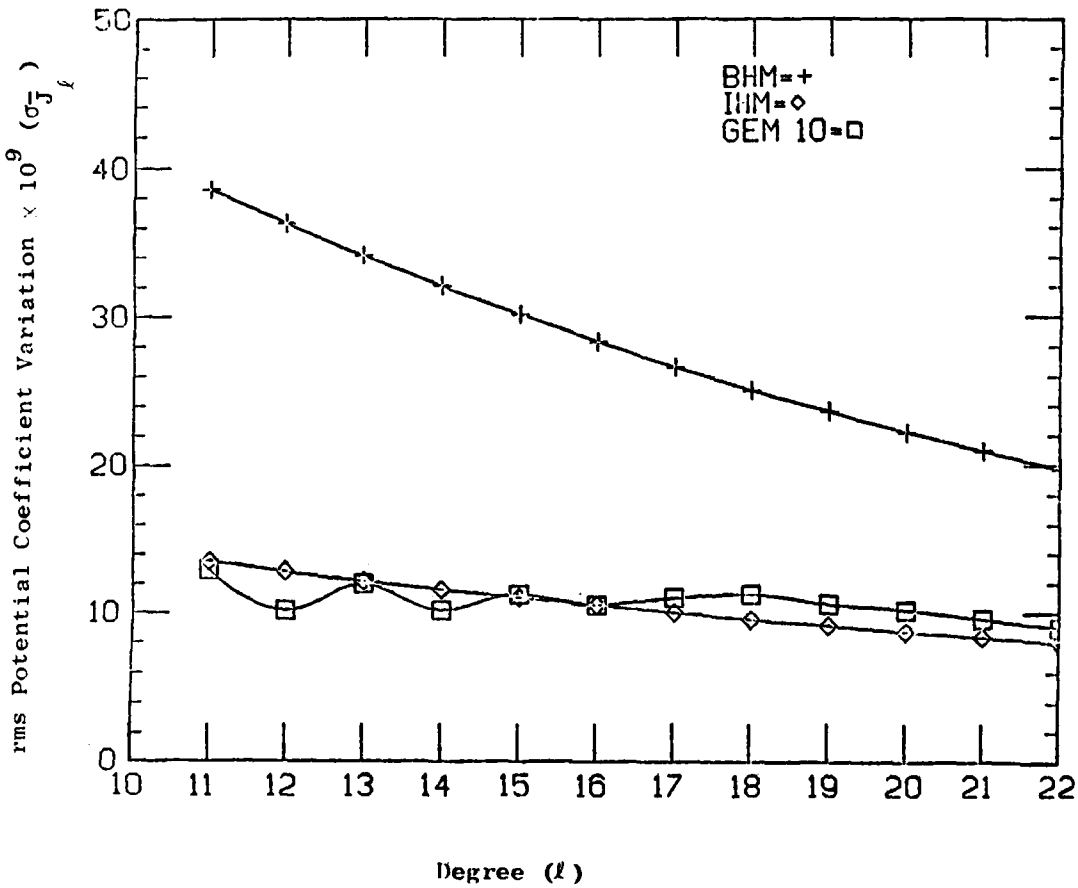

FIG. III-2 GEM 10 DATA - HELLER MODEL COMPARISON

The improved Heller model (IHM) was a necessary development in the course of this research as explained above. To alleviate any confusion in deciding which Heller model was used in the comparisons to come, great care has been taken to clearly mark each case.

Thus far in the discussion all of the power spectral densities have been based on spatial as opposed to time variation. In the following chapters, PSDs based on time will be required. The conversion from spatial to time variation for a carrier vehicle with constant velocity simply involves the carrier speed as follows

$$\Phi^{s}(\omega^{s}) = \Phi^{t}(\omega^{t}) \times V \ . \tag{3.17}$$

Note also the spatial-to-time frequency variable transformation

$$\omega^{t} = \omega^{s} \times V \tag{3.18}$$

which will be used for consistency in writing various PSD expressions.

Chapter IV

APPROXIMATE REAL TIME FILTERS

In this chapter the basic theory for deriving filters for the estimation of INS position and velocity error is presented. Gradiometer outputs, and in some cases the externally obtained vehicle velocity measurement, are used as inputs to these filters. Figure IV-1 shows a schematic of the real time gradiometer application scheme which is simply added on to the basic navigation loop shown in Fig. II-1.

The scope of this thesis permitted at most two gradiometer measurements in-track or cross-track. The output signal of a single Bell RGG with its spin axis vertical is

$$\frac{1}{2}(\Gamma_{yy} - \Gamma_{xx}) \sin 2\Omega t + \Gamma_{xy} \cos 2\Omega t^{\dagger}$$

where $\bar{\bar{\Gamma}}$ is the gravity gradient tensor prior to differencing with the reference gravity gradient, Ω is the gradiometer rotation rate, and t is time. After demodulation to separate the sine and cosine terms and differencing the gradient components with the reference values, the following outputs are obtained

$$\frac{1}{2}(\Gamma_{yy} - \Gamma_{xx})^{\ddagger}$$

and

$$\Gamma_{xy}{}^{\ddagger}$$

where $\bar{\bar{\Gamma}}$ is the difference gradient.

---

† The navigation axes x and y to which the sensor is aligned are not necessarily principal axes of the gravity gradient. In the plane of rotation of the sensor the principal axes are at an angle with respect to the x and y axes. If a phase angle is introduced in the equation indicated by this footnote it would indicate the orientation of the principal axes when the cross-gradient component is zero. Thus the gradient can also be represented by an angle and the maximum difference $(\Gamma_{yy} - \Gamma_{xx})$ in the plane of rotation.

‡ The outputs obtainable from a single spherical gradiometer manufactured by the Draper Lab. are different in form from those of the Bell RGG. It is an easy matter, however, to alter the analysis given in this thesis to accommodate the Draper gradiometer. An overview of the operation and outputs of the spherical gradiometer is given by Trageser[15].

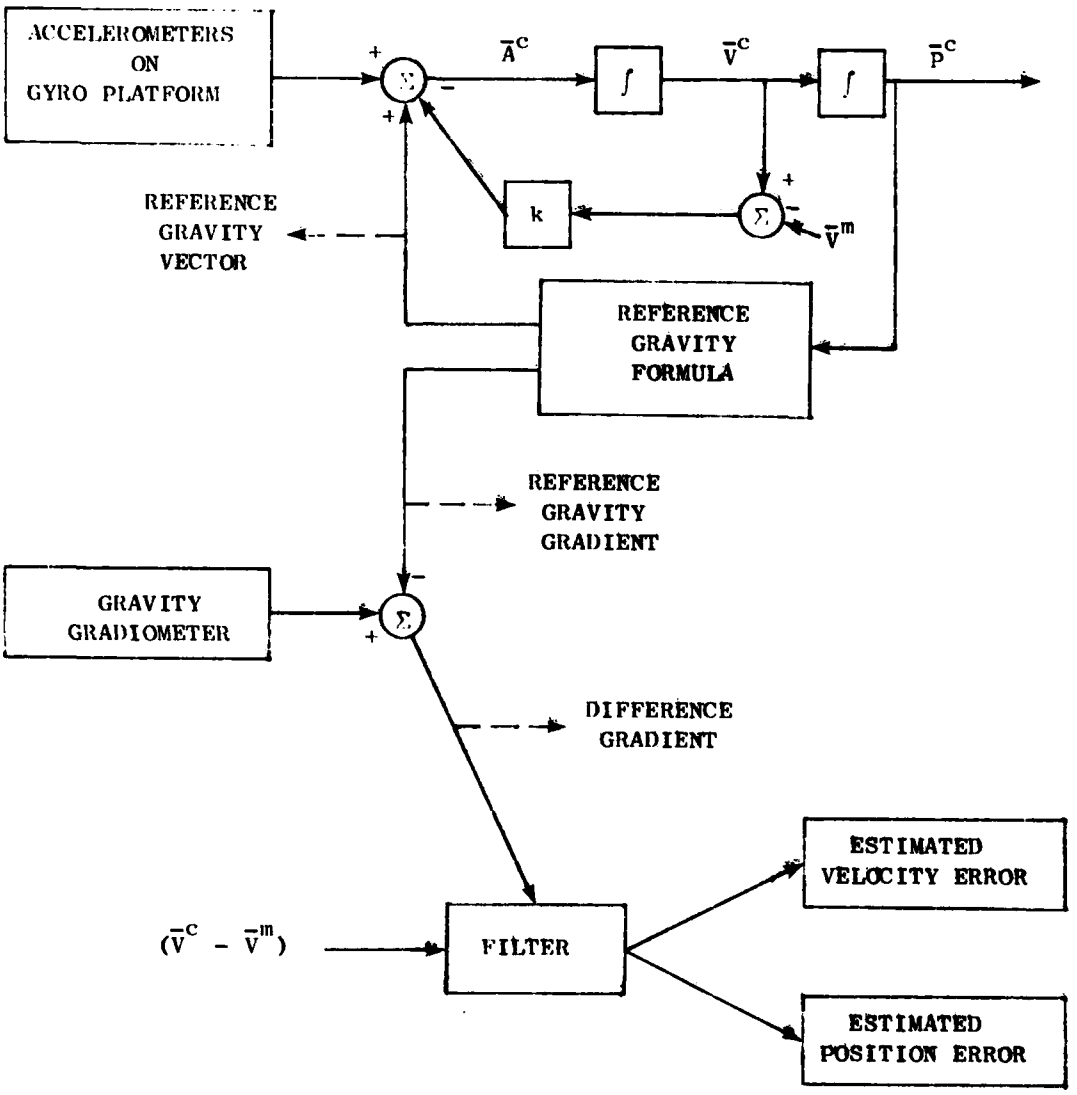

FIG. IV-1 SCHEMATIC OF REAL TIME FILTER APPLICATION

A cyclic permutation of these subscripts gives the outputs for instruments with spin axes aligned in-track and cross-track respectively. Recall from Ch. III that only the cross-gradients Γ_{xy} and Γ_{yz} can be used as measurements cross-track and only the in-line gradients (Γ_{xx}, Γ_{yy}, Γ_{zz}) and Γ_{xz} can be used as measurements in-track. Thus to obtain two gradiometer measurements cross-track, two instruments are required with spin axes in-track and vertical. The in-line gradient combinations from these same two instruments are used for in-track estimation. This allows for a full evaluation of how two gradiometers can improve horizontal navigation. The best choice for a single cross-track measurement is Γ_{xy} because it is more highly correlated with g_y than is Γ_{yz}. For consistency the in-line output of this same gradiometer is used as a single in-track measurement.

Table IV-1 lists each of the measurement combinations used.

Table IV-1

CROSS-TRACK AND IN-TRACK MEASUREMENT COMBINATIONS

Measurement Combination Code	Difference Gradient Components
CT-1	$[\Gamma_{xy}]$
CT-2	$\begin{bmatrix} \Gamma_{xy} \\ \Gamma_{yz} \end{bmatrix}$
IT-1	$[\Gamma_{xx}]$
IT-2	$[\Gamma_{xx} + \frac{1}{2}\Gamma_{zz}]$
IT-3	$\begin{bmatrix} \Gamma_{xx} + \frac{1}{2}\Gamma_{zz} \\ \frac{1}{2}\Gamma_{xx} + \Gamma_{zz} \end{bmatrix}$

The significance of each is given below.

CT-1. This combination corresponds to using the cross-gradient output of one Bell rotating gravity gradiometer (RGG) with its spin axis mounted vertically. Because this tensor component is the in-track spatial derivative of the cross-track deflection it is the tensor component most highly correlated with g_y.

CT-2. To obtain this set of measurements two RGGs are required. The spin axes of these instruments point vertically and in-track respectively. The improvement over the CT-1 combination is small.

IT-1. Because the in-line gradients come from the Bell RGG linearly combined (e.g., for spin axis vertical $\frac{1}{2}(\Gamma_{xx} - \Gamma_{yy})$), Γ_{xx}, the most highly correlated component with g_x is not directly obtainable. However, for comparison purposes this fictitious case of a direct Γ_{xx} measurement is included.

IT-2. This case illustrates the situation where the direct in-line composite output (modified by Laplace's equation) of one vertical RGG is used as a measurement. This is inferior to the IT-1 case.

IT-3. In this situation the direct composite outputs of two RGGs are used where the instrument spin axes are vertical and in-track. This combination is comparable in information to the IT-1 case.

A. VELOCITY ERROR ESTIMATION THEORY

A-1 Excluding the External Velocity Measurement

To obtain the measurement combinations just discussed the basic difference gradient vector required is

$$\bar{\Gamma} = \begin{bmatrix} \Gamma_{xx} \\ \Gamma_{xy} \\ \Gamma_{xz} \\ \Gamma_{yz} \\ \Gamma_{zz} \end{bmatrix}^{\dagger} \tag{4.1}$$

The measurements may then be written as

$$\underset{z}{m\times 1} = \underset{H}{m\times 5}\ \underset{\bar{\Gamma}}{5\times 1} + \underset{\bar{\epsilon}}{m\times 1} \tag{4.2}$$

where $\bar{\epsilon}$ is the white measurement noise vector.

Let the estimated velocity error be

$$\hat{\delta v}_x(s) = \underset{\psi(s)}{1\times m}\ \underset{\bar{z}}{m\times 1} = \psi(s)[H\bar{\Gamma} + \bar{\epsilon}] \ . \tag{4.3}$$

where $\psi(s)$ is the velocity error filter expressed in the Laplace domain.

---

† This vector requires only these five components because any single channel output of a Bell RGG with axes oriented along the x, y, z directions can be reproduced with these elements and the proper H matrix. If all the elements of the gravity perturbation tensor are required three orthogonal RGGs are required. These instruments must be mounted so that a significant component of gravity is perpendicular to the spin axis of each instrument. This is necessary for proper operation of the scale factor calibration loops.

Note here that (4.3) is written with subscript x indicating the in-track direction. Because the basic INS error equations have the same form IT or CT the velocity error estimation equations will be written IT but are immediately applicable CT simply by changing the x subscripts to y. Taking the Laplace transform of (2.5) and (2.7) and solving for δV_x gives

$$\delta V_x(s) = \frac{sg_x}{(+)} + \frac{sk\delta V_x^m}{(+)} \tag{4.4}$$

where

$$(+) = s^2 + ks + \omega_s^2 \tag{4.5}$$

is called the positive Schuler factor and conversely, (-) will be used to denote the negative Schuler factor $(s^2 - ks + \omega_s^2)$. Subtracting (4.4) from (4.3) the estimate error is

$$\tilde{\delta V}_x(s) = \psi(s)H\bar{\Gamma} + \psi(s)\bar{\epsilon} - \frac{sg_x}{(+)} - \frac{sk\delta V_x^m}{(+)} \quad . \tag{4.6}$$

The PSD of $\tilde{\delta V}_x(s)$ is then

$$\Phi^t_{\tilde{\delta V}_x}(s) = \psi(-s)H\Phi^t_{\bar{\Gamma}\bar{\Gamma}^T}(s)H^T\psi^T(s) + \psi(-s)R\psi^T(s) - \frac{\Phi^t_{g_x}(s)s^2}{(+)(-)} - s^2\frac{k^2q_2}{(+)(-)} - s\frac{\psi(-s)H\Phi^t_{\bar{\Gamma}g_x}(s)}{(+)} + s\frac{\Phi^t_{g_x\bar{\Gamma}^T}(s)H^T\psi^T(s)}{(-)} \tag{4.7}$$

where $R^{m\times m}$ is the PSD matrix of the white noise measurement error vector $(\bar{\epsilon})$. The object of this exercise is to minimize the mean-squared estimation error which may be expressed as

$$\sigma^2_{\tilde{\delta V}_x} = \frac{1}{2\pi j}\int_{-j\infty}^{j\infty} \Phi^t_{\tilde{\delta V}_x}(s)\,ds \quad . \tag{4.8}$$

For $\sigma^2_{\delta V_x}$ to be a minimum its variation due to any change in $\psi(s)$ should be positive. Substituting (4.7) into (4.8) and determining the change in $\sigma^2_{\delta V_x}$ due to a change in $\psi(s)$ gives

$$\Delta\sigma^2_{\delta V_x} = \frac{1}{2\pi j}\int_{-j\infty}^{j\infty}\Delta\psi(-s)\left\{\left[H\Phi^t_{\Gamma\Gamma^T}(s)H^T + R\right]\psi^T(s) - \frac{H\Phi^t_{\Gamma g_y}(s)s}{(+)}\right\}$$

$$+\left\{\psi(-s)\left[H\Phi^t_{\Gamma\Gamma^T}(s)H^T + R\right] + \frac{s\Phi_{g_x\bar{\Gamma}^T}(s)H^T}{(-)}\right\}\Delta\psi^T(s)$$

$$+ \Delta\psi(-s)\left[H\Phi^t_{\Gamma\Gamma^T}(s)H^T + R\right]\Delta\psi^T(s)\,ds\,. \qquad (4.9)$$

Using contour instead of line integrals to evaluate the first two terms in (4.9) yields

$$\Delta\sigma^2_{\delta V_x} = \frac{1}{2\pi j}\oint_{C_1}\Delta\psi(-s)\left\{\left[H\Phi^t_{\Gamma\Gamma^T}(s)H^T+R\right]\psi^T(s) - \frac{H\Phi^t_{\Gamma g_x}(s)s}{(+)}\right\}ds$$

$$+ \frac{1}{2\pi j}\oint_{C_2}\left\{\psi(-s)\left[H\Phi^t_{\Gamma\Gamma^T}(s)H^T+R\right] + \frac{s\Phi^t_{g_x\bar{\Gamma}^T}(s)H^T}{(-)}\right\}\Delta\psi^T(s)\,ds$$

$$+ \frac{1}{2\pi j}\int_{-j\infty}^{j\infty}\Delta\psi(-s)\left[H\Phi^t_{\Gamma\Gamma^T}(s)H^T + R\right]\Delta\psi^T(s)\,ds \qquad (4.10)$$

where the contours C_1 and C_2 are illustrated in Fig. IV-2 and enclose the left and right half complex plane respectively. With these contours it is easy to see, using the Cauchy residue theorem, that if

1) $$\left[H\Phi^t_{\Gamma\Gamma^T}(s)H^T + R\right]\psi^T(s) - \frac{H\Phi^t_{\Gamma g_x}(s)s}{(+)} \qquad (4.11)$$

has no left-half plane poles;

2) The integrands in (4.10) converge properly. (4.12)

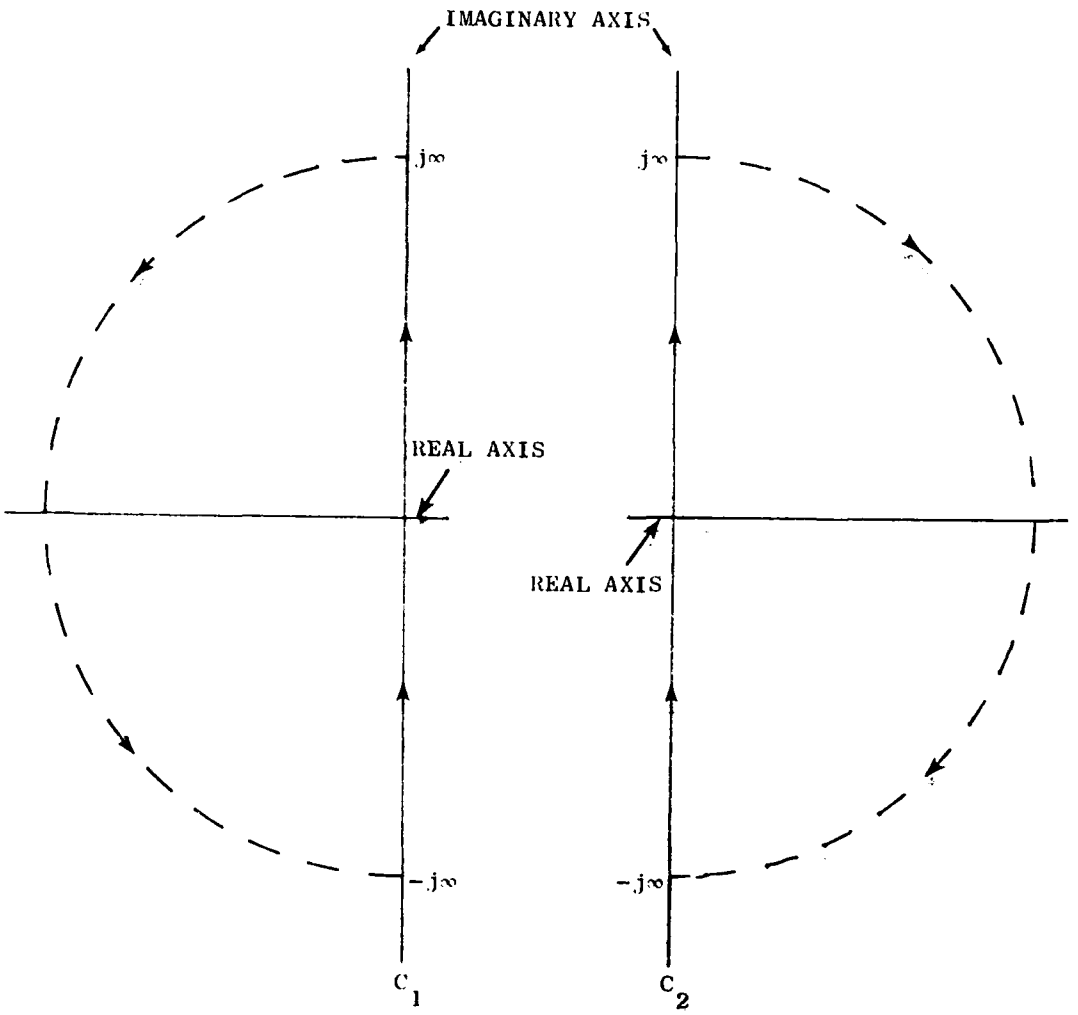

FIG. IV-2 INTEGRATION CONTOURS

Then the contributions of the contour integrals in (4.10) is zero. This means that $\Delta\sigma^2_{\tilde{\delta V}_x}$ is positive since the last integral in (4.10) is always positive and the minimization of $\sigma^2_{\tilde{\delta V}_x}$ is assured.

Note from (4.11) that the poles of $\psi(s)$ must be determined either by setting (+) = 0 or by setting

$$\left|H\Phi^t_{\underline{\Gamma}\underline{\Gamma}^T}(s)H^T + R\right| = 0 .$$

Because of the inherent sensitivity of the INS to Schuler frequency disturbances it will be assumed that the dominant poles come from the Schuler factor (+). In addition, convergence in (4.12) requires that the numerator of $\psi(s)$ be a well selected constant(s). Therefore assume

$$\underset{\psi(s)}{1\times m} = \frac{\underset{\bar{a}}{1\times m}}{(+)} . \tag{4.13}$$

As promised $\psi(s)$ is of relatively low order. The approximate nature of $\psi(s)$ comes from the "Schuler dominance" assumption which is made to determine $\bar{a}$. The idea is that due to INS Schuler sensitivity only the Schuler frequency portion of the estimate error PSD is significant in contributing to $\sigma^2_{\tilde{\delta V}_x}$. This is to say that the estimate error PSD is highly peaked at or near Schuler frequency. With this assumption condition (4.11) is enforced only at $s \cong j\omega_s^t$ to give

$$\bar{a}^T = j\omega_s\left[H\Phi^T_{\underline{\Gamma}\underline{\Gamma}^T}(j\omega_s)H^T + R\right]^{-1} H\Phi^t_{\underline{\Gamma}g_x}(j\omega_s) . \tag{4.14}$$

One way to indirectly show the optimality of the filter just derived is to prove the accuracy of the Schuler dominance assumption. This may be done by substituting (4.13) and (4.7) into (4.8) where the quadrature is performed numerically to give the rms estimate error $\sigma^{NI}_{\tilde{\delta V}_x}$. This value can then be compared to the analytically derived rms estimate error $\sigma^{AF}_{\tilde{\delta V}_x}$ obtained by assuming Schuler dominance. The degree to which $\sigma^{NI}_{\tilde{\delta V}_x}$ agrees with $\sigma^{AF}_{\tilde{\delta V}_x}$ is a direct indication of the validity

of assuming Schuler dominance and an indirect indicator of filter optimality. To derive $\sigma^{AF}_{\tilde{\delta V}_x}$ begin by writing only those parts of (4.7) which will have left-half plane poles if condition (4.11) is assumed satisfied across the frequency spectrum. Substituting (4.13) into he estimate error PSD thus obtained makes it possible to write the mean squared estimation error as

$$\sigma^2_{\tilde{\delta V}_x} = \frac{1}{2\pi j} \oint_{C_1} \left[- \frac{\Phi^t_{g_x}(s)s^2}{(+)(-)} - \frac{s^2k^2q_2}{(+)(-)} + \frac{s\Phi^t_{g_x}\bar{\Gamma}^T(s)H^{T-T}_a}{(+)\ (-)} \right] ds \ . \qquad (4.15)$$

The integral in (4.15) may easily be evaluated using the Cauchy residue theorem if the Schuler portion of the estimate error spectrum is again assumed to be dominant. Under this premise and substituting (4.14) into (4.15) the mean squared estimate error becomes

$$\sigma^2_{\tilde{\delta V}_x} = \frac{1}{2\pi j} \oint_{C_1} \frac{B\omega_s^2 + \omega_s^2k^2q_2}{(+)\ (-)} ds \qquad (4.16)$$

where B is the a posteriori gravity error spectrum defined as

$$B = \Phi^t_{g_x}(j\omega_s) - \Phi^t_{g_x}\bar{\Gamma}^T(j\omega_s)H^T\left[H\Phi^t_{\bar{\Gamma}\bar{\Gamma}^T}(j\omega_s)H^T+R\right]^{-1}H\Phi^t_{\bar{\Gamma}g_x}(j\omega_s) \ . \qquad (4.17)$$

Then the Cauchy residue evaluation of (4.16) yields

$$\sigma^2_{\tilde{\delta V}_x} = \frac{B}{2k} + \frac{kq_2}{2} \ . \qquad (4.18)$$

A-2 Including the External Velocity Measurement

Using the combination

$$V_x^c - V_x^m = \delta V_x - \nu_x^m = (s\delta R_x - \nu_x^m) \tag{4.19}$$

as a measurement,

$$\hat{\delta V}_x = \underset{1\times m}{\psi(s)} \underset{m\times 1}{\bar{z}} + \psi'(s)(s\delta R_x - \nu_x^m) \ . \tag{4.20}$$

The estimate error is then

$$\tilde{\delta V}_x(s) = \psi(s)H\bar{\Gamma} + \psi(s)\bar{\epsilon} + \Phi(s)\frac{sg_x}{(+)} - [1+\Phi(s)-\Phi(s)\frac{sk}{(+)}]\nu_x^m \tag{4.21}$$

where

$$\Phi(s) = \psi'(s) - 1 \ . \tag{4.22}$$

It follows from (4.21) that

$$\Phi^t_{\delta V_x}(s) = [\psi(-s);\Phi(-s)]\left\{[W_1]\begin{bmatrix}\psi(s)\\ \\ \Phi(s)\end{bmatrix} + \begin{bmatrix}0\\ \\ \frac{s^2+\omega_s^2}{(-)}q_2\end{bmatrix}\right\} + (1+\Phi(s)-\Phi(s)\frac{sk}{(+)})q_2 \tag{4.23}$$

where $[W_1]$ is the estimate error characteristic matrix defined as follows

$$[W_1] = \begin{bmatrix} (H\Phi^t_{\bar{\Gamma}\bar{\Gamma}^T}(s)H^T + R) & H\Phi^t_{\bar{\Gamma}g_x}(s)s/(+) \\ \\ \dfrac{-s\Phi^t_{g_x\bar{\Gamma}^T}(s)H^T}{(-)} & \dfrac{-s^2\Phi^t_{g_x}(s) + (s^2+\omega_s^2)^2 q_2}{(+)\ (-)} \end{bmatrix} . \tag{4.24}$$

From Section A-1 recall that the coefficient of $[\psi(-s);\ \phi(-s)]$ in (4.23) must have no left-half plane poles if $\sigma^2_{\delta V_x}$ is to be a minimum. For this to be true the denominators of $\psi(s)$ and $\phi(s)$ must be the left-half plane roots which result from setting the determinant of $[W_1]$ equal to zero. Anticipate that the product of these roots results in a second degree polynomial of the form

$$(+') \quad = \quad s^2 + k's + \omega_s^2 \tag{4.25}$$

where k' is a shifted value of k used in the filter. To determine the value of k' the determinant of (4.24) is set equal to zero the region where

$$s^2 + k's + \omega_s^2 \quad = \quad 0 \tag{4.26}$$

or

$$s^2 + \omega_s^2 \quad = \quad -k's \ . \tag{4.27}$$

For the determinant of $[W_1]$ to equal zero in the Schuler frequency region the following condition must hold

$$(s^2 + \omega_s^2)^2 q_2 \quad = \quad \omega_s^2 H \underline{\Phi}^t_{\bar{\Gamma} g_x}(j\omega_s)[H \underline{\Phi}^t_{\bar{\Gamma}\bar{\Gamma}^T}(j\omega_s)H^T + R]^{-1}$$

$$\times \ \underline{\Phi}^t_{g_x \bar{\Gamma}^T}(j\omega_s)H^T + \omega_s^2 \underline{\Phi}^t_{g_x}(j\omega_s) \tag{4.28}$$

where (4.28) is obtained from reference to the identity

$$\begin{bmatrix} Q_1^{-1} & 0 \\ -Q_2^T Q_1^{-1} & 1 \end{bmatrix} \begin{bmatrix} Q_1 & Q_2 \\ Q_2^T & Q_3 \end{bmatrix} \begin{bmatrix} Q_1^{-1} & -Q_1^{-1}Q_2 \\ 0 & 1 \end{bmatrix} = \begin{bmatrix} Q_1^{-1} & 0 \\ 0 & Q_3 - Q_2^T Q_1^{-1} Q_2 \end{bmatrix} \tag{4.29}$$

where Q_1, Q_2, Q_3 represent the corresponding quantities in $[W_1]$. It is clear that if the determinant of (4.29) is equal to zero then

$$Q_3 = Q_2^T Q_1^{-1} Q_2 . \tag{4.30}$$

Substituting (4.27) into (4.28) yields the following value for k'

$$k'^2 = \frac{B}{q_2} . \tag{4.31}$$

Continuing with the filter derivations, for the coefficient of $[\psi(-s); \phi(s)]$ in (4.23) to have no left-half plane poles, the (+) factors in the second column of $[W_1]$ must be cancelled by the numerator of $\phi(s)$. Therefore assume

$$\phi = -\frac{(+)}{(+')} . \tag{4.32}$$

Substituting (4.32) into (4.21) gives

$$\delta\tilde{V}_x = \psi(s)H\bar{\Gamma} + \psi(s)\bar{\epsilon} - \frac{sg_x}{(+')} - \frac{sk'\delta V_x^m}{(+')} \tag{4.33}$$

which is identical to (4.6) except that k' is substituted for k. From this point on the analysis is the same as in Sect. A-1 resulting in the following equations

$$\overset{1\times m}{\psi}(s) = \frac{\overset{1\times m}{\bar{a}}}{(+')} \tag{4.34}$$

$$\bar{a}^T = j\omega_s\left[H\Phi_{\bar{\Gamma}\bar{\Gamma}}^t{}^T(j\omega_s)H^T + R\right]^{-1} H\Phi_{\bar{\Gamma}\bar{g}_x}^t(j\omega_s) \tag{4.35}$$

and

$$\overset{1\times 1}{\psi'}(s) = \frac{(k' - k)s}{(+')} . \tag{4.36}$$

The analytic and numerically integrated estimate error expressions are also the same as those in Sect. A-1 except for the change in k. The analytic expression may be written

$$(\sigma_{\tilde{\delta V}_x}^{AF})^2 = \frac{B}{2k'} + \frac{k'q_2}{2} = \sqrt{Bq_2} \qquad (4.37)$$

Note that this is the same $(\sigma_{\tilde{\delta V}_x}^{AF})^2$ without the external velocity measurement provided that k is optimized for the mean squared estimation error.

B. POSITION ERROR ESTIMATION THEORY

In contrast to velocity error estimation, position error estimation requires that the low frequency, as well as the Schuler frequency, portion of the estimate error spectrum be considered. This is a consequence of two facts. First the high frequency content of the spatial gravity perturbation spectrum falls off quite rapidly. This is described in the Heller model as an exponential decay. This results in the error contribution from the narrow bandwidth centered at Schuler frequency becoming ever smaller, for decreasing carrier vehicle velocity, when compared to the low frequency spectral content. The second significant observation is that the gravity perturbation spectrum just described is integrated only once to give velocity error but it is integrated twice in the position case. The low frequency error contribution is therefore much more important to position error estimation. This fact is reflected in the following assumed form for the gradiometer measurement position error filters.

$$\psi(s) = \psi_s(s) + \psi_\ell(s) \qquad (4.38)$$

where the s and ℓ indicate Schuler and low frequency portions of the filter. The transfer functions $\psi_s(s)$ and $\psi_\ell(s)$ may always be determined independently of one another if certain logical assumptions are made. These assumptions, to be discussed in the next section, concern the relative size at low frequency of terms contributing to the estimate error.

B-1 Schuler Frequency Filters (In-track or Cross-Track)

As with velocity error estimation, the Schuler portion of the position estimation equations will be written in-track but are immediately applicable cross-track by changing the x subscripts to y. To estimate position error, first without the external velocity measurement, begin as in the velocity case with

$$\bar{z} = H\bar{\Gamma} + \bar{\epsilon} \tag{4.39}$$

and

$$\hat{\delta R}_x(s) = \psi(s)\bar{z} \ . \tag{4.40}$$

The estimate error and estimate error power spectral density can be written as

$$\tilde{\delta R}_x(s) = \psi(s)H\bar{\Gamma} + \psi(s)\bar{\epsilon} - \frac{g_x}{(+)} - \frac{k\delta V_x^m}{(+)} \tag{4.41}$$

and

$$\Phi_{\tilde{\delta R}_x}(s) = \psi(-s)\left[H\Phi^t_{\bar{\Gamma}\bar{\Gamma}^T}(s)H^T + R\right]\psi^T(s) + \frac{\Phi^t_{g_x}(s)}{(+)(-)} + \frac{k^2 q_2}{(+)(-)} - \frac{\psi(-s)H\Phi^t_{\bar{\Gamma}g_x}(s)}{(+)} - \frac{\Phi^t_{g_x\bar{\Gamma}^T}(s)H^T\psi^T(s)}{(-)} \ . \tag{4.42}$$

Following the same reasoning as in velocity error estimation, to minimize $\sigma^2_{\tilde{\delta R}_x}$

$$\left[H\Phi^t_{\bar{\Gamma}\bar{\Gamma}^T}(s)H^T + R\right]\psi^T(s) - \frac{H\Phi^t_{\bar{\Gamma}g_x}(s)}{(+)} \tag{4.43}$$

must have no left-half plane poles. Focusing attention now on Schuler frequency by assuming that $\psi_\ell(j\omega_s)$ is very small compared to $\psi_s(j\omega_s)$ (4.43) may be rewritten as

$$\left[H\Phi^{t}_{\underline{\underline{\Gamma}}\underline{\underline{\Gamma}}^T}(s)H^T + R\right]\psi_s(s) - \frac{H\Phi^{t}_{\underline{\Gamma}_{g_x}}(s)}{(+)} \quad . \tag{4.44}$$

The position error estimation equivalent of (4.12) dictates that the numerator of $\psi_s(s)$ be at most linear. Therefore a first-order factor is used in the numerator of $\psi_s(s)$ while the same Schuler factor is used in the denominator to yield

$$\psi_s(s) = \frac{\underset{1\times m}{\bar{b}}s + \underset{1\times m}{\bar{c}}}{(+)} \quad . \tag{4.45}$$

Substituting (4.45) into (4.44) and assuring no left-half plane poles at the roots of (+) gives

$$\left[H\Phi_{\underline{\underline{\Gamma}}\underline{\underline{\Gamma}}^T}(j\omega_s)H^T + R\right](\bar{b}^T s + \bar{c}^T)\Big|_{s=-\frac{k}{2}+j\omega_s} = H\Phi^{t}_{\underline{\Gamma}_{g_x}}(j\omega_s) \quad . \tag{4.46}$$

From (4.46) both $\bar{b}$ and $\bar{c}$ can be found.

The mean-squared estimation error comparisons are accomplished using the basic formula

$$\sigma^2_{\tilde{\delta R}_x} = \frac{1}{2\pi j}\oint \Phi^{t}_{\tilde{\delta R}_x}(s)\,ds \quad . \tag{4.47}$$

Then $\sigma^{NI}_{\tilde{\delta R}_x}$ is found by substituting (4.45) and the as yet undetermined $\psi_\ell(s)$ into (4.38). Now the complete $\psi(s)$ is used in (4.42) so that

the quadrature in (4.47) may be numerically evaluated. There are two distinct parts to the analytic formula for rms position estimation error, one from the Schuler frequency disturbances and one from the low frequency disturbances expressible as

$$\sigma^{AF}_{\tilde{\delta R}_x} = (\sigma^{AF}_{\tilde{\delta R}_x})_s + (\sigma^{AF}_{\tilde{\delta R}_x})_\ell \,. \tag{4.48}$$

These are found from substituting $\psi(s)$ into that portion of (4.42) that has left-half plane poles, after (4.43) is satisfied. Using (4.42) modified in this manner as the integrand in (4.47)

$$\sigma^2_{\tilde{\delta R}_x} = \frac{1}{2\pi j}\oint \frac{\Phi^t_{g_x}(s)}{(+)(-)} + \frac{k^2 q_2}{(+)(-)} - \frac{\Phi^t_{g_x \bar{\Gamma}^T}(s) H^T \psi^T_s(s)}{(-)}\, ds$$
$$- \frac{1}{2\pi j}\oint \frac{\Phi^t_{g_x \bar{\Gamma}^T}(s) H^T \psi^T_\ell(s)}{(-)}\, ds \tag{4.49}$$

where the first integral represents

$$(\sigma^{AF}_{\tilde{\delta R}_x})^2_s \times (2\pi j)$$

and the second

$$(\sigma^{AF}_{\tilde{\delta R}_x})^2_\ell \times (-2\pi j) \,.$$

Using (4.45) in the Cauchy residue evaluation of the first integral in (4.49) gives

$$(\sigma^{AF}_{\tilde{\delta R}_x})^2_s = \frac{B}{2k\omega_s^2} + \frac{kq_2}{2\omega_s^2} . \tag{4.50}$$

where this expression is equal to $(\sigma^{AF}_{\tilde{\delta V}_x})^2$ in (4.18) divided by ω_s^2. This is a standard form for the Schuler mean-squared estimation error. The form for the low frequency counterpart to this quantity, however, has no such standard form but varies with the number and location of low frequency poles. For this reason the quantity $(\sigma^{AF}_{\tilde{\delta R}_x})_\ell$ will be derived on an individual basis for the measurement combinations specified in Table IV-1.

The external velocity measurement may be included as a measurement by writing $\hat{\delta R}_x$ as

$$\hat{\delta R}_x = \psi(s)\bar{z} + \psi'(s)(s\delta R_x - \delta V_x^m) \tag{4.51}$$

which gives an estimate error equation of the form

$$\tilde{\delta R}_x(s) \quad \psi(s)H\bar{\Gamma} + \psi(s)\bar{\epsilon} + \frac{\Phi(s)g_x}{(+)} - \left[\frac{1+\Phi(s)}{s} - \frac{k\Phi(s)}{(+)}\right]\delta V_x^m \tag{4.52}$$

where

$$\Phi(s) \quad \psi'(s)s - 1 . \tag{4.53}$$

Writing the estimate error power spectral density for the position error in the same matrix format as was used in (4.2) yields

$$\Phi_{\delta\tilde{R}_x}(s) = \left[\psi(-s),\ \phi(-s)\right]\left\{[W_2]\begin{bmatrix}\psi(s)\\ \phi(s)\end{bmatrix} + \begin{bmatrix}0\\ -\frac{s^2+\omega_s^2}{s^2(-)}\,q_2\end{bmatrix}\right\} - \frac{1}{s}\left(\frac{1+\phi(s)}{s} - \frac{k\phi(s)}{(+)}\right)q_2 \qquad (4.54)$$

where

$$[W_2] = \begin{bmatrix} H\Phi\overline{\overline{\Gamma\Gamma}}^{T}(s)H^T + R & \dfrac{H\Phi\overline{\Gamma}g_x(s)}{(+)} \\ \dfrac{\Phi^t g_x \bar{\Gamma}^T(s)H^T}{(-)} & \dfrac{\Phi^t g_x(s)}{(+)(-)} - \dfrac{(s^2+\omega_s^2)^2}{s^2(+)(-)}\,q_2 \end{bmatrix} . \qquad (4.55)$$

Reasoning identical to that used in Sect. A-2 yields the following Schuler frequency form for $\phi(s)$:

$$\phi(s) = -\frac{(+)}{(+')} . \qquad (4.56)$$

Notice that the low frequency behavior of (4.56) gives

$$\phi(s)\Big|_{\text{small } s} \cong -1 . \qquad (4.57)$$

This results in highly desirable behavior because it minimizes the contribution of the $1 + \phi(s)/s$ term in (4.52). This term, for small s and $\phi(s) \neq -1$, might be very large even for reasonable levels of external velocity measurement noise. Therefore it will be assumed that the $\delta V_x^m/s$ term in (4.52) is large at low frequency making $\phi(s) = -[(+)/(+')]$ an ideal choice at both low and Schuler frequency.

Substituting this value for $\phi(s)$ into (4.52) yields

$$\delta\tilde{R}_x(s) = \psi(s)H\bar{\Gamma} + \psi(s)\bar{\epsilon} - \frac{g_x}{(+')} - \frac{k'\delta V_x^m}{(+')} \qquad (4.58)$$

which is identical to (4.41) except that k is replaced with k'. Therefore

$$\psi_s(s) = \frac{\bar{b}s + \bar{c}}{(+')}$$

where $\bar{b}$ and $\bar{c}$ are determined from the condition

$$\left[H\Phi^t_{\bar{\Gamma}\bar{\Gamma}^T}(j\omega_s)H^T + R\right](\bar{b}^T s + \bar{c}^T)\Big|_{s=-\frac{k'}{2}+j\omega_s} = H\Phi^t_{\bar{\Gamma}g_x}(j\omega_s) \; . \qquad (4.59)$$

The estimate error PSD is expressible as

$$\Phi_{\delta\tilde{R}_x}(s) = \psi(-s)\left[H\Phi^t_{\bar{\Gamma}\bar{\Gamma}^T}(s)H^T + R\right]\psi^T(s) + \frac{\Phi^t_{g_x}(s)}{(+')(-')} + \frac{k'^2 q_2}{(+')(-')} \qquad (4.60)$$

$$- \frac{\psi(-s)H\Phi^t_{\bar{\Gamma}g_x}(s)}{(+')} - \frac{\Phi^t_{g_x\bar{\Gamma}^T}(s)H^T\psi^T(s)}{(-')}$$

where

$$(-') = s^2 - k's + \omega_s^2 \; , \qquad (4.61)$$

and $\sigma^{AF}_{\delta\tilde{R}_x}$ and $\sigma^{NI}_{\delta\tilde{R}_x}$ are determined as previously explained except that again k' is used in place of k. The resulting Cauchy residue evaluation of $(\sigma^{AF}_{\delta\tilde{R}_x})_s$ gives

$$(\sigma^{AF}_{\delta\tilde{R}_x})^2_s = \frac{B}{2k'\omega_s^2} + \frac{k'q_2}{2\omega_s^2} = \frac{\sqrt{Bq_2}}{\omega_s^2} \; . \qquad (4.62)$$

where again this expression is related to $(\sigma^{AF}_{\delta\tilde{V}_x})^2$ in (4.37) by the factor ω_s^2.

In the next two sections the various forms for $\Psi_\ell(s)$ for the cross-track and in-track directions will be found. These filter forms will be constant whether or not the external velocity measurement is used as a measurement. This is a direct result of choosing $\Phi(s)$ as in (4.56) which gives

$$\Psi'(s)\Big|_{\text{small } s} \cong 0 . \tag{4.63}$$

Simply stated the external velocity measurement is assumed to add very little low frequency information and therefore does not change the low frequency part of the gradiometer measurement filters.

B-2 Low Frequency Filters, Cross-Track

The reason for the low frequency filter variation from cross-track to in-track is solely a manifestation of the assumed low frequency forms for $\Phi_{g_x}(s)$ and $\Phi_{g_y}(s)$ from the Heller model. The low frequency PSD (power spectral density) matrix in (3.11) transformed to a time variation is

$${}^{t}[M]^{LF}_{1-D} = \begin{bmatrix} -k_1^C s^2 & 0 & k_2^C s & 0 & -2k_3^B s \\ 0 & 2k_3^C & 0 & -6k_4^B & 0 \\ -k_2^C s & 0 & 2k_3^C & 0 & -6k_4^B \\ 0 & -6k_4^B & 0 & 24k_5^A & 0 \\ 2k_3^B & 0 & -6k_4^B & 0 & 24k_5^A \end{bmatrix} . \tag{4.64}$$

where k_j^A, k_j^B, and k_j^C are low frequency time spectral density coefficients defined as

$$k_j^A = \frac{k_j}{v_x^{(6-j)}} \tag{4.65}$$

$$k_j^B = \frac{k_j}{v_x^{(5-j)}} \tag{4.66}$$

$$k_j^C = \frac{k_j}{v_x^{(4-j)}} \tag{4.67}$$

and

$$s = j\omega_x^t \, . \tag{4.68}$$

From (4.64), $\Phi_{g_x}(s)$ and $\Phi_{g_y}(s)$ are of degree two and zero, respectively. This difference ultimately produces low frequency filters of orders two and one. This means that the results from this and the next section are applicable to any other gravity perturbation model whose low frequency behavior for $\Phi_{g_x}(s)$ and $\Phi_{g_y}(s)$ matches that given in (4.64).

The cross-track low frequency filter derivation begins by writing (4.43) for small s. Then

$$\left[H\Phi^t_{\bar{\Gamma}\bar{\Gamma}^T}(s)H^T + R\right]\Psi^T_\ell(s) - \left.\frac{H\Phi^t_{\bar{\Gamma}g_y}(s)}{s^2}\right|_{\text{small } s} \tag{4.69}$$

must have no left-half plane poles. To satisfy (4.69) it is immediately clear that the denominator of $\Psi^T_\ell(s)$ must be the left-half plane roots of

$$\left|H\Phi^t_{\bar{\Gamma}\bar{\Gamma}^T}(s)\, H^T + R\right|_{\text{small } s} = 0 \, . \tag{4.70}$$

In the cross-track direction this results in a single real root annotated

$$s = -\beta \, . \tag{4.71}$$

To assure that the low frequency peak in the estimate error spectrum dies out at the upper end of the low frequency range, the numerator of $\psi_\ell(s)$ must again be a well chosen constant(s). This is equivalent to satisfying the position error estimation equivalent of the convergence condition in (4.12), at low frequency. Therefore $\psi_\ell(s)$ has the form

$$\psi_\ell(s) = \frac{1 \underline{\times} m}{\frac{\alpha}{s + \beta}} . \tag{4.72}$$

To find α note that (4.69) must not only be without left-half plane poles but to assure convergence

$$\left\{ [H\Phi^t_{\bar{\Gamma}\bar{\Gamma}^T}(s)H^T] \frac{\bar{\alpha}^T}{s} - \frac{1}{\sigma_s^2} H\Phi^t_{\bar{\Gamma}g_y} \right\}\Bigg|_{\text{"large s"}} = 0 \tag{4.73}$$

where the quotes indicate "large s" in the low frequency range. Note also that (4.73) is applied only to the higher powers of s. It may be assumed that $\Phi^t_{\bar{\Gamma}\bar{\Gamma}^T}(s)$ has a dominant s^2 term and that $\Phi^t_{\bar{\Gamma}g_y}(s)$ has a dominant s term when estimating position error cross-track. To reduce (4.73) to one nontrivial equation using these facts, write

$$\Phi^t_{\bar{\Gamma}\bar{\Gamma}^T}(s) \underline{\times} \frac{s^2 \Phi^{t''}_{\bar{\Gamma}\bar{\Gamma}^T}(s)}{2} \tag{4.74}$$

$$\Phi^t_{\bar{\Gamma}g_y}(s) \underline{\times} s\Phi^{t'}_{\bar{\Gamma}g_y}(s) \tag{4.75}$$

where the primes indicate differentiation with respect to s. Note that (4.74) and (4.75) only hold for the highest powers of s. Substituting (4.74) and (4.75) into (4.73) yields

$$\frac{1}{2}\, H\Phi^{t''}_{\bar{\Gamma}\bar{\Gamma}^T}(s) H^T \bar{\alpha}^T = \frac{1}{\omega_s^2}\, H\Phi^{t'}_{\bar{\Gamma} g_y}(s)\Big|_{\text{"large s"}} . \tag{4.76}$$

From (4.76) one component of $\bar{\alpha}$ may be found. The other components may be found by enforcing (4.69) at the low frequency pole. This relationship is

$$\left[H\Phi^{t}_{\bar{\Gamma}\bar{\Gamma}^T}(s)\, H^T + R \right] \bar{\alpha}^T \Big|_{s=-\beta} = 0 . \tag{4.77}$$

Recall that to calculate $(\sigma^{AF}_{\delta R_x})_\ell$ this last integral in (4.49) must be evaluated. Using the Cauchy residue theorem to perform this quadrature gives no standardized form as was the case for $(\sigma^{AF}_{\delta R_x})_s$, primarily because $\Phi_{g_x \bar{\Gamma}^T}(s)$ is a function of s at low frequency. Because of this and the nontrivial nature of the low frequency filter constant determinations, detailed derivations for the in-track and cross-track low frequency filter constants are given in App. C. These derivations apply to measurement combinations listed in Table IV-1 and include the resulting detailed formulas for $(\sigma^{AF}_{\delta R_x})_\ell$.

B-3 Low Frequency Filters, In-Track

The denominators of the in-track filters are again found from (4.70). For the assumed second degree form of $\Phi_{g_x}(s)$, however, the left-half plane roots, after some approximations explained in App. C, turn out to be a complex conjugate pair expressed as the factor $(\ell+)$. The exact location of these poles vary with the exact measurement combination used and are given in App. C. The low frequency filters can be written as

$$\psi_\ell(s) = \frac{{}^{1\times m}\bar{d}s + {}^{1\times m}\bar{e}}{(\ell+)} \tag{4.78}$$

where the first-order numerator satisfies convergence at low frequency while ensuring sufficient estimation accuracy. The convergence and low frequency pole conditions (Sect. B-2) are used to find $\bar{d}$ and $\bar{e}$. These conditions are stated below for the in-track direction

$$\left\{\left[H\Phi^{t}_{\bar{\bar{\Gamma}}\bar{\bar{\Gamma}}^T}(s)H^T\right]\frac{\bar{d}^T s + \bar{e}^T}{(\ell+)} - \frac{1}{{}^{(n)}_{s}}\, H\Phi^{t}_{\bar{\Gamma}g_x}(s)\right\}\Big|_{u_{\text{large } s^n}} = 0\,, \tag{4.79}$$

and

$$\left[H\Phi^{t}_{\bar{\bar{\Gamma}}\bar{\bar{\Gamma}}^T}(s)H^T + R\right](\bar{d}^T s + \bar{e}^T)\Big|_{\substack{s=\text{roots}\\ \text{of } (\ell+)}} = 0\,. \tag{4.80}$$

The details of finding $\bar{d}$ and $\bar{e}$ are again peculiar to the particular measurement combination considered.

C. LOW FREQUENCY FILTER RESULTS

The results from the low frequency filter derivations in App. C are given in Tables IV-2 and IV-3.

Table IV-2
LOW FREQUENCY FILTER RESULTS
(CROSS-TRACK MEASUREMENT COMBINATIONS)

	CROSS-TRACK 1	CROSS-TRACK 2
$\bar{z} - \bar{\epsilon}$	$[\Gamma_{xy}]$	$\begin{bmatrix} \Gamma_{xy} \\ \Gamma_{yz} \end{bmatrix}$
H	$[0 \quad 1 \quad 0 \quad 0 \quad 0]$	$\begin{bmatrix} 0 & 1 & 0 & 0 & 0 \\ 0 & 0 & 0 & 1 & 0 \end{bmatrix}$
R	r_1	$\begin{bmatrix} r_1 & 0 \\ 0 & r_2 \end{bmatrix}$
ρ	$\left(\frac{r_1}{2k_3^A}\right)^{\frac{1}{2}}$	$\left[\frac{r_1(r_2 + 24k_5^A)}{(48k_3^A k_5^A - 36(k_4^A)^2 + 2k_3^A r_2)}\right]^{\frac{1}{2}}$
$\bar{\alpha}$	$\frac{V_x}{\omega_s^2}$	$\left[\frac{V_x}{\omega_s^2}; - \frac{6k_4^A \rho V_x}{\omega_s^2(24k_5^A + r_2)}\right]$
$\left(\sigma^{AF}_{\dot{R}_y}\right)^2_{\ell}$	$\frac{2k_3^B \alpha \rho}{\omega_s^2}$	$\frac{2k_3^B \alpha_1 \rho + 6k_4^B \alpha_2}{\omega_s^2}$

These measurement combinations assume the state vector defined in (4.1)

Table IV-3
LOW FREQUENCY FILTER RESULTS
(IN-TRACK MEASUREMENT COMBINATIONS)

	IN-TRACK 1	IN-TRACK 2	IN-TRACK 3
$\bar{z} - \bar{\epsilon}$	(Γ_{xx})	$\left[\Gamma_{xx} + \frac{1}{2}\Gamma_{zz}\right]$	$\begin{bmatrix} \Gamma_{xx} + \frac{1}{2}\Gamma_{zz} \\ \frac{1}{2}\Gamma_{xx} + \Gamma_{zz} \end{bmatrix}$
H	$[1\ 0\ 0\ 0\ 0]$	$[1\ 0\ 0\ 0\ \frac{1}{2}]$	$\begin{bmatrix} 1 & 0 & 0 & 0 & \frac{1}{2} \\ \frac{1}{2} & 0 & 0 & 0 & 1 \end{bmatrix}$
R	r_1	r_1	$\begin{bmatrix} r_1 & 0 \\ 0 & r_2 \end{bmatrix}$
L	$\left(\frac{4k_1^A}{r_1}\right)^{\frac{1}{4}}$	--	$\left(\frac{4\left(\frac{27}{2}k_1^A k_5^A + \frac{3}{2}(k_3^A)^2 + \frac{5}{4}k_1^A r_1\right)}{(30k_5^A + r_1)r_1}\right)^{\frac{1}{4}}$
$\bar{d}$	$\frac{V_x}{\omega_s^2}$	$\frac{V_x}{\omega_s}$	$\left(\frac{4V_x}{3\omega_s^2}\ ;\ -\frac{2V_x}{3\omega_s^2}\right)$
$\bar{e}$	$\frac{2V_x}{L\omega_s^2}$	$\frac{2\omega_N\delta_1 V_x}{\omega_s^2}$	$\left(\frac{8V_x}{3L\omega_s^2}\ ;\ -\frac{4V_x}{3L\omega_s^2}\right)$
$\left(\sigma^{AF}_{\delta\tilde{R}_x}\right)^2_\ell$	$\frac{2k_1^B e}{\omega_s^2 L^2}$	$-k_1^B d\ell^3[2\delta_1^3 - 2\delta_1\delta_2^2 + 2\delta_1(\delta_1^2 - \delta_2^2)]$ $+ k_1^B e\ell^2[2\delta_1^2 + (\delta_1^2 - \delta_2^2)]$ $- 2k_3^B d\ell\,\delta_1 + k_3^B e/\omega_s^2$	$\frac{2}{\omega_s^2}\left(\frac{A_2}{L^2} - \frac{A_3}{L}\right)$

These measurement combinations assume the state vector defined in (4.1)

Note that to obtain the total analytic position error variance formula for any of the combinations in these tables (4.50) or (4.62) should be added to the appropriate formula for $(\sigma^{AF}_{\tilde{\delta}R_x\,\ell})^2$.

Chapter V

REAL TIME FILTER COVARIANCE STUDY

A. COVARIANCE COMPARISONS OF KALMAN VS APPROXIMATE FILTERS FOR THE CROSS-TRACK DIRECTION

In this section the second-order gravity model is used in a standard Kalman covariance analysis. A comparison is then made with the covariance results obtained from the previously derived approximate filters. The cross-track direction is chosen because the low frequency behavior of the second-order model is similar to that of the Heller model $\Phi^t_{g_y}(s)$ The cross-track gravity perturbation power spectral density from the second-order model is

$$\Phi^t_{g_y}(s) = \frac{q_1}{(s^2 - \beta^2)^2} \cdot \tag{5.1}$$

From this rational expression it follows that

$$\Phi^t_{\Gamma_{xy} g_y}(s) = -\frac{s}{V_x} \times \left(\frac{q_1}{(s^2 - \beta^2)^2} \right) \cdot \tag{5.2}$$

$$\Phi^t_{\Gamma_{xy} \Gamma_{xy}}(s) = -\frac{s^2}{V_x^2} \times \left(\frac{q_1}{(s^2 - \beta^2)^2} \right) \cdot \tag{5.3}$$

The Kalman state space representation is obtained by combining (2.6), (2.8) and (3.3) as follows:

$$\underset{\dot{X}}{\begin{bmatrix} \dot{x}_1 \\ \dot{g}_y \\ \delta\dot{V}_y \\ \delta\dot{R}_y \end{bmatrix}} = \underset{F}{\begin{bmatrix} -\beta & 0 & 0 & 0 \\ 1 & -\beta & 0 & 0 \\ 0 & 1 & -k & -\omega_s^2 \\ 0 & 0 & 1 & 0 \end{bmatrix}} \underset{X}{\begin{bmatrix} x_1 \\ g_y \\ \delta V_y \\ \delta R_y \end{bmatrix}} + \underset{G}{\begin{bmatrix} 1 & 0 \\ 0 & 0 \\ 0 & k \\ 0 & 0 \end{bmatrix}} \underset{\bar{w}}{\begin{bmatrix} w_1 \\ -\delta V_y^m \end{bmatrix}} \qquad (5.4)$$

where

X = state vector

F = state transition matrix

G = process noise transition matrix

$\bar{w}$ = process noise vector .

The measurement is assumed to be

$$\bar{z} = \underset{H}{} \quad \underset{X}{} + \bar{\epsilon}$$

$$\bar{z} = \begin{bmatrix} 1 & -\beta & 0 & 0 \end{bmatrix} \begin{bmatrix} x_1 \\ g_y \\ \delta V_y \\ \delta R_y \end{bmatrix} + \eta V_x \qquad (5.5)$$

where η is the gradiometer error. If the external velocity measurement is included

$$\bar{z} = \begin{bmatrix} 1 & -\beta & 0 & 0 \\ 0 & 0 & 1 & 0 \end{bmatrix} \begin{bmatrix} x_1 \\ g_y \\ \delta V_y \\ \delta R_y \end{bmatrix} + \begin{bmatrix} \eta V_x \\ -\delta V_y^m \end{bmatrix} . \qquad (5.6)$$

The first measurement, here, is obviously $\dot{g}_y$ which can be written

$$\dot{g}_y = \Gamma_{xy} V_x \tag{5.7}$$

which comes from the following identity

$$\bar{\bar{\Gamma}} \cdot \bar{V} = \begin{bmatrix} \dot{g}_x \\ \dot{g}_y \\ \dot{g}_z \end{bmatrix} = \begin{bmatrix} \Gamma_{xx} V_x \\ \Gamma_{xy} V_x \\ \Gamma_{xz} V_x \end{bmatrix} \Bigg|_{V_y = V_z = 0} . \tag{5.8}$$

Comparison of the measurement noise in (5.6) and the process noise in (5.4) shows that the two are correlated. The standard Kalman filter covariance analysis can still be made by deriving an equivalent system described by Bryson and Ho [Ref. 16, pp. 371 and 402-404] where the process and measurement noises are not correlated. The general form for the equivalent system is

$$\dot{\bar{X}} = F'\bar{X} + G'\bar{w}' + D\bar{z} \tag{5.9}$$

where

$$D = GT^T R^{-1} \quad \text{(so that the noise in (5.9) is uncorrelated with } \bar{\epsilon}) \tag{5.10}$$

$$F' = F - DH \tag{5.11}$$

$$G' = \Gamma, -D \tag{5.12}$$

$$\bar{w}' = \begin{bmatrix} \bar{w} \\ \bar{\epsilon} \end{bmatrix} \tag{5.13}$$

$$T\delta(t - \tau) = E[\bar{\epsilon}(t)\, \bar{w}^T(\tau)] \tag{5.14}$$

The specific form for these equations using the unaltered measurements given in (5.6) is

$$D = \begin{bmatrix} 0 & 0 \\ 0 & 0 \\ 0 & k \\ 0 & 0 \end{bmatrix} \tag{5.15}$$

$$T = \begin{bmatrix} 0 & 0 \\ 0 & q_2 \end{bmatrix} \tag{5.16}$$

$$F' = \begin{bmatrix} -\beta & 0 & 0 & 0 \\ 1 & -\beta & 0 & 0 \\ 0 & 1 & 0 & -\omega_s^2 \\ 0 & 0 & 1 & 0 \end{bmatrix} \tag{5.17}$$

$$G' = \begin{bmatrix} 1 & 0 & 0 & 0 \\ 0 & 0 & 0 & 0 \\ 0 & k & 0 & -k \\ 0 & 0 & 0 & 0 \end{bmatrix} \tag{5.18}$$

$$\tilde{w}' = \begin{bmatrix} w_1 \\ -\delta V_y^m \\ \eta V_x \\ -\delta V_y^m \end{bmatrix} \tag{5.19}$$

Equation (5.7) shows that using Γ_{xy} as a measurement is equivalent to the use of $\dot{g}_y$. This means that the covariance results obtained by slightly modifying the CT-1 formulas in Chapter IV can be compared with the covariance results from the foregoing Kalman configuration. Because the low frequency behavior of $\Phi_{g_y}(s)$ is different for the second-order model (SOM) and Heller model (HM) as follows:

$$\Phi^{t^{HM}}_{g_y}(s)\Big|_{\text{small } s} = 2k_3^C \tag{5.20}$$

$$\Phi^{t^{SOM}}_{g_y}(s)\Big|_{\text{small } s} = \frac{q_1}{\beta^4} \ . \tag{5.21}$$

the low frequency root from (4.70) is

$$\beta = \left(\frac{V_x^2\beta^4 r_1}{q_1}\right)^{\frac{1}{2}} \tag{5.22}$$

The value of α found by substituting (5.2) and (5.3) into (4.76) is

$$\alpha = \frac{V_x}{\omega_s^2} \ . \tag{5.23}$$

The analytic low frequency variance formula is altered to give

$$\left(\sigma^{AF}_{\delta\tilde{R}_y}\right)^2_{\ell} = \frac{q_1\alpha\beta}{\beta^4 V_x \omega_s^2} \ . \tag{5.24}$$

The previous results for the determination of $\bar{a}$, $\bar{b}$, and $\bar{c}$ remain unaltered as do the variance formulas except that the spectra in (5.1), (5.2),

and (5.3) are used in place of those from the Heller model.

There are primarily three questions to be answered concerning the real time approximate filters: (1) How optimal are the approximate filters? (2) Over what range of carrier vehicle velocities can these filters be used? (3) What measurement combination produces the most accurate estimates of position and velocity error? Tables V-1 through V-4 seek to answer the first two questions by comparing the Kalman filter rms estimate errors with these same quantities resulting from use of the approximate filters. The assumed second-order model and inertial navigation system quantitative characteristics, taken from Heller [10] are as follows:

$$\delta V_y^m : \text{0.2 percent of } V_x \text{ - band limited white noise with a two second correlation time.} \tag{5.25}$$

$$\sigma_{g_y}^2 = 1.4466 \times 10^{-7} \quad m^2/sec^4 \tag{5.26}$$

$$k = 7.5 \times 10^{-5} \quad 1/sec\ . \tag{5.27}$$

Because the Bell and Draper gradiometers are accurate to approximately 1 Eötvos, this would seem a realistic value to use and, in fact, all of the results in this research assume a gradiometer with this accuracy. In addition, the gradiometer is assumed to have a 10 sec averaging time. This determines the gradiometer measurement error power spectral density necessary for computation of the Kalman filter.

Looking at Tables V-1 to V-4 the most important results appear in the rms estimate error columns. As explained earlier the dominance assumptions made in the filter derivations may be directly checked (which indirectly checks optimality) by comparing the analytically and numerically obtained rms estimate error values. The last two columns of each Table contain these numbers. A comparison of these values shows that nowhere do they differ by more than 6% and routinely differ by less than 1%. A direct check of optimality may be done by comparing the Kalman filter estimate error results in column 2 with the numerically integrated values in the last column. The fact that these values also agree to at least 6%

and routinely to less than 1% provides direct confirmation of approximate filter optimality.

Although the data in these Tables look very promising it must be remembered that a rational second-order model was used. The primary purpose of Tables V-1 through V-4 is to show that confirmation of the dominance assumptions made in the approximate filter derivation coincides with a near optimal filter. From this point on then, confirmation of these dominance assumptions will be considered sufficient proof of near optimality since direct Kalman comparisons are impossible when the Heller Model is used in the next section.

Table V-1

VELOCITY ESTIMATION COVARIANCE
COMPARISON (E/EVM)*: KALMAN VS APPROXIMATE

KF = Kalman Filter, AF = Analytic Formula, NI = Numerically Integrated

Carrier Velocity (m/sec)	Kalman Filter Results $\sigma^{KF}_{\delta V_y}$ (mm/sec)	Approximate Filter Results $\bar{a}$ (m/sec)	$\sigma^{AF}_{\delta V_y}$ (mm/sec)	$\sigma^{NI}_{\delta V_y}$ (mm/sec)
0.5144	0.1079	0.514	0.1079	0.1066
5.144	1.079	5.14	1.079	1.076
51.44	10.79	51.4	10.78	10.77
514.4	103.38	472.4	103.43	103.16

* Excluding the external velocity measurement (EVM)

Table V-2

VELOCITY ERROR ESTIMATION COVARIANCE
COMPARISON (I/EVM)*: KALMAN VS APPROXIMATE

Carrier Velocity (m/sec)	Kalman Filter Results $\sigma^{KF}_{\delta V_y}$ (mm/sec)	Approximate Filter Results $\bar{a}$ (m/sec)	k' (1/sec)	$\sigma^{AF}_{\delta V_y}$ (m/sec)	$\sigma^{NI}_{\delta V_y}$ (mm/sec)
0.5144	0.0511	0.514	$6.376^{\backslash -4}$	0.0519	0.0443
5.144	0.5118	5.14	$6.376^{\backslash -4}$	0.5196	0.4807
51.44	5.118	51.4	$6.376^{\backslash -4}$	5.196	4.88
514.4	50.06	472.4	$6.11^{\backslash -4}$	50.86	47.71

*I/EVM = Including the external velocity measurement

Table V-3

POSITION ERROR ESTIMATION COVARIANCE
COMPARISON (E/EVM): KALMAN VS APPROXIMATE

KF = Kalman Filter, AF = Analytic Formula, NI = Numerically Integrated

Carrier Velocity (m/sec)	Kalman Filter Results $\sigma^{KF}_{\delta V_y}$ (mm/sec)	Approximate Filter Results $\bar{b}$ (m-sec)	$\bar{c}$ (m)	$\bar{\alpha}$ (m-sec)	$\sigma^{AF}_{\delta R_y}$ (m)	$\sigma^{NI}_{\delta R_y}$ (m)
0.5144	9.79	$-3.35\backslash^{5}$	$-2.51\backslash^{1}$	$3.35\backslash^{5}$	9.79	9.79
5.144	17.4	$-3.35\backslash^{6}$	$-2.51\backslash^{2}$	$3.35\backslash^{6}$	17.44	17.43
51.44	32.04	$-3.35\backslash^{7}$	$-2.51\backslash^{3}$	$3.35\backslash^{7}$	32.17	32.11
514.4	96.95	$03.074\backslash^{8}$	$-2.12\backslash^{4}$	$3.35\backslash^{8}$	99.87	97.82

Table V-4

POSITION ERROR ESTIMATION COVARIANCE
COMPARISON (I/EVM): KALMAN VS APPROXIMATE

Carrier Velocity (m/sec)	Kalman Filter Results $\sigma^{KF}_{\delta R_y}$ (m)	Approximate Filter Results $\bar{b}$ (m-sec)	$\bar{c}$ (m)	$\bar{\alpha}$ (m-sec)	k' (1/sec)	$\sigma^{AF}_{\delta R_y}$ (m)	$\sigma^{NI}_{\delta R_y}$ (m)
0.5144	9.23	$-2.646\backslash^{5}$	$-1.68\backslash^{2}$	$2.646\backslash^{5}$	$6.376\backslash^{-4}$	9.238	9.231
5.144	16.41	$-2.646\backslash^{6}$	$-1.687\backslash^{3}$	$2.646\backslash^{6}$	$6.376\backslash^{-4}$	16.43	16.42
51.44	29.31	$-2.646\backslash^{7}$	$-1.687\backslash^{4}$	$2.646\backslash^{7}$	$6.376\backslash^{-4}$	29.45	29.39
514.4	59.98	$-2.476\backslash^{8}$	$-1.389\backslash^{5}$	$2.646\backslash^{8}$	$6.11\backslash^{-4}$	63.47	61.61

B. SINGLE GRADIOMETER MEASUREMENT ANALYTIC VS NUMERICAL COVARIANCE COMPARISONS

The next step in proving the accuracy of the approximate filters is to show their near optimality when the more realistic Heller model is used. This is done by making the same type of comparisons as in Sect. A but with the following changes: (1) The Kalman covariance is excluded; (2) The exact formulas for Ch. IV are used. (3) The IT-1 measurement combination is included. The impetus to improve the Heller model came from studies done in this section. Therefore all the comparisons in Tables V-5 to V-12 were done assuming the BHM (Baseline Heller Model). In addition these data also assume the EVM (external velocity measurement) noise and the value of k as defined in Sect. A.

The primary focus in Tables V-5 through V-12 is the agreement of the rms estimate error values in the last two columns of each Table. As with the preceding Tables in this Chapter these numbers agree to within 6% for both velocity and position error, with the exception of the lowest velocity case, in all of the velocity error Tables. This is due to the fact that the low frequency portion, as assumed, of the estimate error power spectral density (PSD) is dominant. The exponential decrease in the Heller gravity perturbation spectrum results in very small gravity perturbation PSD values at the short spatial wavelengths corresponding to Schuler frequency at low speed which in turn causes the low frequency dominance. In order for the velocity filters to be meaningful at low velocities some form of low frequency compensation would have to be included.

By comparing the data which includes and excludes the external velocity measurement, it is possible to determine the impact of using this potential data source. The rms estimate error values in Table V-7 vs Table V-8 and Table V-11 vs Table V-12 show that the external velocity measurement contributes little to enhance position error estimation. Conversely Table V-5 vs Table V-6 and Table V-9 vs Table V-10 demonstrate that an average increase in accuracy of 50% is possible for velocity error estimation.

Table V-5

IN-TRACK VELOCITY ERROR ESTIMATION COVARIANCE
COMPARISON (E/EVM): ANALYTIC VS NUMERICAL
AF = Analytic Formula, NI = Numerically Integrated

Carrier Velocity (m/sec)	$\bar{a}$ (m/sec)	$\sigma^{AF}_{\tilde{\delta V}_x}$ (mm/sec)	$\sigma^{NI}_{\tilde{\delta V}_x}$ (mm/sec)
0.5144	$1.985\backslash^{-21}$	0.0126	7.098
5.144	5.144	1.078	1.078
51.44	51.43	10.78	10.78
514.4	470.0	103.16	102.89

Table V-6

IN-TRACK VELOCITY ERROR ESTIMATION COVARIANCE
COMPARISON (I/EVM): ANALYTIC VS NUMERICAL

Carrier Velocity (m/sec)	$\bar{a}$ (m/sec)	k' (1/sec)	$\sigma^{AF}_{\tilde{\delta V}_x}$ (mm/sec)	$\sigma^{NI}_{\tilde{\delta V}_x}$ (mm/sec)
0.5144	$1.985\backslash^{-21}$	$3.96\backslash^{-14}$	$4.1\backslash^{-7}$	7.098
5.144	5.144	$6.376\backslash^{-4}$	0.5196	0.493
51.44	51.43	$6.376\backslash^{-4}$	5.195	4.93
514.4	470.0	$6.095\backslash^{-4}$	50.8	47.62

Table V-7

IN-TRACK POSITION ERROR ESTIMATION COVARIANCE COMPARISON (E/EVM): ANALYTIC VS NUMERICAL

Carrier Velocity (m/sec)	$\bar{b}$ (m-sec)	$\bar{c}$ (m)	$\bar{d}$ (m-sec)	$\bar{e}$ (m)	$\sigma^{AF}_{\delta R_x}$ (m)	$\sigma^{NI}_{\delta R_x}$ (m)
0.5144	$-1.292\backslash-15$	$-3.739\backslash-40$	$3.347\backslash5$	$4.379\backslash-2$	4.137	4.09
5.144	$-3.347\backslash6$	$-2.51\backslash2$	$3.347\backslash6$	7.788	9.849	9.528
51.44	$-3.346\backslash7$	$-2.51\backslash3$	$3.347\backslash7$	$1.385\backslash3$	24.83	23.72
514.4	$-3.058\backslash8$	$-2.096\backslash4$	$3.347\backslash8$	$2.463\backslash5$	99.74	97.15

Table V-8

IN-TRACK POSITION ERROR ESTIMATION COVARIANCE COMPARISON (I/EVM): ANALYTIC VS NUMERICAL

Carrier Velocity (m/sec)	$\bar{b}$ (m-sec)	$\bar{c}$ (m)	$\bar{d}$ (m-sec)	$\bar{e}$ (m)	k' (1/sec)	$\sigma_{\tilde{R}_x}^{AF}$ (m)	$\sigma_{\tilde{R}_x}^{NI}$ (m)
0.5144	$-1.021\backslash-15$	$-1.56\backslash-49$	$2.647\backslash5$	$3.266\backslash-2$	$3.961\backslash-14$	3.79	3.73
5.144	$-2.646\backslash6$	$-1.688\backslash3$	$2.647\backslash6$	5.808	$6.376\backslash-4$	8.988	8.71
51.44	$-2.646\backslash7$	$-1.687\backslash4$	$2.647\backslash7$	$1.033\backslash3$	$6.376\backslash-4$	21.47	20.58
514.4	$-2.646\backslash8$	$-1.373\backslash5$	$2.647\backslash8$	$1.837\backslash5$	$6.095\backslash-4$	56.71	58.76

Table V-9

CROSS-TRACK VELOCITY ERROR ESTIMATION COVARIANCE
COMPARISON (E/EVM): ANALYTIC VS NUMERICAL

Carrier Velocity (m/sec)	$\bar{a}$ (m/sec)	$\sigma^{AF}_{\tilde{\delta V}_y}$ (mm/sec)	$\sigma^{NI}_{\tilde{\delta V}_y}$ (mm/sec)
0.5144	$2.257\backslash^{-23}$	0.0126	4.088
5.144	5.143	1.079	1.077
51.44	$5.142\backslash^{1}$	10.78	10.77
514.4	$4.926\backslash^{2}$	105.58	105.53

Table V-10

CROSS-TRACK VELOCITY ERROR ESTIMATION COVARIANCE
COMPARISON (I/EVM): ANALYTIC VS NUMERICAL

Carrier Velocity (m/sec)	$\bar{a}$ (m/sec)	k' (1/sec)	$\sigma^{AF}_{\tilde{\delta V}_y}$ (mm/sec)	$\sigma^{NI}_{\tilde{\delta V}_y}$ (mm/sec)
0.5144	$2.575\backslash^{-23}$	$4.51\backslash^{-15}$	$1.382\backslash^{-7}$	4.089
5.144	5.143	$6.376\backslash^{-4}$	0.519	0.493
51.44	$5.142\backslash^{1}$	$6.376\backslash^{-4}$	5.195	4.965
514.4	$4.926\backslash^{2}$	$6.24\backslash^{-4}$	51.39	50.98

Table V-11

CROSS-TRACK POSITION ERROR ESTIMATION COVARIANCE COMPARISON (E/EVM): ANALYTIC VS NUMERICAL

AF = Analytic Formula, NI = Numerically Integrated

Carrier Velocity (m/sec)	$\bar{b}$ (m-sec)	$\bar{c}$ (m)	$\bar{\alpha}$ (m-sec)	$\sigma^{AF}_{\delta R_y}$ (m)	$\sigma^{NI}_{\delta R_y}$ (m)
0.5144	$-1.675\backslash^{17}$	$-6.291\backslash^{-44}$	$3.347\backslash^{5}$	12.625	12.618
5.144	$-3.346\backslash^{6}$	$-2.51\backslash^{2}$	$3.347\backslash^{6}$	22.47	22.4
51.44	$-3.345\backslash^{7}$	$-2.51\backslash^{3}$	$3.347\backslash^{7}$	40.85	40.52
514.4	$-3.205\backslash^{8}$	$-2.30\backslash^{4}$	$3.347\backslash^{8}$	110.76	108.96

Table V-12

CROSS-TRACK POSITION ERROR ESTIMATION COVARIANCE COMPARISON (I/EVM): ANALYTIC VS NUMERICAL

Carrier Velocity (m/sec)	$\bar{b}$ (m-sec)	$\bar{c}$ (m)	$\bar{\alpha}$ (m-sec)	k' (1/sec)	$\sigma^{AF}_{\delta\tilde{R}_y}$ (m)	$\sigma^{NI}_{\delta\tilde{R}_y}$ (m)
0.5144	$-1.325\backslash^{-17}$	$-2.993\backslash^{-54}$	$2.647\backslash^{5}$	$4.512\backslash^{-15}$	11.9	11.89
5.144	$-2.646\backslash^{6}$	$-1.687\backslash^{3}$	$2.647\backslash^{6}$	$6.376\backslash^{-4}$	21.17	21.12
51.44	$-2.646\backslash^{7}$	$-1.646\backslash^{7}$	$2.647\backslash^{7}$	$6.376\backslash^{-4}$	37.83	37.54
514.4	$-2.560\backslash^{8}$	$-1.529\backslash^{5}$	$2.647\backslash^{8}$	$6.240\backslash^{-4}$	76.42	74.77

The IHM (improved Heller Model) was developed after noting the excessively long characteristic settling times associated with the low frequency filter poles for some of the cases studied in this section. To best see this problem, Table V-13 catalogs these settling times for the CT-1 and IT-1 (cross-track and in-track) measurement combinations.

Table 13

LOW FREQUENCY POLE CHARACTERISTIC SETTLING TIMES FOR THE BHM*

Carrier Velocity (m/s)	CT-1 Settling Time (days) (1/β)	IT-1 Settling Time (days) (1/L)
0.5144	1647	176.9
5.144	52.1	9.95
51.44	1.647	0.56
514.4	0.052	0.0315

* BHM = Baseline Heller Model

Note the settling time of 1.647 days even at 51.44 m/sec.

The most desirable way to deal with this problem is to update the low frequency knowledge of the gravity field thus reducing the low frequency residual in the Heller gravity perturbation model. This is precisely what was done in Ch. II to obtain the IHM. The updated characteristic times for the IHM are shown, along with the values for the BHM in Table V-14.

Table V-14

LOW FREQUENCY POLE CHARACTERISTIC SETTLING TIMES FOR THE IHM

Carrier Velocity (m/sec)	CT-1 Settling Time (days) (1/β)	IT-1 Settling Time (days) (1/L)
0.5144	1157.74 (1647)*	106.995 (176.9)*
5.144	36.612 (52.1)	6.017 (9.95)
51.44	1.158 (1.647)	0.338 (0.56)
514.4	0.037 (0.052)	0.019 (0.0315)

*numbers in parentheses indicate BHM values

There is some improvement shown in Table V-14 but in the low velocity cases the times are still inordinately long.

C. LOW FREQUENCY POLE PLACEMENT TECHNIQUE

There is another way to decrease the settling times but it is less advantageous because acceptable filter performance is balanced against estimation accuracy. This simply involves moving the low frequency poles to the left on the negative real axis to a point where the time response is acceptable. These new pole locations are nonoptimal, thus degrading estimation accuracy. The hope is that estimation accuracy sensitivity to low frequency pole movement is small. Table V-15 shows this relationship for a velocity of 51.44 m/sec only. The results for 5.144 m/sec and below indicate that the extreme root relocation necessary to give acceptable low frequency behavior produces an unacceptable degradation in estimation accuracy. At very high carrier velocities the low frequency settling times are already on the order of hours or even minutes and do not require severe adjustment.

TABLE V-15

SUBOPTIMAL VS APPROXIMATELY OPTIMAL TIME CONSTANTS AND ESTIMATION ACCURACIES FOR V_x = 51.44 m/sec

TC = time constant AO = approximately optimal SO = suboptimal

Measurement Combination	TC_{ℓ}^{AO} (hours)	TC_{ℓ}^{SO} (hours)	$\sigma_{\tilde{\delta}R}^{AO}$ (m)	$\sigma_{\tilde{\delta}R}^{SO}$ (m)
IT-1 (E/EVM)	8.12	0.812	19.1	70.92
IT-1 (I/EVM)	8.12	0.812	16.04	16.4
CT-1 (E/EVM)	27.79	0.2779	34.38	68.91
CT-1 (I/EVM)	27.79	0.2779	31.60	35.85

This Table uses the IHM

Note that for the cases where the EVM is excluded the estimation accuracy is degraded by a factor of 2 to 3. When the EVM is included the degradation is at most 20% and may be as small as a few percent. Therefore pole shifting may be a reasonable way to hasten filter convergence particularly if the EVM is included as a filter input.

Another way to see the effect of the pole shifts is to look at plots of the estimate error PSDs (power spectral densities) for approximately optimal and suboptimal pole locations. Figure V-1 shows these PSDs for the IT-1 measurement combination excluding the EVM assuming a carrier velocity of 51.44 m/sec. The low frequency suboptimal PSD is

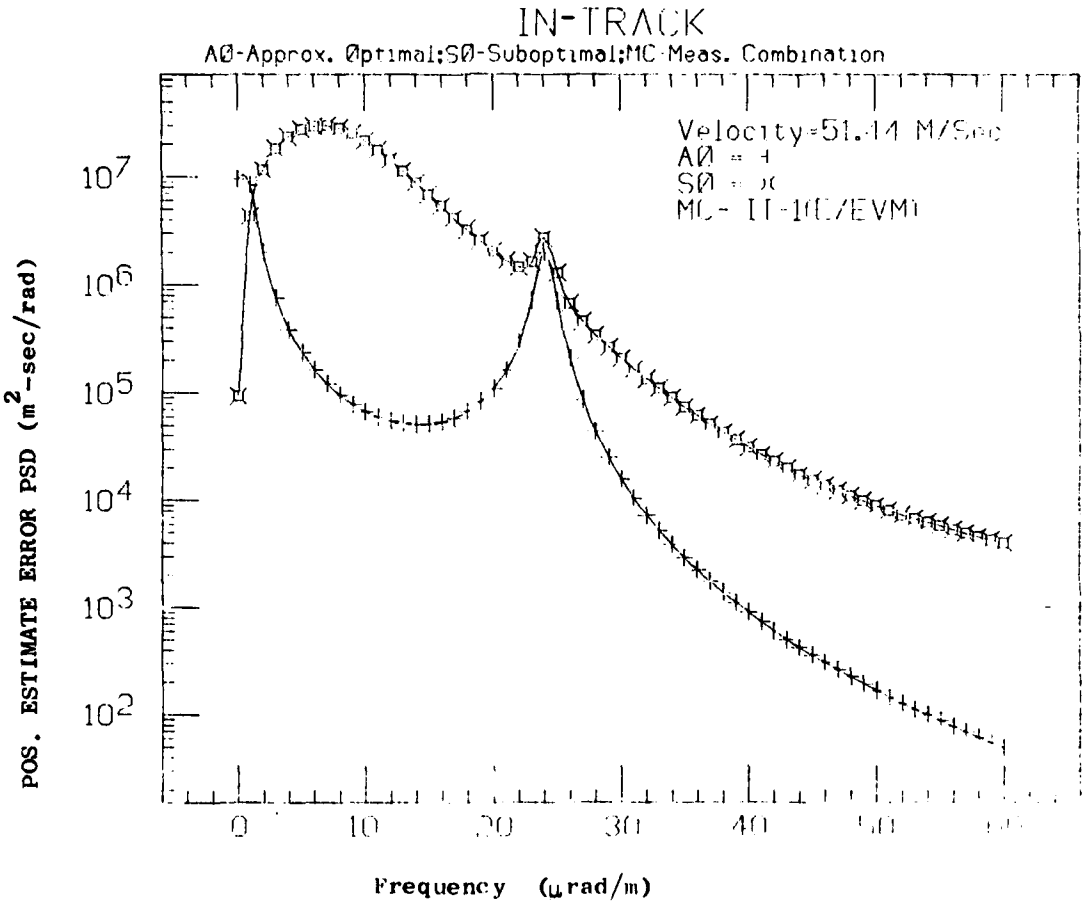

FIG. V-1 APPROXIMATELY OPTIMAL VS SUBOPTIMAL POSITION ERROR ESTIMATE ERROR POWER SPECTRAL DENSITY COMPARISON.

much greater than the same portion of the approximately optimal spectrum while the same Schuler peak is produced in both curves.

D. MULTIPLE GRADIOMETER MEASUREMENT ANALYTIC COVARIANCE COMPARISONS

Up to this point only the CT-1 and IT-1 measurement combinations have been explored. Do the other combinations provide significant improvement over the single, pure gradiometer measurement cases? This question is answered in Tables V-16 through V-29. The covariance data in these Tables was all obtained from the analytic formulas using the IHM. It was deemed unnecessary to show numerical corroboration since the optimality of the approximate filter technique has been shown in the preceding sections of this chapter. The lowest velocity case is omitted for velocity error estimation because approximate filters are not optimal at such low speeds, as explained in Sect. B of this chapter.

The most significant information occurs in the last columns of Tables V-16 through V-29. Two types of comparisons may be done with this rms estimate error data.

1. The different measurement combinations may be examined to determine the optimal (lowest rms estimate error) combination. This requires that the estimate error values in the 1st, 3rd and 5th rows or the 2nd, 4th, and 6th rows be compared for the in-track Tables. In the cross-track Tables the numbers in the 1st and 3rd or 2nd and 4th rows should be examined. This process clearly segregates the data depending upon the use or non-use of the external velocity measurement. The most significant conclusion is that the IT-2 measurement combination is inferior for in-track navigation when compared to the IT-1 or IT-3 combinations, particularly in the cases where the external velocity measurement is omitted. Therefore it would take at least two Bell RGGs (IT-3 measurement combination) to improve significantly in-track navigation. The cross-track data shows no great improvement when two RGGs (CT-2 measurement combination) are used instead of only one (CT-1 measurement combination). These trends confirm the intuitively obvious fact that the best information comes from the in-track derivative of the desired gravity perturbation component, Γ_{xx} in-track, and Γ_{xy} cross-track. Unfortunately one RGG will supply a measurement of Γ_{xy} but it takes two RGGs to adequately determine Γ_{xx}.

2. The improvement in estimation accuracy possible through the use of the external velocity measurement can be found by comparing the E/EVM and I/EVM cases for each measurement combination. The information added by the external velocity measurement improves velocity error estimation by an average of 50% and position error estimation by not more than 10%.

Table V-16

IN-TRACK(IT) VELOCITY ERROR ANALYTIC COVARIANCE COMPARISON

FOR V_x = 5.144 m/sec

Measurement Combination	$\bar{a}$ (m/sec)	k' (1/sec)	$\sigma^{AF}_{\Delta V_x}$ (mm·sec)
IT-1 (E/EVM)	5.144	—	1.079
IT-1 (I/EVM)	5.144	$6.376\backslash^{-4}$	0.52
IT-2 (E/EVM)	$1.076\backslash^{1}$	—	91.95
IT-2 (I/EVM)	$1.076\backslash^{1}$	$5.473\backslash^{-2}$	4.814
IT-3 (E/EVM)	$\begin{bmatrix} 6.858 \\ -3.43 \end{bmatrix}$	—	1.602
IT-3 (I/EVM)	$\begin{bmatrix} 6.858 \\ -3.43 \end{bmatrix}$	$9.505\backslash^{-4}$	0.634

† AF = analytic formula

Table V-17

IN-TRACK(IT) VELOCITY ERROR ANALYTIC COVARIANCE COMPARISON

FOR V_x = 51.44 m/sec

Measurement Combination	$\tilde{a}$ (m/sec)	k' (1/sec)	$\sigma^{AF\dagger}_{\tilde{\delta}V_x}$ (mm/sec)
IT-1 (E/EVM)	$5.143\backslash^{1}$	--	10.79
IT-1 (I/EVM)	$5.143\backslash^{1}$	$6.376\backslash^{-4}$	5.195
IT-2 (E/EVM)	7.139	--	693.53
IT-2 (I/EVM)	7.139	$4.128\backslash^{-2}$	41.81
IT-3 (E/EVM)	$\begin{bmatrix} 6.855\backslash^{1} \\ -3.428\backslash^{1} \end{bmatrix}$	--	16.01
IT-3 (I/EVM)	$\begin{bmatrix} 6.855\backslash^{1} \\ -3.428\backslash^{1} \end{bmatrix}$	$9.503\backslash^{-4}$	6.34

† AF = analytic formula

Table V-18

IN-TRACK(IT) VELOCITY ERROR ANALYTIC COVARIANCE COMPARISON

FOR V_x = 514.4 m/sec

Measurement Combination	$\bar{a}$ (m/sec)	k' (1/sec)	$\sigma^{AF}_{\delta\tilde{V}_x}$ (mm/sec)
IT-1 (E/EVM)	$3.423\backslash^2$	--	88.29
IT-1 (I/EVM)	$3.423\backslash^2$	$5.202\backslash^{-4}$	46.93
IT-2 (E/EVM)	5.216	--	149.4
IT-2 (I/EVM)	5.216	$8.842\backslash^{-4}$	61.18
IT-3 (E/EVM)	$\begin{bmatrix} 3.152\backslash^2 \\ -1.593\backslash^2 \end{bmatrix}$	--	109.11
IT-3 (I/EVM)	$\begin{bmatrix} 3.152\backslash^2 \\ -1.593\backslash^2 \end{bmatrix}$	$6.45\backslash^{-4}$	52.26

Table V-19

CROSS-TRACK(CT) VELOCITY ERROR ANALYTIC COVARIANCE COMPARISON

FOR V_x = 5.144 m/sec

Measurement Combination	$\bar{a}$ (m/sec)	k' (1/sec)	$\sigma^{AF}_{\delta V_x}$ (mm/sec)
CT-1 (E/EVM)	5.143	—	1.079
CT-1 (I/EVM)	5.143	$6.377\backslash^{-4}$	0.520
CT-2 (E/EVM)	$\begin{bmatrix} 5.148 \\ j3.421\backslash^{-3} \end{bmatrix}^*$	—	1.079
CT-2 (I/EVM)	$\begin{bmatrix} 5.148 \\ j3.421\backslash^{-3} \end{bmatrix}^*$	$6.379\backslash^{-4}$	0.5197

* In the cross-track direction, that member of $\bar{a}$ calculated from Eq. (4.14) corresponding to the measurement of Γ_{yz} is an imaginary quantity. This indicates that the numerator of the transfer function associated with Γ_{yz} should be written with a first degree s term as

$$a_{\Gamma_{yz}} = a'_{\Gamma_{yz}} s\Big|_{s=j\omega_s} .$$

The foregoing footnote applies to Tables V-19 to V-21.

Table V-20

CROSS-TRACK VELOCITY ERROR ANALYTIC COVARIANCE COMPARISON

FOR V_x = 51.44 m/sec

Measurement Combination	$\bar{a}$ (m/sec)	k' (1/sec)	$\sigma^{AF}_{\tilde{\delta V}_x}$ (mm/sec)
CT-1 (E/EVM)	$5.142\angle 1$	--	10.78
CT-1 (I/EVM)	$5.142\angle 1$	$6.375\angle -4$	5.195
CT-2 (E/EVM)	$\begin{bmatrix} 5.137\angle 1 \\ -j1.656\angle -2* \end{bmatrix}$	—	10.78
CT-2 (I/EVM)	$\begin{bmatrix} 5.137\angle 1 \\ -j1.656\angle -2* \end{bmatrix}$	$6.373\angle -4$	5.194

* See footnote Table V-19

Table V-21

CROSS-TRACK VELOCITY ERROR ANALYTIC COVARIANCE COMPARISON

FOR V_x = 514.4 m/sec

Measurement Combination	$\bar{a}$ (m/sec)	k' (1/sec)	$\sigma^{AF}_{\delta V_x}$ (mm/sec)
CT-1 (E/EVM)	$4.802\angle 2$	—	104.26
CT-1 (I/EVM)	$4.802\angle 2$	$6.161\angle -4$	51.07
CT-2 (E/EVM)	$\begin{bmatrix} 4.674\angle 2 \\ -j2.079 \end{bmatrix}$ *	—	102.9
CT-2 (I/EVM)	$\begin{bmatrix} 4.674\angle 2 \\ -j2.079 \end{bmatrix}$ *	$6.079\angle -4$	50.73

See footnote Table V-19

Table V-22

IN-TRACK POSITION ERROR ANALYTIC COVARIANCE COMPARISON FOR V_x = 0.5144 m/sec

Measurement Combination	$\bar{b}$ (m-sec)	$\bar{c}$ (m)	$\bar{d}$ (m-sec)	$\bar{e}$ (m)	k' (1/sec)	$\sigma^{AF}_{\delta R_x}$ (m)
IT-1 (E/EVM)	$-1.292\backslash-15$	$-3.739\backslash-40$	$3.347\backslash5$	$7.24\backslash-2$	--	3.218
IT-1 (I/EVM)	$-1.021\backslash-15$	$-1.562\backslash-49$	$2.646\backslash5$	$5.4\backslash-2$	$3.961\backslash-14$	2.95
IT-2 (E/EVM)	$-6.337\backslash-16$	$-2.376\backslash-20$	$3.347\backslash5$	2.09	--	533.1
IT-2 (I/EVM)	$-6.337\backslash-16$	$-1.252\backslash-29$	$3.347\backslash5$	2.09	$3.95\backslash-15$	533.07
IT-3 (E/EVM)	$\begin{bmatrix} -6.337\backslash-16 \\ 6.587\backslash-16 \end{bmatrix}$	$\begin{bmatrix} -2.376\backslash-20 \\ 2.47\backslash-20 \end{bmatrix}$	$\begin{bmatrix} 4.462\backslash5 \\ -2.231\backslash5 \end{bmatrix}$	$\begin{bmatrix} 1.17\epsilon\backslash-1 \\ -5.879\backslash-3 \end{bmatrix}$	--	4.32
IT-3 (I/EVM)	$\begin{bmatrix} -6.337\backslash-16 \\ 6.587\backslash-16 \end{bmatrix}$	$\begin{bmatrix} -1.252\backslash-29 \\ 1.301\backslash-29 \end{bmatrix}$	$\begin{bmatrix} 4.462\backslash5 \\ -2.231\backslash5 \end{bmatrix}$	$\begin{bmatrix} 1.176\backslash-1 \\ -5.879\backslash-3 \end{bmatrix}$	$3.95\backslash-14$	4.32

Table V-23

IN-TRACK POSITION ERROR ANALYTIC COVARIANCE COMPARISON FOR V_x = 5.144 m/sec

Measurement Combination	$\bar{b}$ (m-sec)	$\bar{c}$ (m)	$\bar{d}$ (m-sec)	$\bar{e}$ (m)	k' (1/sec)	$\sigma^{AF}_{\delta R_x}$ (m)
IT-1 (E/EVM)	$-3.347\backslash 6$	$-2.510\backslash 2$	$3.347\backslash 6$	$1.288\backslash 1$	--	7.68
IT-1 (I/EVM)	$-2.646\backslash 6$	$-1.687\backslash 3$	$2.646\backslash 6$	9.602	$6.376\backslash -4$	6.99
IT-2 (E/EVM)	$-6.999\backslash 6$	$-2.625\backslash 2$	$3.347\backslash 6$	$2.09\backslash 2$	--	538.2
IT-2 (I/EVM)	$-6.999\backslash 6$	$-1.916\backslash 5$	$3.347\backslash 6$	$2.09\backslash 2$	$5.473\backslash -2$	533.1
IT-3 (E/EVM)	$\begin{bmatrix} -4.462\backslash 6 \\ 2.231\backslash 6 \end{bmatrix}$	$\begin{bmatrix} -1.673\backslash 2 \\ 8.367\backslash 1 \end{bmatrix}$	$\begin{bmatrix} 4.462\backslash 6 \\ -2.231\backslash 6 \end{bmatrix}$	$\begin{bmatrix} 2.091\backslash 1 \\ -1.045\backslash 1 \end{bmatrix}$	--	10.34
IT-3 (I/EVM)	$\begin{bmatrix} -4.462\backslash 6 \\ 2.231\backslash 6 \end{bmatrix}$	$\begin{bmatrix} -2.12\backslash 3 \\ 1.060\backslash 3 \end{bmatrix}$	$\begin{bmatrix} 4.462\backslash 6 \\ -2.231\backslash 6 \end{bmatrix}$	$\begin{bmatrix} 2.091\backslash 1 \\ -1.045\backslash 1 \end{bmatrix}$	$9.505\backslash -4$	10.27

Table V-24

IN-TRACK POSITION ERROR ANALYTIC COVARIANCE COMPARISON FOR V_x = 51.44 m/sec

Measurement Combination	$\bar{b}$ (m-sec)	$\bar{c}$ (m)	$\bar{d}$ (m-sec)	$\bar{e}$ (m)	k' (1/sec)	$\sigma^{AF}_{\delta R_x}$ (m)
IT-1 (E/EVM)	$-3.346\backslash^{7}$	$-2.509\backslash^{3}$	$3.347\backslash^{7}$	$2.289\backslash^{3}$	—	20.07
IT-1 (I/EVM)	$-2.646\backslash^{7}$	$-1.687\backslash^{4}$	$2.646\backslash^{7}$	$1.707\backslash^{3}$	$6.376\backslash^{-4}$	16.78
IT-2 (E/EVM)	$-4.645\backslash^{6}$	$-1.742\backslash^{2}$	$3.347\backslash^{7}$	$2.09\backslash^{4}$	—	772.7
IT-2 (I/EVM)	$-4.645\backslash^{6}$	$-9.587\backslash^{4}$	$3.347\backslash^{7}$	$2.09\backslash^{4}$	$4.128\backslash^{-2}$	534.1
IT-3 (E/EVM)	$\begin{bmatrix} -4.459\backslash^{7} \\ 2.229\backslash^{7} \end{bmatrix}$	$\begin{bmatrix} -1.672\backslash^{3} \\ 8.362\backslash^{2} \end{bmatrix}$	$\begin{bmatrix} 4.462\backslash^{7} \\ -2.23\backslash^{7} \end{bmatrix}$	$\begin{bmatrix} 3.718\backslash^{2} \\ -1.859\backslash^{3} \end{bmatrix}$	—	27.54
IT-3 (I/EVM)	$\begin{bmatrix} -4.459\backslash^{7} \\ 2.229\backslash^{7} \end{bmatrix}$	$\begin{bmatrix} -2.119\backslash^{4} \\ 1.059\backslash^{4} \end{bmatrix}$	$\begin{bmatrix} 4.462\backslash^{7} \\ -2.23\backslash^{7} \end{bmatrix}$	$\begin{bmatrix} 3.718\backslash^{2} \\ -1.859\backslash^{3} \end{bmatrix}$	$9.503\backslash^{-4}$	24.86

Table V-25

IN-TRACK POSITION ERROR ANALYTIC COVARIANCE COMPARISON FOR $V_{\bar{x}}$ = 514.4 m/sec

Measurement Combination	$\bar{b}$ (m-sec)	$\bar{c}$ (m)	$\bar{d}$ (m-sec)	$\bar{e}$ (m)	k' (1/sec)	$\sigma^{AF}_{\delta R_x}$ (m)
IT-1 (E/EVM)	$-2.229\backslash^{8}$	$-1.112\backslash^{4}$	$3.347\backslash^{8}$	$4.07\backslash^{5}$	--	83.09
IT-1 (I/EVM)	$-1.833\backslash^{8}$	$-6.344\backslash^{4}$	$2.647\backslash^{8}$	$3.036\backslash^{5}$	$5.202\backslash^{-4}$	45.94
IT-2 (E/EVM)	$3.393\backslash^{6}$	$1.272\backslash^{2}$	$3.347\backslash^{8}$	$2.09\backslash^{6}$	--	546.7
IT-2 (I/EVM)	$3.393\backslash^{6}$	$1.500\backslash^{3}$	$3.347\backslash^{8}$	$2.09\backslash^{6}$	$8.842\backslash^{-4}$	535.6
IT-3 (E/EVM)	$\begin{bmatrix} -2.051\backslash^{8} \\ 1.036\backslash^{8} \end{bmatrix}$	$\begin{bmatrix} -7.69\backslash^{3} \\ 3.885\backslash^{3} \end{bmatrix}$	$\begin{bmatrix} 4.462\backslash^{8} \\ -2.231\backslash^{8} \end{bmatrix}$	$\begin{bmatrix} 6.621\backslash^{5} \\ -3.311\backslash^{5} \end{bmatrix}$	—	105.3
IT-3 (I/EVM)	$\begin{bmatrix} -2.051\backslash^{8} \\ 1.036\backslash^{8} \end{bmatrix}$	$\begin{bmatrix} -6.615\backslash^{4} \\ 3.342\backslash^{4} \end{bmatrix}$	$\begin{bmatrix} 4.462\backslash^{8} \\ -2.331\backslash^{8} \end{bmatrix}$	$\begin{bmatrix} 6.621\backslash^{5} \\ -3.311\backslash^{5} \end{bmatrix}$	$6.451\backslash^{-4}$	71.54

Table V-26

CROSS-TRACK POSITION ERROR ANALYTIC COVARIANCE COMPARISON

FOR V_x = 0.5144 m/sec

Measurement Combination	$\bar{b}$ (m-sec)	$\bar{c}$ (m)	$\bar{\alpha}$ (m-sec)	k' (1/sec)	$\sigma^{AF}_{\tilde{\Delta}R_y}$ (m)
CT-1 (E/EVM)	$-1.675\backslash^{-17}$	$-6.291\backslash^{-44}$	$3.347\backslash^{5}$	--	10.58
CT-1 (I/EVM)	$-1.325\backslash^{-17}$	$-2.993\backslash^{-54}$	$2.647\backslash^{5}$	$4.512\backslash^{-15}$	9.98
CT-2 (E/EVM)	$\begin{bmatrix} -1.666\backslash^{-17} \\ 2.111\backslash^{-34} \end{bmatrix}$	$\begin{bmatrix} -6.246\backslash^{-22} \\ -2.156\backslash^{-20} \end{bmatrix}$	$\begin{bmatrix} 3.347\backslash^{5} \\ -1.314\backslash^{2} \end{bmatrix}$	--	9.48
CT-2 (I/EVM)	$\begin{bmatrix} -1.666\backslash^{-17} \\ 1.756\backslash^{-44} \end{bmatrix}$	$\begin{bmatrix} -3.746\backslash^{-32} \\ -2.156\backslash^{-20} \end{bmatrix}$	$\begin{bmatrix} 3.347\backslash^{5} \\ -1.314\backslash^{2} \end{bmatrix}$	$4.499\backslash^{-15}$	9.48

Table V-27

CROSS-TRACK POSITION ERROR ANALYTIC COVARIANCE COMPARISON

FOR V_x = 5.144 m/sec

Measurement Combination	$\bar{b}$ (m-sec)	$\bar{c}$ (m)	$\bar{\alpha}$ (m-sec)	k' (1/sec)	$\sigma^{AF}_{\tilde{\delta}R_y}$ (m)
CT-1 (E/EVM)	$-3.346\backslash 6$	$-2.509\backslash 2$	$3.347\backslash 6$	—	18.84
CT-1 (I/EVM)	$-2.646\backslash 6$	$-1.687\backslash 3$	$2.647\backslash 6$	$6.376\backslash -4$	17.75
CT-2 (E/EVM)	$\begin{bmatrix} -3.349\backslash 6 \\ 3.03\backslash -10 \end{bmatrix}$	$\begin{bmatrix} -1.256\backslash 2 \\ 2.76 \end{bmatrix}$	$\begin{bmatrix} 3.347\backslash 6 \\ -4.154\backslash 3 \end{bmatrix}$	—	16.87
CT-2 (I/EVM)	$\begin{bmatrix} -3.349\backslash 6 \\ 1.403\backslash -10 \end{bmatrix}$	$\begin{bmatrix} -1.068\backslash 3 \\ 2.76 \end{bmatrix}$	$\begin{bmatrix} 3.347\backslash 6 \\ -4.154\backslash 3 \end{bmatrix}$	$6.379\backslash -4$	16.86

Table V-28

CROSS-TRACK POSITION ERROR ANALYTIC COVARIANCE COMPARISON

FOR V_x = 51.44 m/sec

Measurement Combination	$\bar{b}$ (m-sec)	$\bar{c}$ (m)	$\bar{\alpha}$ (m-sec)	k' (1/sec)	$\sigma^{AF}_{\tilde{\delta R}_y}$ (m)
CT-1 (E/EVM)	$-3.345\backslash 7$	$-2.508\backslash 3$	$3.347\backslash 7$	--	34.58
CT-1 (I/EVM)	$-2.646\backslash 7$	$-1.686\backslash 4$	$2.646\backslash 7$	$6.375\backslash -4$	31.78
CT-2 (E/EVM)	$\begin{bmatrix} -3.342\backslash 7 \\ 5.172\backslash -11 \end{bmatrix}$	$\begin{bmatrix} -1.253\backslash 3 \\ -1.336\backslash 1 \end{bmatrix}$	$\begin{bmatrix} 3.347\backslash 7 \\ -1.313\backslash 5 \end{bmatrix}$	--	31.2
CT-2 (I/EVM)	$\begin{bmatrix} -3.342\backslash 7 \\ -5.539\backslash -10 \end{bmatrix}$	$\begin{bmatrix} -1.065\backslash 4 \\ -1.336\backslash 1 \end{bmatrix}$	$\begin{bmatrix} 3.347\backslash 7 \\ -1.313\backslash 5 \end{bmatrix}$	$6.373\backslash -4$	30.26

Table V-29

CROSS-TRACK POSITION ERROR ANALYTIC COVARIANCE COMPARISON

FOR V_x = 514.4 m/sec

Measurement Combination	$\bar{b}$ (m-sec)	$\bar{c}$ (m)	$\bar{\alpha}$ (m-sec)	k' (1/sec)	$\sigma^{AF}_{\tilde{\alpha}R_y}$ (m)
CT-1 (E/EVM)	$-3.124\backslash^{8}$	$-2.187\backslash^{4}$	$3.347\backslash^{8}$	--	102.92
CT-1 (I/EVM)	$-2.51\backslash^{8}$	$-1.443\backslash^{5}$	$2.647\backslash^{-4}$	$6.161\backslash^{-4}$	67.02
CT-2 (E/EVM)	$\begin{bmatrix} -3.041\backslash^{8} \\ -5.161\backslash^{-10} \end{bmatrix}$	$\begin{bmatrix} -1.140\backslash^{4} \\ -1.677\backslash^{3} \end{bmatrix}$	$\begin{bmatrix} 3.347\backslash^{8} \\ -4.152\backslash^{6} \end{bmatrix}$	--	98.68
CT-2 (I/EVM)	$\begin{bmatrix} -3.041\backslash^{8} \\ -5.840\backslash^{-10} \end{bmatrix}$	$\begin{bmatrix} -9.242\backslash^{4} \\ -1.677\backslash^{3} \end{bmatrix}$	$\begin{bmatrix} 3.347\backslash^{8} \\ -4.152\backslash^{6} \end{bmatrix}$	$6.079\backslash^{-4}$	67.26

Chapter VI

GRAVITY GRADIOMETER SURVEYING TO IMPROVE THE GRAVITY PERTURBATION MODEL

The gradiometer may be used as a survey tool divorced from any direct INS application. Gradiometer survey data, and in fact any survey data which provides gravity information, may be used to improve the reference gravity model used in the INS (inertial navigation system) and consequently reduce velocity and position error.

The rms velocity and position error can be found by first writing (4.4) in the following form

$$\delta V = \frac{sg}{(+)} - \frac{sk\delta V^m}{(+)} \tag{6.1}$$

where the x or y subscripts have been omitted as the equation can be used in either the IT or CT directions. The velocity and position error power spectra are given by

$$\Phi^t_{\delta R}(s) = \frac{\Phi^t_g(s)}{(+)(-)} - \frac{k^2 q_2}{(+)(-)} \quad . \tag{6.2}$$

and

$$\Phi^t_{\delta V}(s) = \frac{s^2\Phi^t_g(s)}{(+)(-)} - \frac{s^2k^2q_2}{(+)(-)} \quad . \tag{6.3}$$

Recalling the variance formulas in (4.8) and (4.47) the position and velocity error variance can be expressed as

$$\sigma^2_{\delta R} = \frac{kq_2}{2\omega_s^2} + \frac{1}{\pi j}\int_0^{j\infty} \frac{\Phi^t_g(s)}{(+)(-)}\,ds \tag{6.4}$$

and

$$\sigma^2_{\delta V} = \frac{kq_2}{2} + \frac{1}{\pi j}\int_0^{j\infty} \frac{s^2\Phi^t_g(s)}{(+)(-)}\,ds \quad . \tag{6.5}$$

Again the integrals in (6.4) and (6.5) can be evaluated either numerically or analytically. Assuming a reduced low frequency perturbation content due to the added survey information, the analytic integral evaluations consider only the Schuler poles. The validity of this assumption can again be tested by comparing the analytic and numerically obtained variance values. The analytic formulas are

$$\sigma^2_{\delta R} = \frac{kq_2}{2\omega_s^2} + \frac{\Phi^t_g(j\omega_s)}{2k\omega_s^2} \tag{6.6}$$

and

$$\sigma^2_{\delta V} = \frac{kq_2}{2} + \frac{\Phi^t_g(j\omega_s)}{2k} \quad . \tag{6.7}$$

The basic theory used to determine the updated gravity perturbation spectrum $(\Phi^t_g(s))$ is taken from Breakwell [12]. It is presented here for completeness. The objective is to estimate some scalar function $\Psi(x,y)$ related to the surface perturbation potential ΔU by

$$\Psi(\bar{\omega}^s;\ h_1) = f(\bar{\omega}^s)\Delta U(\bar{\omega}^s;\ 0) \tag{6.8}$$

where (6.8) is written in the Fourier domain and h_1 is the height above sea level at which the estimate of Ψ is to be made. The measurement equation may be expressed as

$$\underset{\bar{z}}{\overset{m\times 1}{}}(\bar{\omega}^s;\, h_2) \;=\; \underset{\bar{H}}{\overset{m\times 1}{}}(\bar{\omega}^s)\,\Delta U(\bar{\omega}^s;\, 0) + \bar{\epsilon} \tag{6.9}$$

where h_2 is the height above sea level at which the survey is taken. Assume that the estimate of η at height h is given by

$$\hat{\eta}(\bar{\omega}^s;\, h_1) \;=\; \psi^T(\bar{\omega}^s)\,\bar{z}(\bar{\omega}^s;\, h_2)\ . \tag{6.10}$$

The resulting estimation error is

$$\begin{aligned}\tilde{\eta}(\bar{\omega}^s;\, h_1) \;&=\; \hat{\eta}(\bar{\omega}^s;\, h_1) - \eta(\bar{\omega}^s;\, h_1) \\ &=\; [\psi^T(\bar{\omega}^s)H(\bar{\omega}^s) - f(\bar{\omega}^s)]\Delta U(\bar{\omega}^s;0) + \psi^T(\omega^s)\bar{\epsilon}\end{aligned} \tag{6.11}$$

which means that the estimate error spectral density is expressible as

$$\begin{aligned}\Phi_{\tilde{\eta}}(\bar{\omega}^s;h_1) \;&=\; [\psi^T(-\bar{\omega}^s)H(-\bar{\omega}^s) - f(-\bar{\omega}^s)]\Phi^s_{\Delta U}(\bar{\omega}^s;0) \\ &\quad\times [H^T(\bar{\omega}^s)\ \psi(\bar{\omega}^s) - f(\bar{\omega}^s)] + \psi^T(-\bar{\omega}^s)R\psi(\bar{\omega}^s)\ .\end{aligned} \tag{6.12}$$

In this situation causality is not a factor as it was in the real time filter case. Therefore to assure the minimum mean squared estimation error, given by

$$\sigma^2_{\tilde{\eta}} \;=\; \frac{1}{4\pi^2}\int_{-\infty}^{\infty}\int \Phi^s_{\tilde{\eta}}(\bar{\omega}^s;\, h_1)\,d\omega^s_x\,d\omega^s_y\ , \tag{6.13}$$

it is sufficient to minimize (6.12) with respect to $\psi(\bar{\omega}^s)$. This results in the statistically best weighting of the measurements for estimating η, written as

$$\psi(\bar{\omega}^s) \;=\; [H(-\bar{\omega}^s)\Phi^s_{\Delta U}(\bar{\omega}^s;0)H^T(\bar{\omega}^s)+R]^{-1}H(-\bar{\omega}^s)\Phi^s_{\Delta U}(\bar{\omega}^s;0)f(\bar{\omega}^s)\ . \tag{6.14}$$

Substituting (6.14) into (6.12) yields the following compact expression

$$\Phi^{s}_{\tilde{\eta}}(\bar{\omega}^{s};\ h) \;=\; \frac{\Phi^{s}_{\Delta U}(\bar{\omega}^{s};\ 0) f(-\bar{\omega}^{s}) f(\bar{\omega}^{s})}{1 + \Phi^{s}_{\Delta U}(\bar{\omega}^{s};\ 0) H^{T}(\bar{\omega}^{s}) R^{-1} H(-\bar{\omega}^{s})} \qquad (6.15)$$

Notice that the numerator of this expression represents the a priori knowledge of $\tilde{\eta}$ and the second term in the denominator represents the information added by the survey. To obtain the required one dimensional spectrum, (6.15) must be integrated with respect to ω^{s}_{y}. In addition the time variation spectrum, required in (6.4) through (6.7), is found simply by dividing the one-dimensional spacial spectrum by the IT velocity. The desired spectrum may then be expressed as

$$\Phi^{t}_{\tilde{\eta}}(\bar{\omega}^{t};\ h_{1}) \;=\; \frac{1}{v_{x}} \int_{0}^{\infty} \left\{ \frac{\Phi^{s}_{\Delta U}(\bar{\omega}^{s};0) f(-\bar{\omega}^{s}) f(\bar{\omega}^{s})}{1 + \Phi^{s}_{\Delta U}(\bar{\omega}^{s};0) H^{T}(\bar{\omega}^{s}) R^{-1} H(-\bar{\omega}^{s})} \right\} d\omega^{s}_{y}. \qquad (6.16)$$

Equation (6.16) may be used to determine the updated spectrum $\Phi^{t}_{g}(s)$ in (6.4) and (6.5) if $\tilde{\eta}$ is equal to g. This, in fact, is the case when the updated gravity model is used in the basic navigation loop.

In the covariance analyses in the next section, two survey schemes are used. The first is a ground level gradiometer survey (GS) where the measurement is assumed to be the vertical perturbation gradient, Γ_{zz}. Recall that at least two Bell RGGs are required to obtain this quantity. In all the a priori studies the BHM is taken as the gravity perturbation model to be updated. Therefore the surface potential fluctuations, from (3.4), are described as

$$\Phi^{s}_{\Delta U}(\bar{\omega}^{s};\ 0) \;=\; \sum_{i=1}^{3} \Phi_{i}\, e^{-2\left|\bar{\omega}^{s}\right| D_{i}}. \qquad (6.17)$$

The functional relationship between (6.17) and Γ_{zz} is found to be

$$H(\bar{\omega}^s) = |\bar{\omega}^s|^2 e^{-|\bar{\omega}^s| h_2} \tag{6.18}$$

and

$$H(\bar{\omega}^s)H(-\bar{\omega}^s) = |\bar{\omega}^s|^4 e^{-2|\bar{\omega}^s| h_2} . \tag{6.19}$$

The second type of survey used is the proposed low-low GRAVSAT configuration where two low earth satellites follow each other in circular polar orbits and are connected by a very accurate Doppler rate indicator. The relative velocity changes between the two satellites indicate gravitational field perturbations. The functional relationship between the Doppler data and the potential perturbations is

$$V_x^{\text{satellite 1}} - V_x^{\text{satellite 2}} = \Delta V_x = \frac{e^{-|\bar{\omega}^s| h_2}}{V_{cir}} 2j \sin \frac{\omega_x^s \Delta}{2} \Delta U(\bar{\omega}^s; 0) \tag{6.20}$$

where $V_{c_{ir}}$ is the unperturbed circular velocity and Δ is the satellite distance spacing. Assuming that the perturbations of interest have wavelengths substantially greater than Δ then $H(\bar{\omega}^s)$ from (6.20) may be approximated as

$$H(\bar{\omega}^s) = \frac{e^{-|\bar{\omega}^s| h_2}}{V_{cir}} j|\bar{\omega}^s| \Delta \cos \alpha \tag{6.21}$$

where α denotes the direction of $\bar{\omega}^s$. Then

$$H(\bar{\omega}^s)H(-\bar{\omega}^s) = \frac{e^{-2|\bar{\omega}^s| h_2}}{V_{cir}^2} |\bar{\omega}^s|^2 \Delta^2 \cos^2 \alpha . \tag{6.22}$$

It is possible to modify (6.22) to compensate for the rotation of the earth under the satellite ground track as explained by Breakwell [Ref. 12, p. 338]. This correction is necessary since the north-south and south-north satellite ground tracks are not parallel. These tracks diverge at an angle θ having a value of approximately 1/16 radian at low latitude. To compensate for this effect (6.22) should be replaced by

$$H(\bar{\omega}^s)H(-\bar{\omega}^s) = \frac{1}{2}\frac{e^{-2|\bar{\omega}^s|h_2}}{V_{cir}^2}|\bar{\omega}^s|^2\Delta^2[\cos^2(\alpha-\theta)+\cos^2(\alpha+\theta)] \qquad (6.23)$$

or simplifying (6.23) using trigonometric identities

$$H(\bar{\omega}^s)H(-\bar{\omega}^s) = \frac{e^{-2|\bar{\omega}^s|h_2}\Delta^2}{V_{cir}^2}[\bar{\omega}_x^{s\,2}\cos^2\theta + \bar{\omega}_y^{s\,2}\sin^2\theta]\,. \qquad (6.24)$$

For both the gradiometer and satellite surveys the measurement error is given by the following formula in the scalar case

$$R = \frac{\sigma_{ME}^2}{N/AS} \qquad (6.25)$$

where σ_{ME}^2 is the mean-squared measurement error, N is the number of survey measurements, and AS is the area surveyed.

The analysis in the following section investigates both the IT and CT directions. The transfer functions relating g_x and g_y to the BHM perturbation potential are respectively

$$f(\bar{\omega}^s)f(-\bar{\omega}^s) = (\omega_y^s)^2 e^{-2|\bar{\omega}^s|h_1} \qquad (6.26)$$

$$f(\bar{\omega}^s)f(-\bar{\omega}^s) = (\bar{\omega}_x^s)^2 e^{-2|\bar{\omega}^s|h_1}\,. \qquad (6.27)$$

With these relationships the error spectra from (6.16) and subsequently the INS position and velocity error may be determined for the following four separate direction/survey options.

IT/GS (in-track/gradiometer survey). This combination indicates alteration of the g_x spectrum using gradiometer survey data. For this case (6.16) becomes

$$\Phi^t_{g_x}(\bar{\omega}^t;h_1) = \frac{(\omega^s_x)^2}{V_x\pi}\int_0^\infty \left\{ \frac{\sum_{i=1}^{3} \Phi_i e^{-2|\bar{\omega}^s|h_1'}}{1 + \frac{N/AS}{\sigma^2_{\Gamma_{zz}}}|\bar{\omega}^s|^4 \sum_{i=1}^{3}\Phi_i e^{-2|\bar{\omega}^s|h_2'}} \right\} d\omega^s_y \quad . \qquad (6.28)$$

IT/SS (in-track/satellite survey). This again indicates alteration of the g_x residual but this time with a low-low GRAVSAT satellite survey. The updated g_x spectrum may be written as

$$\Phi^\dagger_{g_x}(\bar{\omega}^t;\, h_1) = \frac{(\omega^s_x)^2}{V_x\pi}\int_0^\infty \left\{ \frac{\sum_{i=1}^{3} \Phi_i e^{-2|\bar{\omega}^s|h_1'}}{1 + C(\bar{\omega}^s)[(\bar{\omega}^s_x)^2\cos^2\theta + (\bar{\omega}^s_y)^2\sin^2\theta]} \right\} d\omega^s_y \qquad (6.29)$$

where

$$C(\bar{\omega}^s) = \frac{N/AS}{\sigma^2_{Doppler}}\left(\frac{\Delta}{V_{cir}}\right)^2 \sum_{i=1}^{3}\Phi_i e^{-2|\bar{\omega}^s|h_2'} \quad . \qquad (6.30)$$

CT/GS (cross-track/gradiometer survey). This again indicates alteration of the g_y residual but this time with a low-low GRAVSAT satellite survey. The updated g_y spectrum may be written as

$$\Phi_{g_y}^{t}(\bar{\omega}^{t};\, h_1) = \frac{1}{V_x \pi} \int_0^{\infty} \left\{ \frac{(\omega_y^s)^2 \sum_{i=1}^{3} \Phi_i \, e^{-2|\bar{\omega}^s| h_1'}}{1 + \frac{N/AS}{\sigma_{zz}^2} |\bar{\omega}^s|^4 \sum_{i=1}^{3} \Phi_i \, e^{-2|\bar{\omega}^s| h_2'}} \right\} d\omega_y^s \,. \quad (6.31)$$

CT/SS (cross-track/satellite survey). Here the g_y spectrum formula updated by satellite data appears as

$$\Phi_{g_y}^{t}(\bar{\omega}^{t};\, h_1) = \frac{1}{V_x \pi} \int_0^{\infty} \left\{ \frac{(\omega_y^s)^2 \sum_{i=1}^{3} \Phi_i \, e^{-2|\bar{\omega}^s| h_1'}}{1 + C(\bar{\omega}^s)[(\omega_x^s)^2 \cos^2\theta + (\omega_y^s)^2 \sin^2\theta]} \right\} d\omega_y^s \,. \quad (6.32)$$

The first step in doing the covariance comparisons in the next chapter is to numerically carry out the quadratures in (6.28) through (6.32) to obtain the updated gravity perturbation spectra. These spectra are subsequently used in the numerical evaluation of (6.4) and (6.5) to be compared with the position and velocity errors obtained from (6.6) and (6.7) where the Schuler values from the updated spectra are used in the analytic formulas.

Chapter VII

COVARIANCE COMPARISON FOR REAL TIME VS SURVEY USE OF A GRADIOMETER

The objective in this Chapter will be to compare the real time estimation errors in Sect. B of Ch. V with the velocity and position errors resulting from the use of an updated gravity model. To obtain a valid comparison the survey parameters must be chosen judiciously, particularly in the case of the gradiometer survey. The survey vehicle velocity and gradiometer averaging time are the principal parameters. Assuming that the latter is fixed it is important that the gradiometer survey and carrier vehicles have the same speeds to assure equal wavelength resolution in the real time and survey applications. Actually, the important parameter in the survey situation is the number of survey measurements per unit area (N/AS). If the survey track spacing is set at a distance equal to the minimum wavelength information desired (10 km), and with a fixed gradiometer averaging time, the survey velocity completely determines the measurements per unit area and the time to survey a specified area. Then the claim of equal survey and carrier speeds ensuring equal resolution is contingent on the track spacing chosen. From a practical standpoint, the survey times for a given area are of interest. Table VII-1 gives the survey times for an area of 1×10^{12} square meters, about 1/15 of the continental United States.

Table VII-1

SURVEY TIMES FOR 1×10^{12} SQUARE METERS

Survey Velocity (m/sec)	Survey Time (days)
0.5144	2250
5.144	225
51.44	22.5
514.4	2.25

Note that the lower velocities take excessive survey times. Gradiometer survey height also influences the resolution question. Thus to maintain equality the gradiometer survey and carrier vehicles will also have equal assumed altitudes. With these facts in mind the gradiometer survey parameters are as follows:

survey height: zero km

survey velocity: carrier velocity

gradiometer averaging time: 10 sec

track spacing: 10 km

gradiometer accuracy: 1 Eötvos .

The GRAVSAT mission parameters are more interdependent and consequently less flexible than the gradiometer survey quantities. Nevertheless, the GRAVSAT survey provides an interesting alternative to the gradiometer survey with very real possibilities. Nominal parameters for a low-low GRAVSAT mission might be

satellite altitude: 180 km

circular velocity: 7.796 km/sec

Doppler accuracy: 1×10^{-6} m/sec

satellite separation: 3 deg (341.87 km)

length of mission: 6 months

time between measurements: 8 sec

Assuming these survey parameters, Tables VII-2 and VII-3 compare the real time data from Tables V-5 through V-12 with the variances obtained from (6.6) and (6.7). In order to standardize the data the optimal value of k is used for both the real time and survey applications. In the real time case the optimal k is given in (4.31) (x or y subscript as

Table VII-2

REAL TIME VS SURVEY VELOCITY ERROR COVARIANCE COMPARISON

EVM = External Velocity Measurement
GS = Gradiometer Survey
SS = Satellite Survey

Measurement Combination	RMS Velocity or Velocity Estimate Error (mm/sec)	CARRIER VELOCITY (m/sec) 0.5144	5.144	51.44	514.4
IT-1 (I/EVM)	$\sigma^{AF}_{\tilde{\delta V}_x}$	$4.1^{\backslash -7}$	0.5196	5.195	50.8
	$\sigma^{NI}_{\tilde{\delta V}_x}$	7.098	0.493	4.93	47.62
IT/GS	$\sigma^{AF}_{\delta V_x}$	$4.095^{\backslash -7}$	0.456	2.574	14.46
	$\sigma^{NI}_{\delta V_x}$	0.0177	0.422	2.541	14.32
IT/SS	$\sigma^{AF}_{\delta V_x}$	$4.095^{\backslash -7}$	8.295	16.94	10.72
	$\sigma^{NI}_{\delta V_x}$	6.923	5.95	23.14	11.54
CT-1 (I/EVM)	$\sigma^{AF}_{\tilde{\delta V}_y}$	$1.382^{\backslash -7}$	0.519	5.195	51.39
	$\sigma^{NI}_{\tilde{\delta V}_y}$	4.089	0.4934	4.965	50.98
CT/GS	$\sigma^{AF}_{\delta V_y}$	$1.382^{\backslash -7}$	0.4022	2.544	14.46
	$\sigma^{NI}_{\delta V_y}$	$6.556^{\backslash -3}$	0.386	2.52	14.32
CT/SS	$\sigma^{AF}_{\delta V_y}$	$1.382^{\backslash -7}$	5.18	30.37	57.18
	$\sigma^{NI}_{\delta V_y}$	3.99	4.46	22.77	56.54

Note: Data assumes BHM (Baseline Heller Model) prior to survey update

Table VII-3

REAL TIME VS SURVEY POSITION ERROR COVARIANCE COMPARISON

EVM = External Velocity Measurement
GS = Gradiometer Survey
SS = Satellite Survey

Measurement Combination	RMS Position or Position Estimate Error (m)	CARRIER VELOCITY (m/sec) 0.5144	5.144	51.44	514.4
IT-1 (I/EVM)	$\sigma^{AF}_{\delta\tilde{R}_x}$	3.79	8.988	21.47	56.71
	$\sigma^{NI}_{\delta\tilde{R}_x}$	3.73	8.71	20.58	58.76
IT/GS	$\sigma^{AF}_{\delta R_x}$	$3.3\backslash^{-7}$	0.367	2.076	11.67
	$\sigma^{NI}_{\delta R_x}$	0.219	0.556	2.297	11.72
IT/SS	$\sigma^{AF}_{\delta R_x}$	$3.03\backslash^{-7}$	6.691	13.66	8.646
	$\sigma^{NI}_{\delta R_x}$	108.8	5.55	11.55	8.46
CT-1 (I/EVM)	$\sigma^{AF}_{\delta\tilde{R}_y}$	11.9	21.17	37.83	76.42
	$\sigma^{NI}_{\delta\tilde{R}_y}$	11.89	21.12	37.54	74.77
CT/GS	$\sigma^{AF}_{\delta R_y}$	$1.115\backslash^{-7}$	0.3244	2.05	11.67
	$\sigma^{NI}_{\delta R_y}$	0.113	0.468	2.23	11.75
CT/SS	$\sigma^{AF}_{\delta R_y}$	$1.115\backslash^{-7}$	4.18	24.47	46.12
	$\sigma^{NI}_{\delta R_y}$	110.82	34.29	25.94	46.23

Note: This data assumes BHM prior to survey update.

applicable) which is attained in practice by simply including the external velocity measurement in the IT-1 or CT-1 combinations. For the survey case, k, used in the basic navigation loop is chosen using (4.31) except that the update of $\Phi_g^t(j\omega_s)$ is done a priori so that

$$B = \Phi_g^t(j\omega_s) \tag{7.1}$$

where the value on the right hand side of (7.1) comes from the updated gravity perturbation spectrum.

From Tables VII-2 and VII-3 three things are immediately apparent. First, for the low velocity survey cases, agreement between the analytic and numerical standard deviations is poor for velocity and position error. This is not surprising when it is remembered that neither the analytic velocity nor position results take into account any low frequency contribution. The existence of a dominant low frequency contribution produces the observed discrepancies. The second obvious fact that the gradiometer survey always produces more accurate results than the real-time gradiometer. Reflecting upon the situation, this too is is an expected result since the gradiometer survey gathers information along many tracks while the real-time gradiometer has knowledge only along the present vehicle track. The third and most difficult trend to explain is the GRAVSAT vs gradiometer survey behavior. In general, the gradiometer survey gives better results than GRAVSAT. The high frequency gravitational potential is attenuated with increasing altitude. This makes the ground-level, 1 Eötvos gradiometer more sensitive to short spatial wavelengths (characteristic of Schuler frequency at low velocity) than the 10^{-6} m/sec Doppler at satellite altitude. However, a second consideration working against this trend is that as the carrier velocity increases, so too does the spatial wavelength corresponding to Schuler frequency. It just so happens that for the highest velocity IT case the Schuler spatial wavelength is so long that GRAVSAT has a superior signal-to-noise ratio when compared with that of the gradiometer at ground level. Had speeds above 514.4 m/sec been considered, trends in the data suggest this same type behavior might appear in the CT direction also.

Chapter VIII

CONCLUSIONS AND RECOMMENDATIONS FOR FUTURE RESEARCH

A. CONCLUSIONS

The conclusions resulting from this work can be classified in two areas: those resulting from the real time work, and those from the survey application of the gradiometer to inertial navigation.

A-1 Real Time Gradiometer Application

It has been shown that the modified Wiener filter analysis produces low-order filters for inertial navigation system velocity and position error estimation.

Analysis of the accuracy of these filters is accomplished in several ways. If Kasper's rational gravity model is used, covariance comparisons with the Kalman filter show agreement in the rms position and velocity error estimate error typically to within 1%. An indirect method of proof is needed for the more accurate Heller gravity model. This is done by a comparison of analytically and numerically obtained estimate error results. Agreement of the analytically and numerically obtained estimate error values is always within 10%, on the average about 5%, and in some cases below 1%. This assumes that for velocity estimation the carrier vehicle has a velocity at or above 5.144 m/sec (10 knots). Therefore for the single gradiometer measurement cases used in the above covariance comparisons the approximate low order filters are very nearly optimal.

The approximate nature of the derived filters leads to the carrier vehicle velocity limitation mentioned in the previous paragraph. Fully stated this limitation requires that the position and velocity filters be used only on carrier vehicles traveling at or above 5.144 m/sec (for the assumed levels of external velocity measurement noise and gradiometer accuracy) to avoid at least two problems that arise. These problems are:

(1) the velocity filters contain insufficient low frequency gravity perturbation compensation which makes them inaccurate at low velocity where there is a large low frequency gravity perturbation contribution; (2) The position error filters do compensate low frequency gravity disturbances which unfortunately produces excessively long low frequency pole characteristic settling times in the low velocity cases. In spite of a pole placement technique which is marginally successful for mid-range velocities, and the improvement of the Heller model to reduce the low frequency portion of the gravity potential perturbation spectrum, the under 5,144 m/sec velocity range is unsuitable for approximate filter application at the present time. Lower velocities may be more suitable as future gradiometer and GRAVSAT surveys provide greater knowledge of the earth's gravity field.

The ability of the Wiener technique to produce approximate filters for multiple measurement situations makes it possible to compare the advantages of using two gradiometers as compared to only one. The effect of using the external velocity measurement as a filter input may also be explored. In the cross-track direction using one gradiometer (CT-1 measurement combination) as opposed to two (CT-2 measurement combination) produces a degradation in estimation accuracy of not more than 2% for velocity error estimation and 11% for position error estimation. However, using one gradiometer in-track (IT-2 measurement combination) as opposed to two gradiometers (IT-3 measurement combination) yields a degradation in velocity error estimation accuracy of from 0.5 to 1.5 orders of magnitude and in position error estimation accuracy of from 1 to 2 orders of magnitude. Clearly, if significant improvement over the a priori position and velocity error values is desired, two gradiometers are required in-track while one will suffice cross-track. Additional estimation accuracy may also be obtained for a given gradiometer measurement combination by simply including the external velocity measurement as a filter input. In most cases of velocity error estimation this results in an improvement of about 50%. The improvements in position error estimation accuracy are much more modest, being generally on the order of a few percent, due to the increased effect of low

frequency disturbances as opposed to those at Schuler frequency.

A-2 Survey Gradiometer Application

Of the gradiometer and GRAVSAT surveys considered in this research the gradiometer option is more accurate by at least a factor of four, except for the highest velocity in-track case. As expected, the data show that the gradiometer survey always produces more accurate results than does the real time gradiometer scheme. However, it may not be possible to obtain gradiometer surveys over all potential carrier vehicle routes. Even the GRAVSAT survey with worldwide coverage showed resolution problems at spatial wavelengths greater than its altitude caused by high frequency attenuation of the gravity potential. Therefore, in spite of the excellent INS accuracy attainable with the gradiometer survey, the most likely scenario for improving INS accuracy involves immediate real-time use of the gradiometer with a gradual improvement of the gravity model from data collected in surveys. These data could come from any source supplying gravity information, even the stored real-time gradiometer outputs. One final question is the ability to store aboard a carrier vehicle the large number of coefficients necessary to describe a world-wide gravity model with a desired resolution of approximately 10 km. One solution to this storage problem might be to use an alternative gravity field description consisting of strategically placed mass concentrations in the projected area of vehicle operation. This makes it unnecessary to store a world-wide model thus alleviating the storage problem while making the actual computation of gravity simpler.

B. RECOMMENDATIONS FOR FUTURE RESEARCH

The approximate filters used to estimate position and velocity error from the real time gradiometer/INS combination were derived by assuming "white" gradiometer and external velocity measurement noises. Real gradiometer noise is colored. Data already obtained from the gradiometer manufacturers and processed by the Analytic Science Corp. could be used, along with Navy test data, when it becomes available,

to develop more discriminating filters. Fitting the assumed external velocity measurement noise to a particular carrier vehicle's measurement equipment would also help to develop better filters.

The method used in this research to analyze the error spectrum of the gravity field improved by survey data provides several options for further study. This error spectrum analysis method could be used to optimize gradiometer survey parameters. Additionally it could be used to compare different measurement schemes as was done with the low-low GRAVSAT and ground level gradiometer surveys in this research. Two other survey questions that might be explored are: (1) The possible problems and merits associated with storing real time gradiometer/INS data for post processing and gravity model improvement; (2) The advantages of flying a gradiometer on board the GRAVSAT spacecraft as an additional data source.

APPENDIX A

POISSON'S FORMULA FOR UPWARD CONTINUATION OF THE EARTH'S POTENTIAL

To prove Poisson's formula it is necessary to relate the following spherical harmonic forms for the earth's potential:

$$U(R_{\oplus}, \theta, \phi) = \frac{\mu}{R_{\oplus}} \sum_{\ell=0}^{\infty} \sum_{m=-\ell}^{\ell} \bar{J}_{\ell m} \bar{Y}_{\ell m}(\theta, \phi) \tag{A.1}$$

$$U(r, \theta, \phi) = \frac{\mu}{R_{\oplus}} \sum_{\ell=0}^{\infty} \sum_{m=-\ell}^{\ell} \left(\frac{R_{\oplus}}{r}\right)^{\ell+1} \bar{J}_{\ell m} \bar{Y}_{\ell m}(\theta, \phi) \tag{A.2}$$

where

$$\bar{Y}_{\ell m} = K_{\ell m} P_{\ell m}(\sin \theta) e^{im\lambda} \quad \text{for} \quad m \geq 0 \tag{A.3}$$

$$\bar{Y}_{\ell m} = K_{\ell m} P_{\ell m}(\sin \theta) e^{-i|m|\lambda} \quad \text{for} \quad m \leq 0 \, . \tag{A.4}$$

Note from (A.1) that

$$\oint U(R_{\oplus}, \theta, \phi) \bar{Y}^*_{\ell_2 m_2}(\theta, \phi) d\Omega = \frac{\mu}{R_{\oplus}} \oint \sum_{\ell_1=0}^{\infty} \sum_{m_1=-\ell}^{\ell} \times \bar{J}_{\ell_1 m_1} \bar{Y}_{\ell_1 m_1}(\theta,\phi) \bar{Y}^*_{\ell_2 m_2}(\theta,\phi) d\Omega \tag{A.5}$$

where the integral specified is over the entire earth's surface. Assuming that the $Y_{\ell m}$'s are not only orthogonal over the sphere but suitably (fully) normalized [17] then

$$\oint \bar{Y}_{\ell_1 m_1}(\theta, \phi) \bar{Y}^*_{\ell_2 m_2}(\theta, \phi) d\Omega = 4\pi \delta_{\ell_1 \ell_2} \delta_{m_1 m_2} \tag{A.6}$$

Substituting (A.6) into (A.5) yields

$$\oint U(R_{(p)}, \theta, \phi)\bar{Y}^*_{\ell m}(\theta, \phi)d\Omega = 4\pi \frac{\mu}{R_{(p)}} \bar{J}_{\ell m} . \qquad (A.7)$$

Therefore

$$\bar{J}_{\ell m} = \frac{R_{(p)}}{\mu 4\pi} \oint U(R_{(p)}, \theta, \phi)\bar{Y}^*_{\ell m}(\theta, \phi)\, d\Omega . \qquad (A.8)$$

Substituting (A.8) into (A.2)

$$U(r, \theta, \phi) = \frac{1}{4\pi} \oint \sum_{\ell=0}^{\infty} \left(\frac{R_{(p)}}{r}\right)^{\ell+1} \sum_{m=-\ell}^{\ell} \bar{Y}_{\ell m}(\theta, \phi) \times \bar{Y}_{\ell m}(\theta', \phi')\, U(R_{(p)}, \theta', \phi')d\Omega' ; \qquad (A.9)$$

Making use of the identity

$$P_\ell(\cos \psi) = \frac{1}{2\ell+1} \sum_{m=-\ell}^{\ell} \bar{Y}_{\ell m}(\theta,\phi)\bar{Y}^*_{\ell m}(\theta', \phi') \qquad (A.10)$$

where ψ is the angle between $(1, \theta, \phi)$ and $(1, \theta', \phi')$, (A.9) can be written as

$$U(r,\theta,\phi) = \frac{1}{4\pi} \oint \sum_{\ell=0}^{\infty} \left(\frac{R_{(p)}}{r}\right)^{\ell+1} (2\ell+1)P_\ell(\cos \psi)U(R_{(p)},\theta',\phi')d\Omega' . \qquad (A.11)$$

Since ψ is the angle between $\bar{R}_{(p)}$ and $\bar{r}$ then

$$D = |\bar{R}_{(p)} - \bar{r}| = \left\{r^2\left[1 + \left(\frac{R_{(p)}}{r}\right)^2 - 2\frac{R_{(p)}}{r}\cos \psi\right]\right\}^{\frac{1}{2}} . \qquad (A.12)$$

Using the generating function for $P_\ell(\xi)$ expressed as

$$[1 + \xi'^2 - 2\xi\xi']^{-\frac{1}{2}} = \sum_{n=0}^{\infty} \xi'^n P_n(\xi) \qquad (A.13)$$

and substituting in the quantities

$$\xi' = \frac{R_{\oplus}}{r} \quad \text{and} \quad \xi = \cos\psi \tag{A.14}$$

then from (A.12)

$$[1 + \xi'^2 - 2\xi\xi']^{-\frac{1}{2}} = \frac{r}{D} . \tag{A.15}$$

Substituting (A.14) and (A.15) into (A.13)

$$\frac{1}{D} = [R_{\oplus}^2 + r^2 - 2R_{\oplus} r \cos\psi]^{-\frac{1}{2}} = \frac{1}{R_{\oplus}} \sum_{\ell=0}^{\infty} \left(\frac{R_{\oplus}}{r}\right)^{\ell+1} P_{\ell}(\cos\psi) . \tag{A.16}$$

Taking the negative of the partial with respect to r of (A.16) yields

$$\frac{2rR_{\oplus}(r - R_{\oplus}\cos\psi)}{D^3} = \sum_{\ell=0}^{\infty} 2(\ell+1) \frac{R_{\oplus}^{\ell+1}}{r^{\ell+1}} P_{\ell}(\cos\psi) . \tag{A.17}$$

Subtracting (A.16) from (A.17) yields

$$\frac{2rR_{\oplus}(r - R_{\oplus}\cos\psi) - R_{\oplus}D^2}{D^3} = \sum_{\ell=0}^{\infty} \left\{ \left[(2\ell+2)\left(\frac{R_{\oplus}}{r}\right)^{\ell+1} - \left(\frac{R_{\oplus}}{r}\right)^{\ell+1} \right] P_{\ell}(\cos\psi) \right\} \tag{A.18}$$

or

$$\frac{R_{\oplus}(r^2 - R_{\oplus}^2)}{D^3} = \sum_{\ell=0}^{\infty} (2\ell+1)\left(\frac{R_{\oplus}}{r}\right)^{\ell+1} P_{\ell}(\cos\psi) . \tag{A.19}$$

Putting (A.19) into (A.11) gives

$$U(r, \theta, \phi) = \frac{R_{\oplus}(r^2 - R_{\oplus}^2)}{4\pi} \oint \frac{U(R_{\oplus}, \theta', \phi')}{(r^2 + R_{\oplus}^2 - 2\bar{r}\cdot\bar{R}_{\oplus})^{3/2}} . \tag{A.20}$$

This equation applied to the perturbation potential is the desired result.

Appendix B

SPHERICAL HARMONIC AND HELLER MODEL RMS POTENTIAL COEFFICIENT VARIATION EXPRESSIONS

The GEM 10 [14] data is given in terms of $C_{\ell m}$'s and $S_{\ell m}$'s from the following model

$$U(r,\theta,\phi) = \frac{\mu}{R_D} \sum_{\ell=0}^{\infty} \sum_{m=0}^{\ell} \left(\frac{R_D}{r}\right)^{\ell+1} \bar{P}_{\ell m}(\sin\theta)[C_{\ell m}\cos m\phi + C_{\ell m}\sin m\phi] . \quad (B.1)$$

Therefore the equation for $\sigma^2_{J_\ell}$ (Eq. 3.15) is best derived using the following spherical harmonic form first defined in (A.2)

$$U(r,\theta,\phi) = \frac{\mu}{R_D} \sum_{\ell=0}^{\infty} \sum_{m=-\ell}^{\ell} \left(\frac{R_D}{r}\right)^{\ell+1} \bar{J}_{\ell m} \bar{Y}_{\ell m}(\theta,\phi) \quad (B.2)$$

is is first necessary to establish the relationship between $C_{\ell m}$, $S_{\ell m}$ and $\bar{J}_{\ell m}$. To do this consider the plus and minus m pairs in (B.2) for a given ℓ

$$\frac{\mu}{R_D}\left(\frac{R_D}{r}\right)^{\ell+1}\Big\{\bar{J}_{\ell m}K_{\ell m}\bar{P}_{\ell m}(\sin\theta)[\cos m\phi + i\sin m\phi] + \bar{J}_{\ell(-m)}K_{\ell(-m)} \quad (B.3)$$

$$\times \bar{P}_{\ell(-m)}(\sin\theta)[\cos m\phi - i\sin m\phi]\Big\} .$$

Assuming that

$$\bar{P}_{\ell m}(\sin\theta) = \bar{P}_{\ell(-m)}(\sin\theta) \quad (B.4)$$

$$K_{\ell m} = \frac{(-1)^m}{(2-\delta_{om})!} \quad (B.5)$$

$$K_{\ell(-m)} = \frac{1}{(2 - \delta_{o(-m)})^{\frac{1}{2}}} \tag{B.6}$$

then (B.3) can be written as

$$\frac{\mu}{R_D}\left(\frac{R_D}{r}\right)^{\ell+1} \bar{P}_{\ell m}(\sin\theta)\, \frac{1}{(2-\delta_{om})^{\frac{1}{2}}} \left\{ \bar{J}_{\ell m}(-1)^m [\cos m\phi + i \sin m\phi] + \bar{J}_{\ell(-m)} [\cos m\phi - i \sin m\phi] \right\}. \tag{B.7}$$

Therefore for even m (B.7) becomes

$$\frac{\mu}{R_D}\left(\frac{R_D}{r}\right)^{\ell+1} \bar{P}_{\ell m}(\sin\theta) \left\{ \left[\frac{\bar{J}_{\ell m} + \bar{J}_{\ell(-m)}}{(2-\delta_{om})^{\frac{1}{2}}} \right] \cos m\phi + i \left[\frac{\bar{J}_{\ell m} - \bar{J}_{\ell(-m)}}{(2-\delta_{om})^{\frac{1}{2}}} \right] \sin m\phi \right\} \Bigg|_{\text{even } m} \tag{B.8}$$

and for odd m

$$\frac{\mu}{R_D}\left(\frac{R_D}{r}\right)^{\ell+1} \bar{P}_{\ell m}(\sin\theta) \left\{ \left[\frac{\bar{J}_{\ell(-m)} - \bar{J}_{\ell m}}{(2 - \delta_{om})^{\frac{1}{2}}} \right] \cos m\phi - i \left[\frac{\bar{J}_{\ell m} + \bar{J}_{\ell(-m)}}{(2-\delta_{om})^{\frac{1}{2}}} \right] \sin m\phi \right\} \Bigg|_{\text{odd } m}. \tag{B.9}$$

Then for even m let

$$C_{\ell m}\Big|_{\text{even } m} = \frac{\bar{J}_{\ell m} + \bar{J}_{\ell(-m)}}{(2 - \delta_{om})^{\frac{1}{2}}} \Bigg|_{\text{even } m} \tag{B.10}$$

$$S_{\ell m}\Big|_{\text{even } m} = i \left[\frac{\bar{J}_{\ell m} - \bar{J}_{\ell(-m)}}{(2-\delta_{om})^{\frac{1}{2}}} \right] \Bigg|_{\text{even } m} \tag{B.11}$$

and for odd m let

$$C_{\ell m}\Big|_{\text{odd } m} = \frac{\bar{J}_{\ell(-m)} - \bar{J}_{\ell m}}{(2-\delta_{om})^{\frac{1}{2}}}\Bigg|_{\text{odd } m} \tag{B.12}$$

$$S_{\ell m}\Big|_{\text{odd } m} = -i\left[\frac{\bar{J}_{\ell m} + \bar{J}_{\ell(-m)}}{(2-\delta_{om})^{\frac{1}{2}}}\right]\Bigg|_{\text{odd } m} . \tag{B.13}$$

Substituting (B.10) through (B.13) into (B.8) and (B.9) and summing over the required positive values of ℓ and m gives

$$U(r,\theta,\phi) = \frac{\mu}{R_\oplus}\sum_{\ell=0}^{\infty}\sum_{m=0}^{\ell}\left(\frac{R_\oplus}{r}\right)^{\ell+1}\bar{P}_{\ell m}(\sin\theta)[C_{\ell m}\cos m\phi + S_{\ell m}\sin m\phi] \tag{B.14}$$

which is identical to (B.1).

To solve for $\bar{J}_{\ell m}$ and $\bar{J}_{\ell(-m)}$ in terms of $C_{\ell m}$ and $S_{\ell m}$ first write from (B.10) and (B.11) for even m

$$(2-\delta_{om})^{\frac{1}{2}}C_{\ell m} = \bar{J}_{\ell m} + \bar{J}_{\ell(-m)} \tag{B.15}$$

$$-i(2-\delta_{om})^{\frac{1}{2}}S_{\ell m} = \bar{J}_{\ell m} - \bar{J}_{\ell(-m)} . \tag{B.16}$$

Adding (B.15) and (B.16) yields

$$2\bar{J}_{\ell m} = (2-\delta_{om})^{\frac{1}{2}}[C_{\ell m} - i\,S_{\ell m}] . \tag{B.17}$$

Equation (B.17) is, however, inaccurate for the case $m = 0$ for which the following relation holds

$$\bar{J}_{\ell o} = C_{\ell o} \cdot \tag{B.18}$$

To incorporate (B.18) into (B.17), write 2 as

$$(2 - \delta_{om})^{\frac{1}{2}} (2 - \delta_{om}) = \begin{cases} 2 & m \neq 0 \\ 1 & m = 0 \end{cases} \cdot \tag{B.19}$$

Then

$$\bar{J}_{\ell m} = \frac{1}{(2 - \delta_{om})^{\frac{1}{2}}} [C_{\ell m} - i S_{\ell m}] \Big|_{\text{even } m} \cdot \tag{B.20}$$

After subtracting (B.16) from (B.15) this same type analysis yields for even m

$$\bar{J}_{\ell(-m)} = \frac{1}{(2 - \delta_{om})^{\frac{1}{2}}} [C_{\ell m} + i S_{\ell m}] \Big|_{\text{even } m} \cdot \tag{B.21}$$

Using (B.12) and (B.13) to analyze the odd m case yields

$$\bar{J}_{\ell m} = \frac{1}{(2 - \delta_{om})^{\frac{1}{2}}} [-C_{\ell m} + iS_{\ell m}] \Big|_{\text{odd } m} \cdot \tag{B.22}$$

$$\bar{J}_{\ell(-m)} = \frac{1}{(2 - \delta_{om})^{\frac{1}{2}}} [C_{\ell m} + iS_{\ell m}] \Big|_{\text{odd } m} \cdot \tag{B.23}$$

Rewriting (B.20), (B.21), (B.22), and (B.23) in the following more compact form

$$\bar{J}_{\ell m} = \frac{(-1)^m}{(2 - \delta_{om})^{\frac{1}{2}}} [C_{\ell m} - i S_{\ell m}] , \tag{B.24}$$

$$\bar{J}_{\ell(-m)} = \frac{1}{(2 - \delta_{om})^{\frac{1}{2}}} [C_{\ell m} + i S_{\ell m}] . \tag{B.25}$$

It is also possible to re-express $\bar{Y}_{\ell m}$ as

$$\bar{Y}_{\ell m} = \frac{(-1)^m}{(2 - \delta_{om})^{\frac{1}{2}}} \bar{P}_{\ell m}(\sin \theta) e^{-im\lambda} \tag{B.26}$$

$$\bar{Y}_{\ell(-m)} = \frac{1}{(2 - \delta_{om})^{\frac{1}{2}}} \bar{P}_{\ell m}(\sin \theta) e^{-im\lambda} . \tag{B.27}$$

From (B.24) and (B.25) the following equation may be written

$$\frac{1}{2\ell+1} \sum_{m=-\ell}^{\ell} \bar{J}_{\ell m} \bar{J}^{*}_{\ell m} = \frac{1}{2\ell+1} \sum_{m=0}^{\ell} (C^2_{\ell m} + S^2_{\ell m}) \tag{B.28}$$

The expected value of (B.28) is defined as the rms potential coefficient variation. Therefore

$$\sigma^2_{\bar{J}_\ell} = \frac{1}{2\ell+1} \sum_{m=0}^{\ell} \left[E(C^2_{\ell m}) + E(S^2_{\ell m}) \right] . \tag{B.29}$$

This gives us the first part of (3.15). To derive the Heller model counterpart to $\sigma^2_{\bar{J}_\ell}$ begin by specializing (A.11) to Heller's three layer model

$$U(R_D, \vartheta, \phi) = \frac{1}{4\pi} \sum_{i=1}^{3} \sum_{\ell=0}^{\infty} \oint (2\ell+1) P_\ell(\cos \Psi) \times (R_D - D_i / R_D)^{\ell+1} U(R_D - D_i, \vartheta', \phi') d\omega' . \tag{B.30}$$

Substituting (A.10) into (B.30)

$$U(R_D,\ \theta,\ \phi) = \frac{1}{4\pi} \sum_{i=1}^{3} \sum_{\ell'=0}^{\infty} \left(\frac{R_D - D_i}{R_\Theta}\right)^{\ell'+1} \oint \sum_{m'=-\ell'}^{\ell'} \bar{Y}_{\ell' m'}\ (\theta,\phi)$$

$$\times\ \bar{Y}_{\ell' m'}(\theta',\phi') U(R_D - D_i, \theta', \phi') d\Omega' \ . \qquad \text{(B.31)}$$

Again, going back to App. A, Eq. (A.8)

$$\frac{\mu}{R_D} \bar{J}_{\ell m} = \frac{1}{4\pi} \oint U(R_D,\ \theta,\ \phi)\ \bar{Y}^*_{\ell m}(\theta,\phi) d\Omega \qquad \text{(B.32)}$$

in conjunction with (B.31) yields

$$\frac{\mu}{R_D} \bar{J}_{\ell m} = \frac{1}{16\pi^2} \sum_{i=1}^{3} \oint \oint \sum_{\ell'=0}^{\infty} \sum_{m=-\ell'}^{\ell'} \left(\frac{R_D - D_i}{R_\Theta}\right)^{\ell'+1} \bar{Y}_{\ell' m'}\ (\theta',\ \phi')$$

$$\times\ \bar{Y}_{\ell m}\ (\theta,\phi)\ U(R_D - D_i,\ \theta'\ \phi') d\Omega d\Omega' \ . \qquad \text{(B.33)}$$

But recalling the identity

$$\oint \bar{Y}_{\ell' m'}(\theta,\ \phi) \bar{Y}_{\ell m}(\theta,\phi) d\Omega = 4\pi \delta_{\ell' \ell} \delta_{m' m} \qquad \text{(B.34)}$$

(B.33) simplifies to

$$\frac{\mu}{R_D} \bar{J}_{\ell m} = \frac{1}{4\pi} \sum_{i=1}^{3} \oint \sum_{\ell'=0}^{\infty} \sum_{m'=-\ell}^{\ell} \left(\frac{R_D - D_i}{R_D}\right)^{\ell'+1} \bar{Y}_{\ell' m'}(\theta',\ \phi')$$

$$\times\ U(R_D - D_i,\ \theta',\ \phi') \delta_{\ell' \ell} \delta_{m' m}\ d\Omega' \ . \qquad \text{(B.35)}$$

Since $\ell' = \ell$ and $m' = m$ in (B.35), then for a given ℓ and m only one term in the $\sum_{\ell'} \sum_{m'}$ sequence will be non-zero. Therefore (B.35) may

be written

$$\frac{\mu}{R_0}\bar{J}_{\ell m} = \frac{1}{4\pi}\sum_{i=1}^{3}\oint\left(\frac{R_i-D_i}{R_i}\right)^{\ell+1} Y_{\ell m}(\theta',\phi')U(R_i-D_i,\theta',\phi')d\Omega' \quad . \tag{B.36}$$

Multiplying both sides of (B.36) and their complex conjugates and taking the expected value gives

$$\left(\frac{\mu}{R_0}\right)^2\sigma^2_{\bar{J}_\ell} = E\left\{\frac{1}{16\pi^2}\sum_{i=1}^{3}\sum_{i'=1}^{3}\oint\oint\left(\frac{R_i-D_i}{R_i}\right)^{\ell+1}\left(\frac{R_{i'}-D_{i'}}{R_{i'}}\right)^{\ell+1}\right.$$
$$\times\ Y_{\ell m}(\theta',\phi')Y_{\ell m}(\theta,\phi)U(R_i-D_i,\theta',\phi')$$
$$\left.\times\ U(R_{i'}-D_{i'},\theta,\phi)\,d\Omega'd\Omega\right\}. \tag{B.37}$$

Because the potential variations from different shells are uncorrelated, then

$$E\left\{\oint U(R_i-D_i,\theta,\phi)\,U(R_{i'}-D_{i'},\theta',\phi')f(\theta',\phi')d\Omega'\right\}$$
$$= \begin{cases} 0 & \text{for } i\neq i' \\ \Phi_i/(R_i-D_i)^2 f(\theta,\phi) & \text{for } i = i' \end{cases} \tag{B.38}$$

where $f(\theta,\phi)$ is any function of θ and ϕ. Applying (B.38) to (B.37)

$$\left(\frac{\mu}{R_0}\right)^2\sigma^2_{\bar{J}_\ell} = \frac{1}{16\pi^2}\sum_{i=1}^{3}\left(\frac{R_i-D_i}{R_i}\right)^{2\ell+2}\frac{\Phi_i}{(R_i-D_i)^2} \tag{B.39}$$
$$\times\oint Y_{\ell m}(\theta,\phi)\bar{Y}_{\ell m}(\theta,\phi)d\Omega \quad .$$

However, the integral in (B.39) equals 4π. Therefore simplifying (B.39) using this fact gives the desired result

$$\sigma^2_{\bar{J}_\ell} = \left(\frac{R_0}{\mu}\right)^2\frac{1}{4\pi}\sum_{i=1}^{3}\frac{\Phi_i}{(R_i-D_i)^2}\left(\frac{R_i-D_i}{R_i}\right)^{2\ell+2} \quad . \tag{B.40}$$

Appendix C

LOW FREQUENCY FILTER CONSTANT AND RMS POSITION ERROR ESTIMATE ERROR DERIVATIONS

The measurement combinations used in this research are given below by number preceded by the assumed direction of estimation. Note that these derivations assume the use of the Heller model.

CT-1) If a measurement of

$$\bar{z} = \Gamma_{xy} + \bar{\epsilon} \tag{C.1}$$

is taken then

$$H = [0 \quad 1 \quad 0 \quad 0 \quad 0] \tag{C.2}$$

and

$$R = r_1 \, . \tag{C.3}$$

Equation (4.70) gives the root

$$\beta = \left(\frac{r_1}{2k_3^{\Lambda}}\right)^{\frac{1}{2}} \, . \tag{C.4}$$

Using (4.76) to determine α

$$(\tfrac{1}{2})(-4k_3^{\Lambda})\alpha + \frac{1}{\omega_s^2} 2k_3^{B} = 0 \tag{C.5}$$

then

$$\alpha = \frac{k_3^{B}}{k_3^{\Lambda}} \times \frac{1}{\omega_s^2} = \frac{V_x}{\omega_s^2} \, . \tag{C.6}$$

To obtain $(\sigma^{AF}_{\delta\tilde{R}_y})_{\ell}$ the following integral (from 4.49) must be evaluated

$$-\frac{1}{2\pi j}\oint \frac{\phi^{t}_{g_y}\bar{\Gamma}^{T}(s)H^{T}\psi_{\ell}^{T}(s)}{(-)}\,ds \;-\; -\frac{1}{2\pi j}\oint \frac{2k_3^{B}s\sigma}{\omega_s^{2}(s+\beta)}\,ds\,. \qquad (C.7)$$

Using the Cauchy residue theorem this equals

$$-\frac{1}{2\pi j}\oint \frac{2k_3^{B}s\sigma}{\omega_s^{2}(s+\beta)}\,ds \;=\; \frac{2k_3^{B}\sigma\beta}{\omega_s^{2}}\,. \qquad (C.8)$$

or

$$\left(\sigma^{AF}_{\widetilde{\delta R}_y}\right)^{2}_{\ell} \;=\; \frac{2k_3^{B}\sigma\beta}{\omega_s^{2}}\,. \qquad (C.9)$$

To include the EVM in this and any of the subsequent total estimate error variance formulas the only modification necessary is to change k to k'.

CT-2: In the case where

$$\bar{z} \;=\; \begin{bmatrix}\Gamma_{xy}\\ \Gamma_{yz}\end{bmatrix} + \bar{\varepsilon} \qquad (C.10)$$

then

$$H \;=\; \begin{bmatrix}0 & 1 & 0 & 0 & 0\\ 0 & 0 & 0 & 1 & 0\end{bmatrix} \qquad (C.11)$$

and

$$R \;=\; \begin{bmatrix}r_1 & 0\\ 0 & r_2\end{bmatrix}. \qquad (C.12)$$

The low frequency pole, obtained from (4.70), is

$$\rho = \left\{ \frac{r_1(r_2 + 24k_5^A)}{(48k_3^A k_5^A - 36k_4^{A^2} + 2k_3^A r_2)} \right\}^{\frac{1}{4}} . \qquad (C.13)$$

For multiple measurements the vector $\bar{\alpha}$ is obtained from both (4.76) and (4.77). Equation (4.76) gives

$$\begin{bmatrix} -2k_3^A & 0 \\ 0 & 0 \end{bmatrix} \begin{bmatrix} \alpha_1 \\ \alpha_2 \end{bmatrix} + \frac{1}{\omega_s^2} \begin{bmatrix} 2k_3^B \\ 0 \end{bmatrix} = 0 \qquad (C.14)$$

then

$$\alpha_1 = \frac{k_3^B}{k_3^A} \times \frac{1}{\omega_s^2} = \frac{V_x}{\omega_s^2} . \qquad (C.15)$$

To determine α_2 use (4.77)

$$\begin{bmatrix} r_1 - 2k_3^A s^2 & 6k_4^A s \\ -6k_4^A s & 24k_5^A + r_2 \end{bmatrix} \begin{bmatrix} \alpha_1 \\ \alpha_2 \end{bmatrix} \Bigg|_{s=-\rho} = 0. \qquad (C.16)$$

The second row of this equation gives

$$\alpha_2 = -\frac{6k_4^A \rho V_x}{\omega_s^2(24k_5^A + r_2)} . \qquad (C.17)$$

The last integral in (4.49) can now be expressed as

$$-\frac{1}{2\pi j}\oint \frac{\Phi^{t}_{g_y}\bar{\Gamma}^{T}(s)H^{T}\Psi^{T}_{\ell}(s)}{(-)}\,ds \;-\; -\frac{1}{2\pi j}\oint \frac{2k_3^B s\alpha_1 - 6k_4^B\alpha_2}{\omega_s^2(s+\beta)}\,ds\,. \qquad (C.18)$$

The evaluation of (C.18) gives

$$\left(\sigma^{AF}_{\tilde{R}_y}\right)^2_{\ell} = \frac{2k_3^B\alpha_1\beta + 6k_4^B\alpha_2}{\omega_s^2}\,. \qquad (C.19)$$

IT-1: If the measurement is

$$\tilde{z} = \Gamma_{xx} + \tilde{\epsilon} \qquad (C.20)$$

Then

$$H = [1\ \ 0\ \ 0\ \ 0\ \ 0] \qquad (C.21)$$

and

$$R = r_1\,. \qquad (C.22)$$

The characteristic equation from (4.70) is

$$k_1^A s^4 + r_1 = 0\,. \qquad (C.23)$$

Solving for the two left-half plane poles results in

$$(\ell+) = s^2 + \frac{2}{L}s + \frac{2}{L^2} \qquad (C.24)$$

where L is a low frequency factor coefficient defined as

$$L = \left(\frac{4k_1^A}{r_1}\right)^{1/4}\,. \qquad (C.25)$$

To determine d and e write (4.79) as

$$\left.\frac{k_1^A s}{s^2 + \frac{2}{L}s}\,(ds + e)\right|_{\text{"large s"}} = \left.\frac{1}{\omega_s^2}\,k_1^B\right|_{\text{"large s"}} . \qquad \text{(C.26)}$$

Using the approximation

$$\frac{s}{s^2 + \frac{2}{L}s} \cong \frac{1}{s}\left(1 - \frac{2}{Ls}\right) \qquad \text{(C.27)}$$

(C.26) may be written

$$\left(d - \frac{V_x}{\omega_s^2}\right)s^2 + \left(e - \frac{2d}{L}\right)s - \cancel{\frac{2e}{L}}^{\text{small}} = 0 . \qquad \text{(C.28)}$$

Zeroing the first and second degree s terms gives

$$d = \frac{V_x}{\omega_s^2} \qquad \text{(C.29)}$$

$$e = \frac{2V_x}{L\omega_s^2} . \qquad \text{(C.30)}$$

The low frequency rms variance is obtained by integrating

$$-\frac{1}{2\pi j}\oint \frac{\Phi^t}{g_x}\frac{\bar{\Gamma}^T(s)H^T\psi_\ell^T(s)}{(-)}\,ds = +\frac{1}{2\pi j}\oint \frac{k_1^B s^3(ds + e)}{\omega_s^2(\ell+)}\,ds. \qquad \text{(C.31)}$$

Summing the residues at both left-half plane poles in (C.31) gives

$$\left(\frac{\Delta F}{\sigma_{\delta R_x}}\right)_\ell^2 = \frac{2k_1^B e}{\omega_s^2 L^2} . \qquad \text{(C.32)}$$

LT-2: For a measurement of

$$\bar{z} = \frac{1}{2}\left(\Gamma_{xx} - \Gamma_{yy}\right) + \bar{\epsilon} \qquad \left(\Gamma_{xx} + \frac{1}{2}\Gamma_{zz}\right) + \bar{\epsilon} \ , \tag{C.33}$$

then

$$H = \begin{bmatrix} 1 & 0 & 0 & 0 & \end{bmatrix} \tag{C.34}$$

and

$$R = r_1 \ . \tag{C.35}$$

The characteristic equation from (4.70) is

$$k_1^A s^4 + 2k_3^A s^2 + \left(6k_5^A + r_1\right) = 0 \ . \tag{C.36}$$

The left-half plane poles of (C.34) produce a low frequency factor expressible as

$$(\ell+) \qquad s^2 + 2\omega_N \delta_1 s + \omega_N^2 \tag{C.37}$$

where

$$\xi = \left\{ 6\frac{k_5^A}{k_1^A} + \frac{r_1}{k_1^A} - \left(\frac{k_3^A}{k_1^A}\right)^2 \right\}^{1/2} \tag{C.38}$$

$$\delta_1 = \sin\left(\frac{1}{2}\tan^{-1}\frac{\xi}{k_3^A}\right) \tag{C.39}$$

$$\omega_N = \left[\left(\frac{k_3^A}{k_1^A}\right)^2 + \xi^2\right]^{1/4} \ . \tag{C.40}$$

The convergence condition for this situation is

$$\left[k_1^A s^4 + 2k_3^A s^2 + 6k_5^A\right] \frac{ds + e}{s^2 + 2\omega_N \delta_1 s}\Bigg|_{\text{"large s"}} = \frac{1}{\omega_s^2}\left(k_1^B s^3 + k_3^B s\right)\Bigg|_{\text{"large s"}} . \qquad (C.41)$$

Assuming that the s^4 and s^3 terms dominate for large s and writing

$$\frac{s}{s^2 + 2\omega_N \delta_1 s} \cong \frac{1}{s}\left[1 - \frac{2\omega_N \delta_1}{s}\right] , \qquad (C.42)$$

(C.41) becomes

$$(d - \frac{V_x}{\omega_s^2})s^2 + (e - 2\omega_N \delta_1 d)s - \cancel{2e\omega_N \delta_1}^{\text{small}} = 0 . \qquad (C.43)$$

Cancelling the s^2 and s terms in (C.43) gives

$$d = \frac{V_x}{\omega_s^2} \qquad (C.44)$$

$$e = \frac{2\omega_N \delta_1 V_x}{\omega_s^2} . \qquad (C.45)$$

The expression to be integrated to obtain the low frequency analytic variance is

$$-\frac{1}{2\pi j} \oint \frac{\Phi^t g_x \bar{\Gamma}^T(s) H^T \psi_\ell(s)}{(\ )} ds - \frac{1}{2\pi j} \oint \frac{(k_1^B s^3 + k_3^B s)(ds+e)}{\omega_s^2(\ell+)} ds . \qquad (C.46)$$

Summing the residues at both of the left-half plane poles in (C.44) ultimately gives

$$\left(\frac{\partial^{AF}}{\partial \tilde{R}_x}\right)^2_{\ell} = \left\{-k_1^B d\xi^3 [2\delta_1^3 - 2\delta_1\delta_2^2 + 2\delta_1(\delta_1^2 - \delta_2^2)]\right.$$

$$\left. + k_1^B c\xi [2\delta_1^2 + (\delta_1^2 - \delta_2^2)] - 2k_3^B d\xi \delta_1 + k_3^B c\right\} / \omega_s^2 \qquad \text{(C.47)}$$

where

$$\delta_2 = \cos\left(\frac{1}{2}\tan^{-1}\frac{\xi}{k_3^A}\right) . \qquad \text{(C.48)}$$

IT-3: For a measurement of

$$\bar{z} = \begin{bmatrix} \frac{1}{2}(\Gamma_{xx} - \Gamma_{yy}) \\ \frac{1}{2}(\Gamma_{zz} - \Gamma_{yy}) \end{bmatrix} + \bar{\varepsilon} \qquad \begin{bmatrix} \Gamma_{xx} + \frac{1}{2}\Gamma_{zz} \\ \frac{1}{2}\Gamma_{xx} + \Gamma_{zz} \end{bmatrix} + \bar{\epsilon} \quad , \qquad \text{(C.49)}$$

then

$$H = \begin{bmatrix} 1 & 0 & 0 & 0 & \frac{1}{2} \\ \frac{1}{2} & 0 & 0 & 0 & 1 \end{bmatrix} \qquad \text{(C.50)}$$

$$R = \begin{bmatrix} r_1 & 0 \\ 0 & r_2 \end{bmatrix} . \qquad \text{(C.51)}$$

The characteristic equation, again from (4.70), reduces to

$$(\frac{27}{2}k_1^A k_5^A + \frac{5}{4}k_1^A r_1 + \frac{3}{2}k_3^{A^2})s^4 + (4k_3^A r_1)s^2 + (30k_5^A r_1 + r_1^2) = 0 \qquad \text{(C.52)}$$

where it has been assumed that

$$r_1 = r_2 . \qquad \text{(C.53)}$$

If r_1 is small then the s^2 term in (C.52) is negligible and the equation becomes

$$s^4 = -\frac{(30k_5^A r_1 + r_1^2)}{(\frac{27}{2}k_1^A k_5^A + \frac{3}{2}k_3^{A^2} + \frac{5}{4}k_1^A r_1)} \quad . \tag{C.54}$$

Solving for the left-half plane roots the low frequency factor is

$$(\ell+) = s^2 + \frac{2}{L}s + \frac{2}{L^2} \tag{C.55}$$

where

$$L = \left[\frac{4(\frac{27}{2}k_1^A k_5^A + \frac{3}{2}(k_3^A)^2 + \frac{5}{4}k_1^A r_1)}{(30k_5^A + r_1)r_1}\right]^{1/4} \quad . \tag{C.56}$$

Here the convergence condition (4.79) is

$$\left[\begin{matrix} k_1^A s^4 + 2k_3^A s^2 + 6k_5^A & \frac{1}{2}k_1^A s^4 + \frac{5}{2}k_3^A s^2 + 12k_5^A \\ \frac{1}{2}k_1^A s^4 + \frac{5}{2}k_3^A s^2 + 12k_5^A & \frac{1}{4}k_1^A s^4 + 2k_3^A s^2 + 24k_5^A \end{matrix}\right] \left(\begin{matrix} \frac{d_1 s + e_1}{s^2 + (2/L)s} \\ \frac{d_2 s + e_2}{s^2 + (2/L)s} \end{matrix}\right)\Bigg|_{\text{"large s"}}$$

$$= \frac{1}{\omega_s^2}\left(\begin{matrix} k_1^B s^3 + k_3^B s \\ \frac{1}{2}k_1^B s^3 + 2k_3^B s \end{matrix}\right)\Bigg|_{\text{"large s"}} \quad . \tag{C.57}$$

If the s^4 and s^3 terms dominate, this reduces to

$$\frac{k_1^A s}{s^2 + \frac{2}{L}s}\begin{bmatrix} 1 & \frac{1}{2} \\ \frac{1}{2} & \frac{1}{4} \end{bmatrix}\begin{bmatrix} d_1 s + e_1 \\ d_2 s + e_2 \end{bmatrix}\Bigg|_{\text{"large s"}} = \frac{k_1^B}{\omega_s^2}\begin{bmatrix} 1 \\ \frac{1}{2} \end{bmatrix} . \quad \text{(C.58)}$$

Substituting (C.27) into (C.58) yields

$$\begin{bmatrix} 1 & \frac{1}{2} \\ \frac{1}{2} & \frac{1}{4} \end{bmatrix}\begin{bmatrix} d_1 s^2 + (e_1 - \frac{2d_1}{L})s - \cancel{\frac{2e_1}{L}} \\ d_2 s^2 + (e_2 - \frac{2d_2}{L})s - \cancel{\frac{2e_2}{L}} \end{bmatrix} - \frac{V_x s^2}{\omega_s^2}\begin{bmatrix} 1 \\ \frac{1}{2} \end{bmatrix} = 0 . \quad \text{(C.59)}$$

(small terms)

Using only the first equation in (C.59) since the two are linearly dependent gives

$$\left(d_1 + \frac{d_2}{2} - \frac{V_x}{\omega_s^2}\right) s^2 + \left[(e_1 - \frac{2d_1}{L}) + \frac{1}{2}(e_2 - \frac{2d_2}{L})\right] s = 0 . \quad \text{(C.60)}$$

Zeroing the first and second degree terms in (C.60) gives

$$(e_1 - \frac{2d_1}{L}) + \frac{1}{2}(e_2 - \frac{2d_2}{L}) = 0 \quad \text{(C.61)}$$

$$d_1 + \frac{1}{2} d_2 = \frac{V_x}{\omega_s^2} . \quad \text{(C.62)}$$

This results in four unknowns but only two equations. The remaining two equations come from (4.80) expressed as

$$\left[\begin{matrix} k_1^A s^4 + 2k_3^A s^2 + 6k_5^A + r_1 & \frac{1}{2}k_1^A s^4 + \frac{5}{2}k_3^A s^2 + 12k_5^A \\ \frac{1}{2}k_1^A s^4 + \frac{5}{2}k_3^A s^2 + 12k_5^A & \frac{1}{4}k_1^A s^4 + 2k_3^A s^2 + 24k_5^A + r_2 \end{matrix}\right]\left[\begin{matrix} d_1 s + e_1 \\ d_2 s + e_2 \end{matrix}\right]\Bigg|_{\text{small } s}$$

$$= 0 . \qquad \text{(C.63)}$$

For small s and small r_1 (C.63) reduces to

$$k_5^A \begin{bmatrix} 1 & 2 \\ 2 & 4 \end{bmatrix} \begin{pmatrix} d_1 s + e_1 \\ d_2 s + e_2 \end{pmatrix} = 0 . \qquad \text{(C.64)}$$

Using only the first of the equations in (C.64) because of their linear dependence gives

$$(d_1 + 2d_2)s + (e_1 + 2e_2) = 0 . \qquad \text{(C.65)}$$

This immediately produces the conditions

$$d_1 + 2d_2 = 0 \qquad \text{(C.66)}$$

$$e_1 + 2e_2 = 0 . \qquad \text{(C.67)}$$

Solving (C.61), (C.62), (C.66) and (C.67) simultaneously produces

$$d_1 = \frac{4V_x}{3\omega_s^2} , \qquad \text{(C.68)}$$

$$d_2 = -\frac{2V_x}{3\omega_s^2} , \qquad \text{(C.69)}$$

$$e_1 = \frac{8V_x}{3L\omega_s^2} , \qquad \text{(C.70)}$$

$$e_2 = -\frac{4V_x}{3I\omega_s^2} \quad . \tag{C.71}$$

The analytic low frequency variance integral reduces to

$$-\frac{1}{2\pi j}\oint \frac{\Phi^t g_x \bar{P}^T(s) H^T \Psi_\ell(s)}{(-)} = \frac{1}{2\pi j}\oint \frac{A_1 s^4 + A_2 s^3 + A_3 s^2 + A_4}{\omega_s^2(\ell+)}\, ds \tag{C.72}$$

where

$$A_1 = d_1 k_1^B + \frac{k_1^B}{2} d_2 \tag{C.73}$$

$$A_2 = e_1 k_1^B + \frac{e_2 k_1^B}{2} \tag{C.74}$$

$$A_3 = d_1 k_3^B + 2k_3^B d_2 \tag{C.75}$$

$$A_4 = e_1 k_3^B + 2k_3^B e_2 \quad . \tag{C.76}$$

Solving (C.72) again with the aid of Cauchy's theorem the analytic variance equals

$$\left(\sigma^{\Delta F}_{\delta R_x}\right)^2_\ell = \frac{2}{\omega_s^2}\left(\frac{A_2}{I^2} - \frac{A_3}{L}\right) . \tag{C.77}$$

REFERENCES

1. Hildebrant, R.R., Britting, K.R., and Madden, S.J., "The Effects of Gravitational Uncertainties on the Errors of Inertial Navigation Systems", J. of the Institute of Navigation, Vol. 21, No. 4, Winter 1974-1975.

2. Bell Aerospace Corp., "Gravity Gradiometer Instrument Feasibility Demonstration and Studies and Gravity Gradiometer System Definition Studies Program", Bell Aerospace Corp., Niagara Falls, NY, Vol. 1 Tech. Rept. No. D6441-953001, Oct. 1976.

3. "Advances in Dynamic Gravimetry", Proc. of the Symposium on Dynamic Gravimetry, Mar. 16-17, 1970, Fort Worth, Texas.

4. Pelka, E.J., "On-Line Parameter Estimation and Control for a Rotating Gravity Gradiometer", Ph.D. Dissertation, Stanford University, Dept. Aeronautics and Astronautics, Guidance & Control Lab., Aug. 1977.

5. DeBra, D.B., Schaechter, D., and Kurosaki, M., "Study to Develop Gradiometer Techniques", Air Force Geophysics Laboratory Technical Report, AFGL-TR-78-0046, Dec. 1977 (AFGL/LWG, Hanscom AFB, MA 01731), December 1977.

6. DeBra, D.B., Breakwell, J.V., and Kurosaki, M., "Study to Develop Gradiometer Techniques," Air Force Geophysics Laboratory Technical Report, AFGL-TR-79-0063, January 1979.

7. Heller, W.G., "Free-Inertial and Damped-Inertial Navigation Mechanization and Error Equations", The Analytic Sciences Corp., Reading, Mass., TR-312-1-1, 18 Apr. 1975.

8. Rice, D.A., "A Geoidal Section in the United States", Bulletin Geod., Vol. 65, 1962.

9. Kasper, J.F., Jr., "A Second Order Markov Gravity Anomaly Model", J. of Geophysical Research, Vol. 76, No. 32, Nov. 1971.

10. Heller, W.G., "Gradiometer-Aided Inertial Navigation", The Analytic Sciences Corp., Reading, Mass., TR-312-5, 7 Apr. 1975.

11. Heller, W.G., "A New Self-Consistent Statistical Gravity Field Model", Proc. of the American Geophysical Union, Fall Annual Meeting, San Francisco, CA., Dec. 1976.

12. Breakwell, J.V., "Satellite Determination of Short Wavelength Gravity Variations", J. of Astronautical Sciences, Vol. 37, No. 4, pp. 329-344, Oct-Dec., 1979.

13. Breakwell, J.V., Kurosaki, M., "Real-Time Gravity Filtering from On-Board Gradiometers," AIAA G&C Conf., Boulder, Colorado, Aug. 1979.

14. Lerch, F.J., Klosho, S.M., Laubscher, R.E., and Wagner, C.A., "Gravity Model Improvement Using GEOS-3 (GEM 9 & 10)", Goddard Space Flight Center, Greenbelt, Md., Sept. 1977.

15. Trageser, M.B., "A Status Report on the Floated Gravity Gradiometer", Rept. No. C 3868, The C. Stark Draper Laboratory, Cambridge, Mass., Nov. 30, 1972.

16. Bryson, A.E., and Ho, Y.C., Applied Optimal Control, John Wiley & Sons, Inc., New York, NY, 1975.

17. Heiskanen, W.A., and Moritz, H., Physical Geodesy, W.H. Freeman, San Francisco, CA., 1967.